SAPHYRE

Contract No. FP7-ICT-248001

Basic Limits for System Design (final)
D2.1b

Contractual date:	M30
Actual date:	M30
Authors:	Zuleita Ka-Ming Ho, Christian Scheunert, Eduard Jorswieck, Jan Sýkora, Eleftherios Karipidis, Erik G. Larsson, Johannes Lindblom, David Gesbert
Participants:	TUD, CTU, ECM, LiU
Work package:	WP2
Security:	Public
Nature:	Report
Version:	1.0
Number of pages:	141

Abstract

This report describes final results on basic limits for spectrum sharing considered within SAPHYRE. At first, the spectrum sharing scenario has been modeled by the multi-antenna interference channel. Then different basic limits in terms of achievable rate regions under different assumptions on decoding capabilities of the receivers and channel state information at the transmitters have been derived. Finally, performance and fundamental limits of a novel wireless network coding technique for spectrum sharing have been proposed.

Keywords

Beamforming, Interference Channel, Multiple Antenna, Pareto Optimal, Wireless Network Coding, Performance Region.

Executive Summary

This report is organized in two parts. In the first part (Chapters 2-4) achievable rate regions are derived for the downlink of the spectrum sharing scenario where the multi-antenna base stations (BSs) of different operators transmit over the same channel, each to its own single-antenna mobile station (MS). This scenario is modeled by the multiple-input single-output (MISO) interference channel (IC). In Chapter 2 and 3, we consider the scenario of MSs with single-user decoding (SUD) capabilities with perfect CSI and imperfect CSI at the BSs respectively. In Chapter 4, multi-user decoding (MUD) capabilities at MSs with perfect CSI at BSs are considered. The second part (Chapter 5) focuses on a physical layer (PHY) resource sharing technique, which is based on a hierarchical decode and forward (HDF) strategy. It is a network aware modulation and coding for multi-terminal and multi-relay communications.

Chapter 2 considers the case of SUD, where the MSs treat the interference as additive Gaussian noise. Three different topics regarding Pareto-optimal operation points are discussed in subsequent sections. In Section 2.2, the outer (Pareto) boundary of the MISO IC achievable rate region is characterized. The eigenvector corresponding to the maximum eigenvalue of a weighted sum of Hermitian forms of channel vectors is shown to achieve all points on the boundary. Section 2.3 focuses on the maximum sum-rate operating point, the proportional-fair operating point and the max-min rate point which lead to non-convex optimization problems. A corresponding non-convex optimization framework which takes as much as possible of the problem structure into account has been developed. In contrast to exhaustive search methods, such as a grid search, the proposed approach has the advantage that it can achieve a given accuracy. Section 2.4 proposes an efficient method to find any Pareto-optimal rate pair of the two-user MISO IC achievable rate region. Constrained optimization is used and it is shown that the problem can be formulated as a (sequence of) second-order cone programming (SOCP) feasibility problems. The SOCP problems are convex and they are solved very efficiently using standard off-the-shelf (namely, interior-point) algorithms. The number of SOCP problems that must be solved, for the computation of a Pareto-optimal point, grows only logarithmically with the desired accuracy of the solution. In Section 2.5, the conditions in which non-orthogonal spectrum sharing, e.g. MISO IC, is beneficial as compared to non-sharing baseline scenario e.g. MISO broadcasting channel (BC), are determined. For both the IC and BC, achievable (lower) and upper bounds on the maximum sum-rate are provided. A new fast algorithm is proposed for finding a lower bound on the sum-rate of the BC using linear beamforming. The bounds are used to numerically evaluate the potential gain of non-orthogonal spectrum sharing.

Chapter 3 focuses on the achievable rate region of MISO IC in the scenario with imperfect CSI at the transmitters. In Section 3.1, the robust achievable rate region of MISO is investigated. The transmitters have imperfect CSI with the channel mismatch followed the spherical uncertainty model. Considering the worst case achievable rate of the links, we characterize the beamforming vectors that achieve points on the Pareto boundary of the robust rate region. In addition, we investigate the gain in spectrum sharing under channel information uncertainty compared to time division multiple access (TDMA). The spectral efficiency gain with spectrum sharing is larger in the mid SNR regime. We provide the analytical results of optimal sum rate transmission in asymptotic cases on SNR. Section 3.2 considers the slow-fading two-user MISO IC, where the receivers treat the interference as additive Gaussian noise. We study the rate points that can be achieved, allowing a non-zero outage probability. The points which meet the outage probability specification constitute a so-called outage rate region. There exist several definitions of the outage rate regions for the IC, as for the broadcast and the multiple-access channels. We give four definitions for the outage region of the MISO IC. The definitions differ on whether the rates are declared in outage jointly or individually and whether there is instantaneous or statistical channel state information (CSI) at the transmitters. For the statistical CSI scenario, we discuss how to find the outage probabilities in closed form. We provide interpretations of the definitions and compare the corresponding regions via analytical and numerical results.

Chapter 4 considers the case of MUD, where the MSs have interference decoding capability (IDC) such that the interference, when strong enough, can be decoded and subtracted from the received signal. The achievable rate regions, obtained with this new feature, are explored and the improvement compared with the single-user detection is shown. The achievable rate region of the MISO IC with IDC is not trivial as the additional freedom of interference removal may pose rate constraints on other BSs. The achievable rate region is formulated for the two-user MISO IC with IDC. It is shown that the Pareto-optimal transmit covariance matrices are rank one, i.e. beamforming attains the Pareto boundary. Moreover, the Pareto boundary is characterized, in terms of both power allocation and transmit beamforming vectors.

Chapter 5 (Fundamental Limits for Code, Signal, and Receiver Processing Design) substantially extends the D2.1a deliverable scope by Section 5.4. Section 5.4 deals with the fundamental limits of hierarchical decode and forward (HDF) strategy with *extended* cardinality mapping and the closely related impact of *imperfect* complementary side-information. In simple words, the wireless network coding (WNC) with HDF strategy can use the relay hierarchical symbol mapping with the cardinality higher than the minimal one (i.e. it partially contains information about individual sources) which allows to have imperfect complementary side information at the final destination while still being capable of correctly determining the target data. The relay HDF extends cardinality map therefore allows a trade-off between side information quality and the required throughput over the relay. Such situation captures more realistically the scenarios where sources and destinations are not

collocated. We evaluate quantitatively the limits and the relation between complementary side-information and the relay throughput and we also design a proper extended mapper.

Contents

Notations

Abbreviations

AF	Amplify and Forward
AWGN	Additive White Gaussian Noise
BC	Broadcast Channel
BPSK	Binary Phase Shift Keying
BS	Base Station
C-SI	Complementary Side-Information
CSI	Channel State Information
CSIT	Channel State Information at the transmitter
HBC	Hierarchical Broadcast Channel
HDF	Hierarchical Decode and Forward
HXA	Hierarchical eXclusive Alphabet
HXC	Hierarchical eXclusive Code
IC	Interference Channel
IDC	Interference Decoding Capability
i.i.d.	independent identically distributed
ITC	Interference Temperature Constraint
JDF	Joint Decode and Forward
IFC	Interference Channel
NBS	Nash Bargaining Solution
NC	Network Coding
NCM	Network Coded Modulation
NE	Nash Equilibrium
NP	Non-deterministic Polynomial-time
MAC	Multiple Access Channel
MIMO	Multiple-Input Multiple-Output
MISO	Multiple-Input Single-Output
MRT	Maximum-Ratio Transmission
MS	Mobile Station
MUD	Multi-User Decoding
PDF	Probability Density Function
PHY	Physical Layer
PSK	Phase Shift Keying
QAM	Quadrature Amplitude Modulation
QPSK	Quadrature Phase Shift Keying
SINR	Signal-to-Interference-plus-Noise Ratio

SISO	Single-Input Single-Output
SNR	Signal-to-Noise Ratio
SRN	Source Relay Network
SUD	Single-User Decoding
SOC	Second-Order Cone
SOCP	Second-Order Cone Programming
TC	Topology C
TDMA	Time Division Multiple Access
WNC	Wireless Network Coding
ZF	Zero-Forcing

Mathematical Notations

$\mathbb{C}$	set of complex numbers
$\mathbb{R}$	set of real numbers
$\mathbb{R}_{+}$	set of non-negative real numbers
$\mathbb{R}_{++}$	set of positive real numbers
$x_{k,\ell}$	ℓth component of vector $\boldsymbol{x}_k$
$\|\boldsymbol{a}\|$	Euclidean norm of vector $\boldsymbol{a}$
$\|b\|$	absolute value of $b \in \mathbb{C}$
$v_i(\boldsymbol{Z})$	eigenvector corresponding to the ith eigenvalue of matrix $\boldsymbol{Z}$
$v_{\max}(\boldsymbol{Z})$	eigenvector corresponding to the largest eigenvalue of matrix $\boldsymbol{Z}$
$v_{\min}(\boldsymbol{Z})$	eigenvector corresponding to the smallest eigenvalue of matrix $\boldsymbol{Z}$
$\Pi_{\boldsymbol{Z}}^{\perp}$	orthogonal projector onto the orthogonal complement of the range of $\boldsymbol{Z}$
$\{\cdot\}^H$	the Hermitian (complex conjugate) transpose of a vector or matrix
trace$\{\boldsymbol{X}\}$	the trace of a matrix $\boldsymbol{X}$
rank$\{\boldsymbol{X}\}$	the rank of a matrix $\boldsymbol{X}$
diag$\{\mathbf{x}\}$	a diagonal matrix, whose diagonal elements are the elements in a vector $\mathbf{x}$
E$\{\cdot\}$	the expectation operator

1 Introduction

The objective of SAPHYRE is to come to new approaches to make better use of the spectrum resources that are available for mobile communication services. Beside other options that have been identified and will further be explored, spectrum sharing is of major concern. This deliverable describes final results on basic limits for spectrum sharing which has been modeled by the multi-antenna interference channel.

Interference is known to be one of the major factors that limits the performance of a communication system in a wireless network. This situation is common in multi-user settings when the systems concurrently share the available communication resources. In general interference networks, the performance measure of individual users is described by a utility function. This function depends in a monotonic way on the received signal power, interference signal power and noise power. The joint operation of the systems is efficient if it is not possible to improve the performance of one system without degrading the performance of another. In this case, the operating point is said to be Pareto optimal. It is always desired to design resource allocation schemes that lead to Pareto optimal operation points. In this way, the available communication resources are utilized efficiently to grant efficient operation of the systems. However, developing efficient resource allocation schemes is not straightforward and proves to be difficult.

The deliverable is organized in two parts. In the first part the downlink of a spectrum sharing scenario has been modeled by the MISO IC and corresponding achievable rate regions have been derived under different assumptions on the decoding capabilities of the receivers and different channel state information available at the transmitters. Then, corresponding Pareto-optimal transmission strategies have been identified. In the second part a novel wireless network coding technique has been proposed when both the spectrum and the use of a relay is shared. The performance and fundamental limits of this technique have been studied.

2 Achievable Rate Region of the MISO IC with SUD Capability

2.1 Spectrum-Sharing Paradigm: MISO IC

2.1.1 Related Work

The MISO IC is an example of an interference network where the systems consist of transmitter-receiver pairs. For the two-user case, real-valued parametrization of each transmitter's efficient beamforming vectors is provided in [2]. The beamforming vectors that achieve Pareto optimal points are proven to be a linear combination of zero-forcing (ZF) transmission and maximum ratio transmission (MRT). Based on this characterization, a monotonic optimization framework is developed in [3] to find maximum sum-rate, proportional-fair and minimax operating points. The parametrization in [2] relates to a parametrization using the virtual signal-to-interference-plus-noise-ratio (SINR) framework in [4]. The use of this framework is motivated by the design of distributed algorithms that require local channel state information (CSI) at each transmitter. This framework is extended to the precoding design in MIMO settings in [5]. The concept of combining the MRT and ZF strategies is important for developing so-called distributed bargaining algorithms. These algorithms improve the operation of the systems from the noncooperative outcome [6, 7]. In [6], a distributed bargaining algorithm is developed which requires one bit signaling between the transmitters. Extension to the precoding design in the MIMO case is given in [8]. In [7], a similar distributed beamforming algorithm in the MISO IC is proposed for the case of statistical CSI at the transmitters. Also utilizing the parametrization in [2], a distributed bargaining process is proposed in [9] which requires four bit signaling between the transmitters. The process is proven to converge to an operating point arbitrarily close to the Pareto boundary and dominates the noncooperative outcome of the systems. In [10], the high SINR approximation of the achievable sum-rate of a system pair is utilized to determine suboptimal joint transmission strategies. The achieved performance is shown to be better than the joint MRT and joint ZF strategies.

In the K-user MISO IC, complex-valued parametrization of the Pareto boundary of the MISO IC rate-region is derived in [11] which requires $K(K-1)$ complex-valued parameters in order to attain all Pareto optimal points. In [12], the K-user MISO IC is considered with the capability of time sharing the resources between the links. All points on the Pareto boundary of the MISO IC rate region are achieved with $K(K-1)$ real valued parameters each between 0 and π. In [13], the authors

characterize the Pareto boundary of the MISO IC through controlling interference temperature constraints (ITC) at the receivers. Each Pareto optimal rate tuple is achieved iteratively when each transmitter optimizes its transmission constrained by the ITCs. It is shown that $K(K-1)$ real valued parameters, each between zero and a value depending on the channel vectors, are needed to achieve all Pareto optimal points. ITC is a terminology used in cognitive radio scenarios under the underlay paradigm [14]. It quantifies the amount of interference from the secondary transmitters that is tolerated by the primary users.

In [15], joint linear precoding is investigated taking into account the signaling overhead between the transmitters. The rate-region achieved with joint precoding is larger than the MISO IC rate-region, and all Pareto optimal beamforming vectors are parameterized by $K(K-1)$ complex-valued parameters. For the same setting, a recent result in [16] reduces the number of parameters to $K+L$ real-valued scalars, each between zero and one, where L is the number of linear constraints on the transmission. Linear precoding MIMO IC algorithms are moreover investigated in [17] for a two-user system.

2.1.2 System Model

The MISO IC with K users is studied in [11]. All base stations BS_k have N transmit antennas each, that can be used with full phase coherency. The mobiles MS_k, however, have a single receive antenna each. In Figure 2.1, the MISO IC under study is illustrated for $K = 2$ users and $N = 2$ transmit antennas.

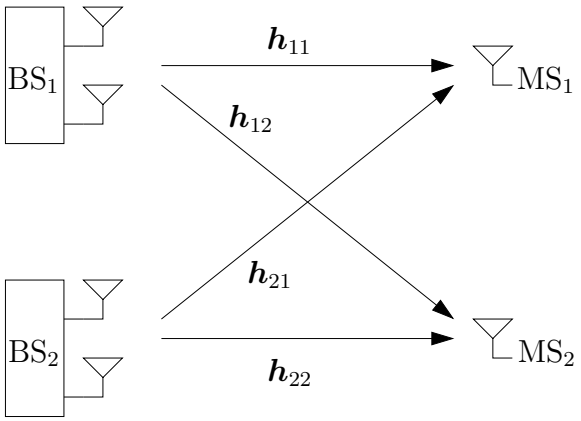

Figure 2.1: The MISO IC for $K = 2$ users and $N = 2$ transmit antennas.

We shall assume that transmission consists of scalar coding followed by beamforming, and that all propagation channels are frequency-flat. This leads to the following basic model for the matched-filtered, symbol-sampled complex baseband data re-

ceived at MS_k:

$$y_k = \boldsymbol{h}_{kk}^T \boldsymbol{w}_k s_k + \sum_{l=1, l\neq k}^{K} \boldsymbol{h}_{lk}^T \boldsymbol{w}_l s_l + e_k, \tag{2.1}$$

where s_l, $1 \leq l \leq K$ is the symbol transmitted by BS_l, $\boldsymbol{h}_{ij}$ is the (complex-valued) $N \times 1$ channel-vector between BS_i and MS_j, and $\boldsymbol{w}_l$ is the beamforming vector used by BS_l. The variables e_k are noise terms which we model as i.i.d. complex Gaussian with zero mean and variance σ^2.

We assume that each base station can use the transmit power P, but that power cannot be traded between the base stations. Without loss of generality, we shall take $P = 1$. This gives the power constraints

$$||\boldsymbol{w}_k||^2 \leq 1, \quad 1 \leq k \leq K \tag{2.2}$$

Throughout, we define the signal-to-noise ratio (SNR) as $1/\sigma^2$. The precoding scheme that we will discuss requires that the transmitters (BS_k) have access to CSI for some of the links. However, at no point we will require phase coherency between the base stations. In [11], a characterization of the beamforming vectors that reach the Pareto boundary of the achievable rate region with interference treated as additive Gaussian noise is provided by a complex linear combination.

Throughout this chapter, we will assume that all receivers treat co-channel interference as noise, i.e. they make no attempt to decode and subtract the interference. We treat the case of multi-user detection in Chapter 4. For a given set of beamforming vectors $\{\boldsymbol{w}_1, \ldots, \boldsymbol{w}_K\}$, the following rate is then achievable for the link $\mathrm{BS}_k \rightarrow \mathrm{MS}_k$, by using codebooks approaching Gaussian ones:

$$R_k(\boldsymbol{w}_1, \ldots, \boldsymbol{w}_K) = \log_2 \left(1 + \frac{|\boldsymbol{w}_k^T \boldsymbol{h}_{kk}|^2}{\sum_{l\neq k} |\boldsymbol{w}_l^T \boldsymbol{h}_{lk}|^2 + \sigma^2} \right). \tag{2.3}$$

We define the *achievable rate region* to be the set of all rates that can be achieved using beamforming vectors that satisfy the power constraint:

$$\mathcal{R} \triangleq \bigcup_{\{\boldsymbol{w}_k : ||\boldsymbol{w}_k||^2 \leq 1, 1 \leq k \leq K\}} \{R_1(\boldsymbol{w}_1, \ldots, \boldsymbol{w}_K), \ldots, R_K(\boldsymbol{w}_1, \ldots, \boldsymbol{w}_K)\} \subset \mathbb{R}_+^K. \tag{2.4}$$

The outer boundary of this region is called the *Pareto boundary*, because it consists of operating points $(R_1, \ldots, R_K)$ for which it is impossible to improve one of the rates, without simultaneously decreasing at least one of the other rates. More precisely we define the *Pareto optimality* of an operating point as follows.

Definition 2.1. A rate tuple $(R_1, \ldots, R_K)$ is said to be Pareto optimal if there exists no other tuple $(Q_1, \ldots, Q_K) \geq (R_1, \ldots, R_K)$ with $(Q_1, \ldots, Q_K) \neq (R_1, \ldots, R_K)$ (the inequality is component-wise). □

2.2 Characterizing the Pareto-Optimal Transmit Strategies

In a multiuser setting, efficient operation of the systems requires the transmitters to maximize the power gain at intended receivers and also minimize the power gain at unintended receivers. In this section, we characterize the transmission strategies of each transmitter that are relevant to achieve Pareto-optimal operating points. Moreover, we parameterize these by real values between zero and one. In this way, the set of efficient transmission strategies is confined and represented by low dimensional real parameters. This result tremendously reduces the complexity of designing efficient resource allocation schemes, and the parametrization can be utilized for low complexity coordination between transmitters.

While previously available results are provided for the MISO IC, the parametrization of efficient transmission strategies in a general multiuser setting is not straightforward. Moreover, neither the ITC-based [13] nor the Lagrangian-based [18, 16] characterizations can be generalized to our framework. A further example of a MISO multiuser setting which can be applied to our framework is when a single transmitter sends common information to K single-antenna receivers. This setting corresponds to multicast transmission. Since the transmission rate depends on the weakest link in the system, the transmitter optimizes its transmission to achieve max-min-fairness at the receivers [19]. The multicast beamforming problem to achieve max-min-fairness is proven to be NP-hard for $K \geq N$ [20], where N is the number of transmit antennas. In [21], the two-user multicast max-min-fair problem is studied, and the set of beamforming vectors which includes the solution of the max-min-fair problem is characterized.

2.2.1 Main Characterization

Following the discussion on the boundary of Ω_k, we formalize the upper boundary following the definitions in [11]. There, this definition was used to derive the solution of a monotonic optimization problem [22].

Definition 2.2. A point $\boldsymbol{y} \in \mathbb{R}^n_+$ is called *upper boundary point* of a normal set $\mathcal{C}$ if $\boldsymbol{y} \in \mathcal{C}$ while the set

$$\mathcal{K}_{\boldsymbol{y}} = \boldsymbol{y} + \mathbb{R}^n_{++} = \{\boldsymbol{y}' \in \mathbb{R}^n_+ | \boldsymbol{y}' > \boldsymbol{y}\} \subset \mathbb{R}^n_+ \setminus \mathcal{C}. \tag{2.5}$$

The set of upper boundary points of $\mathcal{C}$ is called the upper boundary of $\mathcal{C}$ and it is denoted by $\text{part}^+\mathcal{C}$. □

The straightforward extension to include also the right boundary of a convex set $\mathcal{C}$ is to define the upper boundary of $\mathcal{C}$ in direction $\boldsymbol{e}$.

Definition 2.3. A point $\boldsymbol{y} \in \mathbb{R}^n_+$ is called upper boundary point of a normal set $\mathcal{C}$

in direction $\boldsymbol{e}$ if $\boldsymbol{y} \in \mathcal{C}$ while the set

$$\mathcal{K}_{\boldsymbol{y}}(\boldsymbol{e}) = \{\boldsymbol{y}' \in \mathbb{R}_+^n | y'_\ell e_\ell \geq y_\ell e_\ell \; \forall \; 1 \leq \ell \leq n\} \subset \mathbb{R}_+^n \setminus \mathcal{C} \tag{2.6}$$

where the inequality has at least one strict inequality and directional vector $\boldsymbol{e} \in \{-1, 1\}^n$. We denote the set of upper boundary points in direction $\boldsymbol{e}$ as $\text{part}^{\boldsymbol{e}}\mathcal{C}$. □

For the choice $\boldsymbol{e} = \mathbf{1}$ the upper boundary in direction $\boldsymbol{e}$ is the usual upper boundary, i.e., $\text{part}^{+}\mathcal{C} = \text{part}^{\mathbf{1}}\mathcal{C}$.

In the following, we omit the index k when considering only one user for convenience. For efficient operation the boundary points of Ω in all directions (except $\boldsymbol{e} = -\mathbf{1}$) are of interest. Let $\mathcal{E} \triangleq \{-1, 1\}^n \setminus \{-1\}^n$. Then the next result follows immediately from the convexity of the boundary of the gain-region.

Theorem 2.1. *All upper boundary points of the convex set Ω in direction $\boldsymbol{e} \in \mathcal{E}$ can be achieved by*

$$\boldsymbol{w}(\boldsymbol{\lambda}) = \boldsymbol{v}_{max}\left(\sum_{\ell=1}^{K} \lambda_\ell e_\ell \boldsymbol{h}_{k,\ell}\boldsymbol{h}_{k,\ell}^H\right) \tag{2.7}$$

with $\boldsymbol{v}_{\max}(\boldsymbol{Z})$ denoting the eigenvector which belongs to the maximum eigenvalue of the Hermitian matrix $\boldsymbol{Z}$, $\boldsymbol{\lambda} = [\lambda_1, \ldots, \lambda_{K-1}, \; \lambda_1, \ldots, \lambda_{K-1}$ with $0 \leq \lambda_\ell \leq 1$, $1 \leq \ell \leq K-1$ and $\lambda_K = 1 - \sum_{\ell=1}^{K-1} \lambda_\ell$. □

The interesting observation from Theorem 2.1 is that all upper boundary points of the K-dimensional gain-region can be achieved by a parameterization using $K-1$ real parameters between zero and one, i.e.,

$$\boldsymbol{\lambda} \in \boldsymbol{\Lambda} = \{\boldsymbol{\lambda} \in [0, 1]^K : \sum_{\ell=1}^{K} \lambda_\ell = 1\}. \tag{2.8}$$

Depending on the application context different directions or even certain operating points are to be optimized.

Theorem 2.2. *All points of the Pareto boundary of the achievable rate region of the MISO IC can be reached by beamforming vectors*

$$\boldsymbol{w}_k(\boldsymbol{\lambda}_k) = \boldsymbol{v}_{max}\left(\sum_{\ell=1}^{K} \lambda_{k,\ell} e_\ell \boldsymbol{h}_{k,\ell}\boldsymbol{h}_{k,\ell}^H\right) \tag{2.9}$$

with $\boldsymbol{\lambda}_k \in \boldsymbol{\Lambda}$ and

$$e_\ell = \begin{cases} 1 & \ell = k \\ -1 & \textit{otherwise} \end{cases}.$$

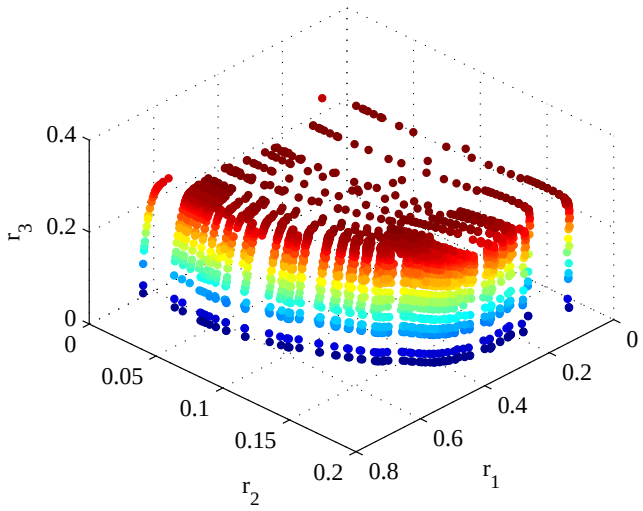

Figure 2.2: Pareto boundary of a three user MISO IC rate-region, where $N = 3$ and SNR = -10 dB.

□

Note that for two users $K = 2$, the characterization in [11, Corollary 1] follows as a special case.

The proof of Theorem 2.2 follows from the observation that the Pareto boundary of the achievable rate region $\mathcal{R}$ in (2.4) corresponds for user k with the upper boundary of Ω_k in direction of $\boldsymbol{e}_k = [-1, \ldots, -1, 1, -1, \ldots, -1]$ with a 1 at the k-th position. The complete proof is provided in [23].

2.2.2 Illustrations

The Pareto boundary of a three user MISO IC rate-region is plotted in Figure 2.2 for SNR $= -10$ dB and in Figure 2.3 for SNR $= 30$ dB. The generated points correspond to the beamforming vectors characterized in Theorem 2.2. The real-valued parameters are varied in a 0.05 step-length. Since we are only interested in revealing the Pareto boundary of the achievable rate-region, we do the following. We randomly choose 10^4 generated rate tuples and remove all points that are dominated by these. In other words, for a randomly chosen rate tuple, all points corresponding to joint rates less than the chosen ones are removed. In addition, we apply the algorithm provided in [24]. This algorithm reduces the number of plotted points in removing points that are not visible from the viewed angle of the figure. This algorithm further reduces the complexity of rendering the generated points.

The two-user MISO IC special case has an appealing form in terms of the parametrization of the Pareto boundary of the achievable rate-region. The efficient beamforming vectors are a linear combination of the MRT and ZF strategies [11, Corollary 2].

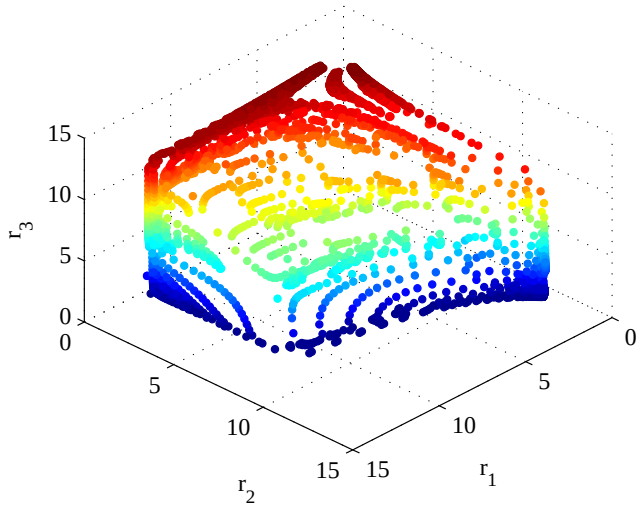

Figure 2.3: Pareto boundary of a three user MISO IC rate-region, where $N = 3$ and SNR $= 30$ dB.

These two strategies have the interpretation of a transmitter being either selfish or altruistic [2, 25]. The efficient beamforming vectors of transmitter $k \in \{1, 2\}$ are given as [11, Corollary 2]

$$\boldsymbol{w}_k(\hat{\lambda}_k) = \frac{\hat{\lambda}_k \boldsymbol{w}_k^{\mathrm{MRT}} + (1-\hat{\lambda}_k)\boldsymbol{w}_k^{\mathrm{ZF}}}{\left\| \hat{\lambda}_k \boldsymbol{w}_k^{\mathrm{MRT}} + (1-\hat{\lambda}_k)\boldsymbol{w}_k^{\mathrm{ZF}} \right\|}, \tag{2.10}$$

where $\hat{\lambda}_k \in [0, 1]$, $\boldsymbol{w}_k^{\mathrm{MRT}} = \frac{\boldsymbol{h}_{kk}}{\|\boldsymbol{h}_{kk}\|}$, and $\boldsymbol{w}_k^{\mathrm{ZF}} = \frac{\boldsymbol{\Pi}_{\boldsymbol{h}_{k\ell}}^{\perp} \boldsymbol{h}_{kk}}{\left\|\boldsymbol{\Pi}_{\boldsymbol{h}_{k\ell}}^{\perp} \boldsymbol{h}_{kk}\right\|}, k \neq \ell$. Next, we prove that the parametrization in (2.10) has the same set of strategies as in Theorem 2.2 for $K = 2$. For this case, the eigenvalue equation for the hermitian matrix in Theorem 2.1 is written as $\left(\lambda_1 \boldsymbol{h}_{11}\boldsymbol{h}_{11}^H - (1-\lambda_1)\boldsymbol{h}_{12}\boldsymbol{h}_{12}^H\right)\boldsymbol{w}_1 = \mu \boldsymbol{w}_1$. This equation can be equivalently formulated to

$$\lambda_1 \|\boldsymbol{h}_{11}\|^2 \frac{\boldsymbol{h}_{11}\boldsymbol{h}_{11}^H}{\|\boldsymbol{h}_{11}\|^2}\boldsymbol{w}_1 - (1-\lambda_1)\|\boldsymbol{h}_{12}\|^2 \frac{\boldsymbol{h}_{12}\boldsymbol{h}_{12}^H}{\|\boldsymbol{h}_{12}\|^2}\boldsymbol{w}_1 = \mu \boldsymbol{w}_1. \tag{2.11}$$

Adding $(1-\lambda_1)\|\boldsymbol{h}_{12}\|^2 \boldsymbol{w}_1$ to both sides of (2.11) gives

$$\left(\lambda_1 \|\boldsymbol{h}_{11}\|^2 \Pi_{\boldsymbol{h}_{11}} + (1-\lambda_1)\|\boldsymbol{h}_{12}\|^2 \Pi_{\boldsymbol{h}_{12}}^{\perp}\right)\boldsymbol{w}_1 = (\mu + (1-\lambda_1)\|\boldsymbol{h}_{12}\|^2)\boldsymbol{w}_1. \tag{2.12}$$

The left hand side of (2.12) states that the principal eigenvector is a linear combination of its orthogonal projection on $\boldsymbol{h}_{11}$ and the orthogonal projection onto the orthogonal complement of $\boldsymbol{h}_{12}$. Since the largest eigenvalue μ is larger or equal to zero, the weight in the right hand side of (2.12) is always positive. Hence, the optimal set of beamforming vectors can be equivalently characterized by (2.10).

2.3 Computing Important Points via Monotonic Optimization

An explicit parameterization of the Pareto boundary for the K-user Gaussian MISO IC, for the case when all multiuser interference is treated as additive Gaussian noise at the receivers, was presented in the previous section. Also, it was shown that for the special case of two users, any point in the rate region can be achieved by choosing beamforming vectors that are linear combinations of the ZF and the MRT beamformers. Hence, all important (i.e., Pareto-efficient) operating points can be expressed by two real-valued parameters between zero and one $0 \leq \boldsymbol{\lambda} = [\lambda_1, \lambda_2] \leq 1$.

In this section, we build on this parameterization and focus on the maximum sum-rate operating point, the proportional-fair operating point and the max-min rate point. The corresponding optimization problems are non-convex problems which are difficult to solve directly. In particular, the max-min problem is non-smooth and therefore derivative-based (gradient) optimization approaches cannot be applied. A suboptimal iterative algorithm based on alternating projection was proposed in [11]. In general, this algorithm converges to a local optimum. Therefore, we are interested in formulating a unified non-convex optimization framework which takes as much as possible of the problem structure into account, and which is able to find the global optimum of the problems.

The main contribution of this work is the development of a *systematic approach* to solve the non-convex optimization problem. In contrast to exhaustive search methods, such as a grid search, the proposed approach has the advantage that it can achieve a given accuracy. The details of the following derivations including proofs and further discussions can be found in [3].

2.3.1 Preliminaries

The following beamformers are well known in literature and their operational meaning in a game-theoretic framework is studied in [26]. The MRT beamforming vectors are given by

$$\boldsymbol{w}_1^{\mathrm{NE}} = \frac{\boldsymbol{h}_{11}^*}{\|\boldsymbol{h}_{11}\|} \qquad \text{and} \qquad \boldsymbol{w}_2^{\mathrm{NE}} = \frac{\boldsymbol{h}_{22}^*}{\|\boldsymbol{h}_{22}\|}. \tag{2.13}$$

The ZF beamformers are given by

$$\boldsymbol{w}_1^{\mathrm{ZF}} = \frac{\Pi_{\boldsymbol{h}_{12}^*}^{\perp} \boldsymbol{h}_{11}^*}{\left\| \Pi_{\boldsymbol{h}_{12}^*}^{\perp} \boldsymbol{h}_{11}^* \right\|} \qquad \text{and} \qquad \boldsymbol{w}_2^{\mathrm{ZF}} = \frac{\Pi_{\boldsymbol{h}_{21}^*}^{\perp} \boldsymbol{h}_{22}^*}{\left\| \Pi_{\boldsymbol{h}_{21}^*}^{\perp} \boldsymbol{h}_{22}^* \right\|} \tag{2.14}$$

for BS_1 and BS_2, respectively, where $\Pi_{\boldsymbol{X}}^{\perp} = \mathbf{I} - \boldsymbol{X}(\boldsymbol{X}^H \boldsymbol{X})^{-1} \boldsymbol{X}^H$ denotes orthogonal projection onto the orthogonal complement of the column space of $\boldsymbol{X}$.

The following Theorem is proved in [11].

Theorem 2.3. *Any point on the Pareto boundary of the rate region is achievable with the beamforming strategies*

$$\boldsymbol{w}_k(\lambda_k) = \frac{\lambda_k \boldsymbol{w}_k^{NE} + (1-\lambda_k)\boldsymbol{w}_k^{ZF}}{\|\lambda_k \boldsymbol{w}_k^{NE} + (1-\lambda_k)\boldsymbol{w}_k^{ZF}\|} \tag{2.15}$$

for some $0 \leq \lambda_k \leq 1$, $k \in \{1,2\}$.

The achievable rates as functions of the parameter vector $\boldsymbol{\lambda} = (\lambda_1, \lambda_2)$ read

$$\begin{aligned} R_1(\boldsymbol{\lambda}) &= \log\left(1 + \frac{|\boldsymbol{w}_1^T(\lambda_1)\boldsymbol{h}_{11}|^2}{\sigma^2 + |\boldsymbol{w}_2^T(\lambda_2)\boldsymbol{h}_{21}|^2}\right) \\ R_2(\boldsymbol{\lambda}) &= \log\left(1 + \frac{|\boldsymbol{w}_2^T(\lambda_2)\boldsymbol{h}_{22}|^2}{\sigma^2 + |\boldsymbol{w}_1^T(\lambda_1)\boldsymbol{h}_{12}|^2}\right). \end{aligned} \tag{2.16}$$

2.3.2 Problem Statement

We are interested in efficient algorithms for finding the following operating points:

1. The weighted sum-rate point:

$$\max_{0\leq\boldsymbol{\lambda}\leq 1} \{\omega R_1(\boldsymbol{\lambda}) + (1-\omega)R_2(\boldsymbol{\lambda})\} \tag{2.17}$$

   where $\omega \in [0,1]$ is a weighting factor.

2. The proportional-fairness operating point:

$$\max_{0\leq\boldsymbol{\lambda}\leq 1} \{R_1(\boldsymbol{\lambda})R_2(\boldsymbol{\lambda})\}. \tag{2.18}$$

3. The max-min optimal point (egalitarian solution):

$$\max_{0\leq\boldsymbol{\lambda}\leq 1} \min\{R_1(\boldsymbol{\lambda}), R_2(\boldsymbol{\lambda})\}. \tag{2.19}$$

All three optimization problems (2.17), (2.18), and (2.19) are non-linear and non-convex. In the following derivation, we propose a new approach that finds the global solution to these problems within a given accuracy and in a finite number of steps.

2.3.3 Monotonic Optimization

The monotonic optimization framework described in [3] is now applied to the problem statements. First, the properties of our objective functions are analyzed and next the programming problems are reformulated in standard form.

First, we show that the atom functions of the individual user rates in (2.16) are strictly increasing. Thus, the user rates can be expressed as the difference of two strictly increasing functions. For future use, we define the functions

$$f_1(\boldsymbol{\lambda}) \triangleq \log\left(\sigma^2 + |\boldsymbol{w}_1^T(\lambda_1)\boldsymbol{h}_{11}|^2 + |\boldsymbol{w}_2^T(\lambda_2)\boldsymbol{h}_{21}|^2\right), \tag{2.20}$$

$$f_2(\boldsymbol{\lambda}) \triangleq \log\left(\sigma^2 + |\boldsymbol{w}_2^T(\lambda_2)\boldsymbol{h}_{22}|^2 + |\boldsymbol{w}_1^T(\lambda_1)\boldsymbol{h}_{12}|^2\right), \tag{2.21}$$

$$g_1(\boldsymbol{\lambda}) \triangleq \log\left(\sigma^2 + |\boldsymbol{w}_1^T(\lambda_1)\boldsymbol{h}_{12}|^2\right), \tag{2.22}$$

$$g_2(\boldsymbol{\lambda}) \triangleq \log\left(\sigma^2 + |\boldsymbol{w}_2^T(\lambda_2)\boldsymbol{h}_{21}|^2\right), \tag{2.23}$$

and further $f \triangleq f_1 + f_2$ and $g \triangleq g_1 + g_2$.

Lemma 2.1. *The functions f, f_1, f_2 as well as g, g_1, g_2 are strictly increasing, i.e., monotonically increasing in λ_1 and λ_2.*

It is shown in [22] that the class of difference of two monotonically increasing functions (d.m. functions) is rich, i.e., it does not only contain the sum or product of R_1 and R_2 but also other combinations including minimization and maximization. The d.m. property is invariant under certain transformations, as detailed in the following proposition.

Proposition 2.1 (Prop. 19 in [22])**.** *If $\mu_1(\boldsymbol{x}), \ldots, \mu_m(\boldsymbol{x})$ are d.m. then*

1. *for any $\alpha_i \in \mathbb{R}$ the function $\sum_{i=1}^m \alpha_i \mu_i(\boldsymbol{x})$ is also d.m.;*
2. *the functions $\max\{\mu_1(\boldsymbol{x}), \ldots, \mu_m(\boldsymbol{x})\}$ and $\min\{\mu_1(\boldsymbol{x}), \ldots, \mu_m(\boldsymbol{x})\}$ is also d.m.*

Based on this result, the next three corollaries show that the weighted sum-rate maximization problem in (2.17) as well as the proportional fair rate maximization problem in (2.18) and the max-min problem in (2.19) are d.m. programming problems.

Corollary 2.1. *The maximum weighted sum-rate problem for weight $0 \leq \omega \leq 1$*

$$\max_{0 \leq \boldsymbol{\lambda} \leq 1} \omega R_1(\boldsymbol{\lambda}) + (1-\omega) R_2(\boldsymbol{\lambda})$$

is a d.m. programming problem.

Corollary 2.2. *The proportional-fair rate maximization problem*

$$\max_{0 \leq \boldsymbol{\lambda} \leq 1} R_1(\boldsymbol{\lambda}) R_2(\boldsymbol{\lambda})$$

is a d.m. programming problem.

From Corollary 2.1 and Corollary 2.2 it can be observed that any linear combination and polynomial in f_1, f_2, g_1, and g_2 can be expressed by expanding and collecting positive and negative parts as a d.m. function.

The following decomposition shows how to deal with the max-min problem in (2.19). The minimum of R_1 and R_2 can be written as

$$\begin{aligned}\min\{R_1, R_2\} &= \min\{f_1 - g_2, f_2 - g_1\} \\ &= \min\{f_1 + g_1 - g_1 - g_2, f_2 + g_2 - g_2 - g_1\} \\ &= \underbrace{\min\{f_1 + g_1, f_2 + g_2\}}_{mon.incr.} - \underbrace{(g_1 + g_2)}_{mon.incr.}.\end{aligned} \tag{2.24}$$

The minimum of the d.m. functions is itself a d.m. function by Proposition 2.1.

Corollary 2.3. *The max-min problem in (2.19)*

$$\max_{0\leq\boldsymbol{\lambda}\leq 1} \min\big(R_1(\boldsymbol{\lambda}), R_2(\boldsymbol{\lambda})\big)$$

is a d.m. programming problem.

Observe that the negative d.m. part of the max-min function in (2.24) is equal to the negative d.m. part of the sum rate function. The difference is only in the positive d.m. function part.

We have seen above that the three problems of interest can be formulated as the following general d.m. problem

$$\max_{\boldsymbol{\lambda}\in[0,1]^2} \phi(\boldsymbol{\lambda}) - \psi(\boldsymbol{\lambda}) \tag{2.25}$$

with strictly increasing functions ϕ and ψ. The way forward that we propose here is to transform the problem in (2.25) to a domain where the parameter space has larger dimension but where the constraints are normal. After this transformation has been performed, the polyblock algorithm can be used to solve the optimization problems.

Specifically, we substitute $\psi(\boldsymbol{\lambda}) = \psi(\mathbf{1})(1-t)$ in (2.25) where the range of t depends on $\boldsymbol{\lambda}$ and obtain the equivalent programming problem with $\boldsymbol{x} = [\lambda_1, \lambda_2, t]$

$$\max \underbrace{\phi(\boldsymbol{x}) + \psi(\mathbf{1})(x_3 - 1)}_{\Phi(\boldsymbol{x})} \qquad \text{s.t.} \quad \boldsymbol{x} \in \mathbb{D} \tag{2.26}$$

with constraint set

$$\mathbb{D} = \big\{\boldsymbol{x} \in \mathbb{R}^3_+ : x_1 \leq 1, x_2 \leq 1, x_3 \leq 1 - \psi(x_1, x_2)/\psi(\mathbf{1})\big\}. \tag{2.27}$$

Note that the function $\Phi(\boldsymbol{x})$ is strictly increasing and it holds that $\psi(\mathbf{1}) \geq 0$.

Lemma 2.2. *The set $\mathbb{D}$ defined in (2.27) is normal.*

Furthermore, the constraint set is compact, bounded, and connected. The programming problem in (2.25) corresponds exactly to the monotonic optimization problem.

Therefore, we can apply the outer polyblock approximation algorithm described in [3] to solve all three problems, the weighted sum-rate maximization in (2.17), the proportional fair problem in (2.18), and the max-min problem in (2.19).

2.3.4 Illustrations

First, the solution by the polyblock algorithm of the weighted sum-rate maximization problem (2.17) is illustrated in the next subsection.

For this example, the channel realization ($n_T = 3$) is given by

$$\begin{aligned}
\boldsymbol{h}_{11} &= [0.0937 + 1.1175i; 1.1264 + 0.0556i; 0.7201 + 0.4820i], \\
\boldsymbol{h}_{12} &= [-0.7245 + 0.3036i; -0.8728 - 0.0395i; 0.2042 + 0.2601i], \\
\boldsymbol{h}_{21} &= [-0.3288 - 1.4935i; 0.2623 + 0.9598i; 0.5150 + 0.7231i], \\
\boldsymbol{h}_{22} &= [0.7339 - 0.2231i; -0.2756 - 1.0983i; -0.9767 - 0.5006i].
\end{aligned}$$

We operate at an SNR of 0 dB. In Figure 2.4, the objective function of the problem (2.17) is illustrated.

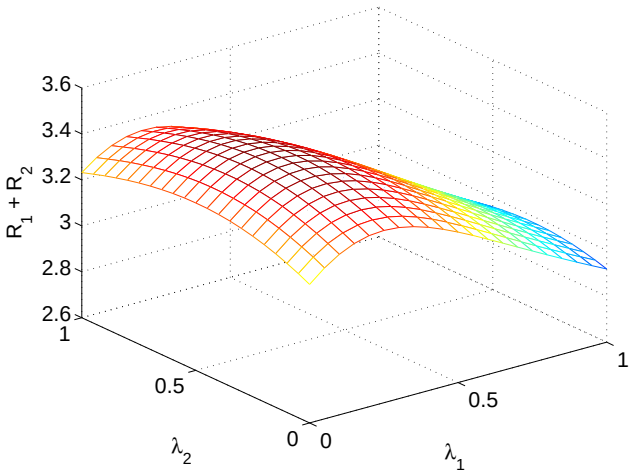

Figure 2.4: Sum-rate $R_1 + R_2$ over $0 \leq \boldsymbol{\lambda} \leq 1$.

The solution found by the polyblock algorithm achieves the individual rates $R_1(\boldsymbol{\lambda}^*) = 1.891$ and $R_2(\boldsymbol{\lambda}) = 1.5713$ and thus a sum-rate of 3.4623. A 20×20 grid search (which corresponds to 400 function evaluations) gives the optimum as $(R_1 + R_2) = 3.4619 < (R_1(\boldsymbol{\lambda}) + R_2(\boldsymbol{\lambda}))$. This shows the advantage of the polyblock algorithm compared to a grid search for one sample channel realization.

Additionally, we computed the average performances of the outer polyblock algorithm and of the grid-search method for 1000 channel randomly chosen realizations, in order to show that the proposed algorithm performs well on the average, too.

Here, the average sum-rate achieved with the outer polyblock algorithm (using at most 100 steps) is 4.374. A 10×10 grid search (100 function evaluations) gives an average sum-rate of 4.364.

2.3.5 SAPHYRE Gain of Operating Points

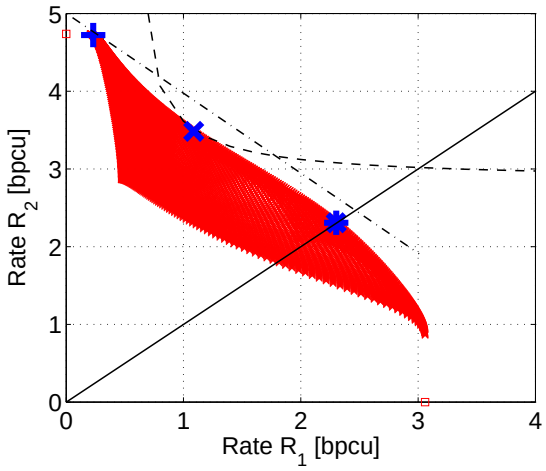

Figure 2.5: Example of the instantaneous achievable rate region for the 2-user MISO IC at SNR 10dB: Egalitarian solution (*), NBS (x), and sum rate maximization solution (+). The red carpet are the points for $0 \leq \lambda_1, \lambda_2 \leq 1$ plotted on a grid with density 0.01. The small red squares on the axes indicate the single-user points (dictatorial solution).

In Figure 2.5, the result of the optimization procedure for the three operating points is shown. The egalitarian solution (*) converges to equal rates $R_1 = R_2 = 2.3$ and the solution is the intersection point between the Pareto boundary and the bisector line. The max sum-rate solution is the tangent point of a line with slope -1 with the Pareto boundary and converges to rates $R_1 = 0.23$ and $R_2 = 4.72$. The NBS converges to the rate tuple $R_1 = 1.08$ and $R_2 = 3.48$ and it is the intersection of the Pareto boundary with the Nash curve $0.4 = (R_1 - R_1^{\mathrm{NE}})(R_2 - R_2^{\mathrm{NE}})$. Finally, the point at the left lower corner of the red carpet corresponds to the NE (threat point). The NE rates are $R_1^{\mathrm{NE}} = 0.47$ and $R_2^{\mathrm{NE}} = 2.86$.

In Figure 2.6, the Pareto boundary is shown for an SNR of 30 dB. The red points are generated from Theorem 2.1 by varying λ_1 and λ_2 over a grid $0 \leq \lambda_1 \leq 1$ and $0 \leq \lambda_2 \leq 1$. The pink circle is the ZF-point. It can be observed that the ZF point is close to the Pareto boundary and to the maximum sum-rate point.

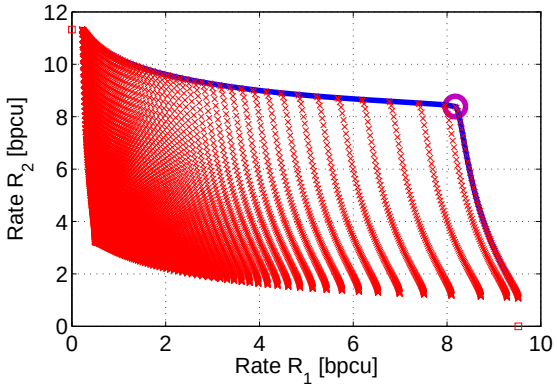

Figure 2.6: Pareto boundary for a sample channel realization with two transmit antennas at 30 dB SNR.

2.4 Computing the Pareto Boundary via Convex Optimization

The main merit of the parameterization derived in [11] is that it provides an analytical tool that has helped to develop an intuitive understanding for what Pareto-optimal beamforming vectors look like. In particular, [25] presented game-theoretic interpretations in terms of "altruistic" and "selfish" strategies. Unfortunately, the parameterization derived in [11] is not particularly efficient when it comes to computing Pareto-optimal beamforming vectors in practice. The main reason for this is that it provides only *necessary* conditions that the beamforming vectors should *separately* fulfil to achieve Pareto-optimality. Hence, using the parameterization as it stands to generate *pairs* of beamforming vectors yields many rate points that are far from optimum, in addition to the desired Pareto-optimal points. We have also earlier presented extensions of the parameterization in [11] to the case where the transmitters only have statistical CSI [27, 7]. Whilst important for analytical studies, these parameterizations are further inefficient for the computation of the Pareto boundary, due to the even larger number of involved parameters.

It becomes apparent, that there is a need to find a way to directly compute pairs of Pareto-optimal beamforming vectors. This need motivated us to propose in [28] an optimization problem, that for each point on the Pareto boundary accepts as input the rate of one link and returns the rate of the other, along with the enabling beamforming vectors. Therein, we considered the scenario where the transmitters have statistical CSI, for which the corresponding (average) rate expressions are involved functions of the beamforming vectors. Because of this, it was hard to solve the proposed optimization problem directly. To overcome this difficulty, we proposed a two-step algorithm to derive a solution. In the first step, the optimization problem was solved separately for each beamforming vector and in the second step the solutions were combined.

In this section, we show that the optimization problem, proposed in [28] to find pairs of Pareto-optimal beamforming vectors, can be solved jointly when the transmitters have perfect CSI. This is now possible because the corresponding (instantaneous) rates are simple functions of the beamforming vectors. Specifically, we exploit the fact that the rates are monotonously increasing with the SINR's and recast the original rate optimization problem as a sequence of SINR feasibility problems. These feasibility problems have nonconvex quadratic constraints, but nevertheless admit an equivalent reformulation as SOCP problems [29]. The SOCP problems are convex [30] and they are solved very efficiently using standard off-the-shelf (namely, interior-point) algorithms [31]. The number of SOCP problems that needs to be solved grows only logarithmically with the desired accuracy of the solution. Taken together, we obtain a computationally very efficient method of calculating the Pareto boundary of the rate region for the MISO IC, that it is achieved when the transmitters have perfect CSI.

2.4.1 Preliminaries

For the two-user MISO, when BS_1 has perfect CSI and MS_1 treats the interference as noise, the achievable instantaneous rate (in bits/channel use) for the link $\mathrm{BS}_1 \to \mathrm{MS}_1$ is [32]

$$R_1(\boldsymbol{w}_1, \boldsymbol{w}_2) = \log_2 \left(1 + \frac{|\boldsymbol{h}_{11}^H \boldsymbol{w}_1|^2}{|\boldsymbol{h}_{21}^H \boldsymbol{w}_2|^2 + \sigma^2} \right). \tag{2.28}$$

It is evident that the instantaneous rate is monotonously increasing with the SINR, which is defined by the ratio within the right-hand-side term of (2.28). Furthermore, the rate depends on the choice of both beamforming vectors. We denote as $p_{11}(\boldsymbol{w}_1)$ the useful signal power received in the direct link $\mathrm{BS}_1 \to \mathrm{MS}_1$ and as $p_{21}(\boldsymbol{w}_2)$ the interference power received in the crosstalk link $\mathrm{BS}_2 \to \mathrm{MS}_1$, i.e.,

$$p_{11}(\boldsymbol{w}_1) \triangleq |\boldsymbol{h}_{11}^H \boldsymbol{w}_1|^2 \quad \text{and} \quad p_{21}(\boldsymbol{w}_2) \triangleq |\boldsymbol{h}_{21}^H \boldsymbol{w}_2|^2. \tag{2.29}$$

It can be easily seen and understood that $R_1(\boldsymbol{w}_1, \boldsymbol{w}_2)$ is monotonously increasing with $p_{11}(\boldsymbol{w}_1)$ for fixed $p_{21}(\boldsymbol{w}_2)$ and monotonously decreasing with $p_{21}(\boldsymbol{w}_2)$ for fixed $p_{11}(\boldsymbol{w}_1)$. A conflict situation is associated with the choice of beamvectors. A beamvector $\boldsymbol{w}_1$ which increases the useful signal power $p_{11}(\boldsymbol{w}_1)$ received by MS_1, might also increase the interference power $p_{12}(\boldsymbol{w}_1)$ experienced at MS_2.

The union of all Pareto-optimal points defines the so-called Pareto boundary of the rate region $\mathcal{R}$. We denote as $\underline{R}_1$ and $\overline{R}_1$ the minimum and maximum, respectively, Pareto-optimal rates of link $\mathrm{BS}_1 \to \mathrm{MS}_1$. The Pareto boundary consists of all Pareto-optimal points on the outer (upper-right) boundary of $\mathcal{R}$, between $(\underline{R}_1, \overline{R}_2)$ and $(\overline{R}_1, \underline{R}_2)$; see Fig. 2.7.

As evidenced by (2.28), the maximum rate $\overline{R}_1$ is achieved when BS_1 operates "selfishly" to maximize the useful signal power $p_{11}(\boldsymbol{w}_1)$ and BS_2 operates "altruistically" to null the interference power $p_{21}(\boldsymbol{w}_2)$. The selfish operation of BS_1 corresponds to the MRT strategy [25]

$$\boldsymbol{w}_1^{\mathrm{MRT}} = \arg \max_{w_1 \in \mathcal{W}} \; p_{11}(\boldsymbol{w}_1) = \frac{\boldsymbol{h}_{11}}{\|\boldsymbol{h}_{11}\|}. \tag{2.30}$$

Note that the computation of the MRT beamforming vector in (2.30) requires knowledge only of the direct channel vector $\boldsymbol{h}_{11}$. That is, the MRT strategy does not take into account the interference that it causes to the other communication link. Contrarily, the altruistic operation maximizes the useful signal power under the hard constraint of causing no interference. The so-called ZF strategy of BS_1 is [25]

$$\boldsymbol{w}_1^{\mathrm{ZF}} = \arg \max_{\substack{w_1 \in \mathcal{W} \\ p_{12}(\boldsymbol{w}_1)=0}} \; p_{11}(\boldsymbol{w}_1) = \frac{\boldsymbol{\Pi}_{\boldsymbol{h}_{12}}^{\perp} \boldsymbol{h}_{12}}{\left\| \boldsymbol{\Pi}_{\boldsymbol{h}_{12}}^{\perp} \boldsymbol{h}_{11} \right\|}, \tag{2.31}$$

where $\boldsymbol{\Pi}_{\boldsymbol{h}_{12}}^{\perp} \triangleq \mathbf{I} - \boldsymbol{h}_{12}(\boldsymbol{h}_{12}^H \boldsymbol{h}_{12})^{-1} \boldsymbol{h}_{12}^H$ is the orthogonal projection onto the orthogonal complement of $\boldsymbol{h}_{12}$ and $\mathbf{I}$ is the identity matrix. In [11], we showed that all the Pareto-optimal transmit strategies can be represented as linear combinations of the MRT and the ZF ones.

The maximum and minimum Pareto-optimal rates on link $\mathrm{BS}_1 \rightarrow \mathrm{MS}_1$ are explicitly written as functions of the MRT and ZF strategies of BS_1 and BS_2 as follows

$$\overline{R}_1 \triangleq R_1(\boldsymbol{w}_1^{\mathrm{MRT}}, \boldsymbol{w}_2^{\mathrm{ZF}}) \quad \text{and} \quad \underline{R}_1 \triangleq R_1(\boldsymbol{w}_1^{\mathrm{ZF}}, \boldsymbol{w}_2^{\mathrm{MRT}}). \tag{2.32}$$

2.4.2 Computation of the Pareto boundary

As discussed previously, we accurately know the endpoints of the Pareto boundary and the transmit strategies that enable them. In this section, we propose an efficient method to calculate the Pareto-optimal pair of beamforming vectors $(\boldsymbol{w}_1^\star, \boldsymbol{w}_2^\star)$ that corresponds to an arbitrary operating point $(R_1^\star, R_2^\star)$ on the Pareto boundary of the achievable rate region. We do so by building on the observation that the Pareto-optimal rates of the two links are related by an one-to-one function. That is, every Pareto-optimal point is uniquely defined when the rate of one communication link is known. The other rate is then the maximum one that can be simultaneously achieved (see Fig. 2.7). This property motivated us to propose the following optimization problem, which accepts as input the coordinate $R_1^\star$ of the sought Pareto-optimal rate pair.

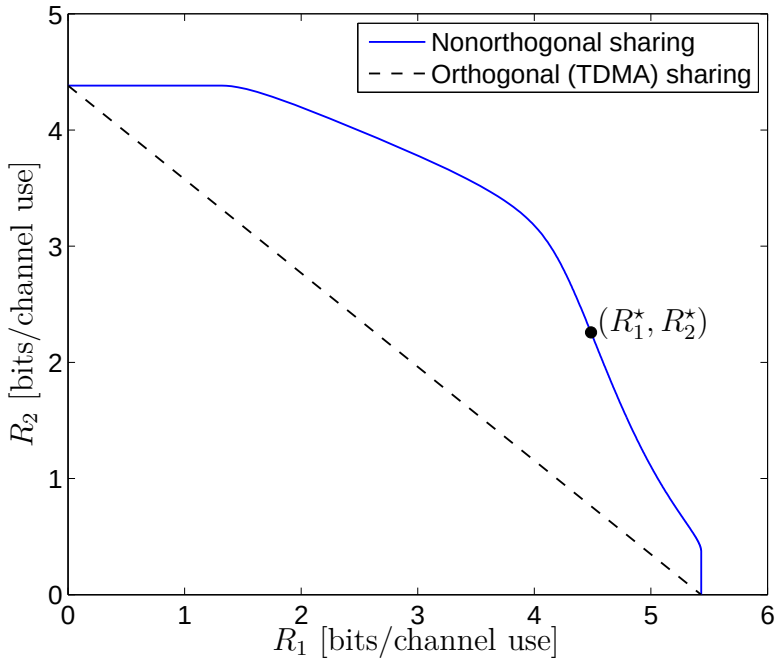

Figure 2.7: Achievable rate region for the two-user MISO IC with perfect CSI

$$\max_{(\boldsymbol{w}_1,\boldsymbol{w}_2)\in\mathcal{W}^2} \quad R_2(\boldsymbol{w}_2,\boldsymbol{w}_1) \tag{2.33}$$

$$\text{s.t.} \qquad R_1(\boldsymbol{w}_1,\boldsymbol{w}_2) = R_1^\star. \tag{2.34}$$

The optimal value of the problem (2.33)–(2.34) is the other coordinate $R_2^\star$. The optimal solution of (2.33)–(2.34) is the pair $(\boldsymbol{w}_1^\star, \boldsymbol{w}_2^\star)$ of transmit strategies that have to be employed in order to achieve $(R_1^\star, R_2^\star)$. It is apparent that the optimization is always feasible and that the entire Pareto boundary can be calculated when $R_1^\star$ is chosen in the range $[\underline{R}_1, \overline{R}_1]$.

In [28], we considered the case where the transmitters only have statistical CSI, for which the achievable rates are computed by averaging over the channel realizations. The resulting rate expressions are involved functions of the beamforming vectors, comprising exponential integrals with quadratic terms in their limits. For this reason, it was difficult in [28] to solve the problem (2.33)–(2.34) directly and we had to break the optimization in two parts, each involving a different beamforming vector. Herein, we assume that the transmitters have perfect CSI. Hence, the corresponding (instantaneous) rate expressions (2.28) are relatively simple functions of the beamforming vectors. As shown in the sequel, this allows us to perform a number of reformulations to the original problem (2.33)–(2.34) in order to eventually

cast it in convex form, that enables us to very efficiently yield the optimal pair of beamforming vectors.

Towards this end, the first step is to replace the rate expression (2.28) in (2.33)–(2.34) and yield

$$\max_{(\boldsymbol{w}_1,\boldsymbol{w}_2)\in\mathcal{W}^2} \ \log_2\left(1+\frac{|\boldsymbol{h}_{22}^H\boldsymbol{w}_2|^2}{|\boldsymbol{h}_{12}^H\boldsymbol{w}_1|^2+\sigma^2}\right) \tag{2.35}$$

$$\text{s.t.} \qquad \log_2\left(1+\frac{|\boldsymbol{h}_{11}^H\boldsymbol{w}_1|^2}{|\boldsymbol{h}_{21}^H\boldsymbol{w}_2|^2+\sigma^2}\right) = R_1^\star. \tag{2.36}$$

Note that the equality constraint (2.36) can be equivalently relaxed to a lower-bounded inequality. It is rather straightforward to show that due to the concept of Pareto optimality, the bound will be tight at the optimum. Furthermore, since the instantaneous rates are monotonously increasing with the SINR's, the rate optimization (2.35)–(2.36) is equivalent to the SINR optimization

$$\max_{(\boldsymbol{w}_1,\boldsymbol{w}_2)\in\mathcal{W}^2} \ \frac{|\boldsymbol{h}_{22}^H\boldsymbol{w}_2|^2}{|\boldsymbol{h}_{12}^H\boldsymbol{w}_1|^2+\sigma^2} \tag{2.37}$$

$$\text{s.t.} \qquad \frac{|\boldsymbol{h}_{11}^H\boldsymbol{w}_1|^2}{|\boldsymbol{h}_{21}^H\boldsymbol{w}_2|^2+\sigma^2} \geq c_1, \tag{2.38}$$

where $c_1 \triangleq 2^{R_1^\star}-1$ is the SINR level which is required to achieve a rate equal to $R_1^\star$.

The objective function (2.37) is a fraction of quadratic terms; hence, it is neither convex nor concave. Since, we are dealing with a maximization problem, we would like to have a concave or a linear objective function. This is easily achieved by performing the standard trick of introducing a nonnegative real auxiliary variable t [30]. The auxiliary variable can now serve as the new objective function, provided that it will also bound from below the original objective function. Implementing these changes, we equivalently reformulate (2.37)–(2.38) as

$$\max_{(\boldsymbol{w}_1,\boldsymbol{w}_2)\in\mathcal{W}^2,\ t\geq 0} \ t \tag{2.39}$$

$$\text{s.t.} \quad \frac{|\boldsymbol{h}_{11}^H\boldsymbol{w}_1|^2}{|\boldsymbol{h}_{21}^H\boldsymbol{w}_2|^2+\sigma^2} \geq c_1, \quad \frac{|\boldsymbol{h}_{22}^H\boldsymbol{w}_2|^2}{|\boldsymbol{h}_{12}^H\boldsymbol{w}_1|^2+\sigma^2} \geq t. \tag{2.40}$$

Since the denominators of the ratios in the left-hand-side terms of the inequalities (2.40) are positive, we can multiply with them and equivalently obtain

$$\max_{(\boldsymbol{w}_1,\boldsymbol{w}_2)\in\mathcal{W}^2,\ t\geq 0} \ t \tag{2.41}$$

$$\text{s.t.} \qquad |\boldsymbol{h}_{11}^H \boldsymbol{w}_1|^2 \geq c_1 |\boldsymbol{h}_{21}^H \boldsymbol{w}_2|^2 + c_1 \sigma^2, \tag{2.42a}$$

$$|\boldsymbol{h}_{22}^H \boldsymbol{w}_2|^2 \geq t |\boldsymbol{h}_{12}^H \boldsymbol{w}_1|^2 + t\sigma^2. \tag{2.42b}$$

Now that the objective function (2.41) is linear, we may focus on the feasible set of (2.41)–(2.42). If this was convex, then the optimization problem would be convex and its global optimal solution could be efficiently found. We observe that the constraint (2.42a) defines a quadratic inequality, which is nonconvex due to the left-hand-side term. As we will later show, this poses no problem since it is possible to recast the quadratic inequality in (2.42a) as a second-order cone (SOC) constraint, which is convex. However, this is not directly possible for the inequality (2.42b), because of the fact that the quadratic term in its right-hand-side is multiplied with the variable t.

In order to overcome this difficulty, we propose solving (2.41)–(2.42) as a sequence of optimization problems for given values of t. We basically need to perform a line search over the values of t to determine which is the maximum feasible value. We can employ the bisection algorithm, because the nonnegative variable t is also bounded from above, since it corresponds to the achievable SINR of the link 2. As initial lower and upper bounds we may set the values that correspond to the endpoints of the Pareto boundary, i.e., $L := 2^{\underline{R}_2} - 1$ and $U := 2^{\overline{R}_2} - 1$, respectively. In each iteration of the bisection algorithm, t takes the value $(U - L)/2$. Since t is not a variable anymore, the formulation (2.41)–(2.42) denotes a feasibility problem with respect to the variables $\boldsymbol{w}_1$ and $\boldsymbol{w}_2$. The feasibility problems are optimization problems with constraints but without an objective function [30]. They return a binary solution to answer the question whether the feasible set, defined by the constraints, is empty or not. If a solution to the feasibility problem exists, then the lower bound is updated with the feasible value of t, i.e., $L := t$. Otherwise, the upper bound is updated with the infeasible value of t, i.e., $U := t$.

Let us now see what is the actual form of the feasibility problem that needs to be solved in each iteration of the bisection algorithm. For a given value of t, (2.41)–(2.42) reads

$$\text{find} \quad (\boldsymbol{w}_1, \boldsymbol{w}_2) \in \mathcal{W}^2 \tag{2.43}$$

$$\text{s.t.} \quad |\boldsymbol{h}_{11}^H \boldsymbol{w}_1|^2 \geq c_1 |\boldsymbol{h}_{21}^H \boldsymbol{w}_2|^2 + c_1 \sigma^2, \quad |\boldsymbol{h}_{22}^H \boldsymbol{w}_2|^2 \geq t |\boldsymbol{h}_{12}^H \boldsymbol{w}_1|^2 + t\sigma^2. \tag{2.44}$$

Now, both constraints in (2.44) are nonconvex quadratic inequalities of the same form. As shown in [29], for the multiuser downlink beamforming problem with SINR constraints, the inequalities of the form (2.44) admit a reformulation as SOC constraints. This is possible because the beamforming vectors are only involved in

homogeneous quadratic terms in problem (2.43)–(2.44). Hence, there is inherent ambiguity on the phases of the optimal beamforming vectors. The trick is to constrain the phases of the beamforming vectors to the values that yield real-valued the signals that are received on the direct links. Then, it is possible to take the square root on the inequalities (2.44) and discard the absolute value operator from the left-hand-side terms. With this change, the feasibility problem (2.43)–(2.44) is now rewritten as

$$\text{find} \quad (\boldsymbol{w}_1, \boldsymbol{w}_2) \tag{2.45}$$

$$\text{s.t.} \qquad \boldsymbol{h}_{11}^H \boldsymbol{w}_1 \geq \sqrt{c_1 |\boldsymbol{h}_{21}^H \boldsymbol{w}_2|^2 + c_1 \sigma^2}, \quad \boldsymbol{h}_{22}^H \boldsymbol{w}_2 \geq \sqrt{t |\boldsymbol{h}_{12}^H \boldsymbol{w}_1|^2 + t\sigma^2}, \tag{2.46a}$$

$$\text{Im}\left\{\boldsymbol{h}_{11}^H \boldsymbol{w}_1\right\} = 0, \quad \text{Im}\left\{\boldsymbol{h}_{22}^H \boldsymbol{w}_2\right\} = 0, \tag{2.46b}$$

$$\|\boldsymbol{w}_1\|^2 \leq 1, \quad \|\boldsymbol{w}_2\|^2 \leq 1. \tag{2.46c}$$

The inequalities (2.46a) define SOC constraints. The equalities (2.46b) which constrain the phases of the beamforming vectors are linear. The constraints (2.46c) explicitly define the power constraints, that have so far been implicitly denoted as $(\boldsymbol{w}_1, \boldsymbol{w}_2) \in \mathcal{W}^2$. They are quadratic norm constraints, which can be seen as special cases of SOC constraints. Thus, taken together problem (2.45)–(2.46) is a convex (specifically, SOCP) feasibility problem.

2.4.3 Computational Complexity

The SOCP problem (2.45)–(2.46) is a small-scale problem involving 2 n-dimensional variables, 4 SOC constraints and 2 linear constraints. It is solved very efficiently, requiring at most $O(n^{3.5})$ arithmetic operations, by modern interior-point algorithms [31]. There exist freely-distributed software packages, e.g. [33], that use interior-point algorithms to yield the optimal solution of such problems.

The number of SOCP problems that needs to be solved to determine the Pareto-optimal pair of beamforming vectors that corresponds to a point on the Pareto boundary is very small. This is because the bisection algorithm converges exponentially fast to the desired accuracy, since the search interval is halved in every iteration. Note that the sought value corresponds to an SINR value; hence, the accuracy of the solution need not be very high. Typically, a handful of iterations suffices to find a solution that is good-enough from engineering perspective.

2.4.4 Discussion

We proposed an efficient method to yield the Pareto boundary of the achievable rate region for the two-user MISO IC when the transmitters have perfect CSI. The merit of the proposed approach, as opposed to previous ones, is that it directly computes pairs of Pareto-optimal beamforming vectors using optimization techniques.

2.5 Achievable rate region in a Spectrum Sharing perspective

2.5.1 Introduction

A series of recent activities have promoted the idea that operators of cellular wireless networks would benefit from sharing spectrum resources. Activities reported in e.g., [34], suggest inter-operator sharing of spectrum on small timescales (comparable to the fading coherence interval), using advanced scheduling and multiple antenna techniques. The sharing concept makes technical sense since spectrum is a finite resource, so whenever one operator does not need all of its resources, another one may borrow from it. In the long run both could gain from doing so. Conceivably, since spectrum is expensive, larger revenues could be generated by better spectrum utilization.

Spectrum sharing comes in two basic forms; orthogonal sharing and non-orthogonal sharing [35]. Orthogonal sharing means that each operator owns and operates in an independent piece of spectrum, but that they can borrow spectrum from each other on a need basis. The borrower can use the borrowed piece of spectrum exclusively.

Non-orthogonal sharing, by contrast, refers to permitting operators to transmit concurrently in the same time-frequency resource. Fundamentally, a scenario with two transmitters (TX_1, TX_2 herein, belonging to the two operators) using the same time-frequency resource to send data to two receivers (RX_1, RX_2 herein, associated with TX_1 and TX_2 respectively) constitutes an interference channel (IC) [36]. For the TX_1-RX_1 and TX_2-RX_2 pairs to achieve good performance, it is required that they coordinate their operations. Multiple antennas at the TXs is thereby a fundamental enabler. With multiple antennas at the TXs but a single antenna at the RXs, we have a multiple-input single-output (MISO) IC. It has been argued that non-orthogonal spectrum sharing can bring substantial benefits in terms of increased sum-rate. The paper [35], for example, reported gains close to a factor of two.

In non-orthogonal sharing, the two operators compete for resources. However, by cooperating in their choice of transmission strategies they can achieve rate pairs that are Pareto optimal [37]. An appropriate approach to analyze the trade-off involved here is to use game theory. Game theoretic analysis in the context of

spectrum sharing and the MISO IC was probably first popularized by [37]. This work has inspired a surge of results on characterization of Pareto-optimal transmit strategies [38]; fast methods for computing such Pareto-optimal outcomes [39, 40]; and various beamforming techniques [40, 41] and extensions to frequency selective channels [42].

One major practical difficulty in making non-orthogonal sharing work is that channel state information (CSI) must be shared between the TXs that belong to different operators. This must be done on a timescale substantially smaller than the channel coherence time and with sufficient accuracy for coherent beamforming to work. This also includes the CSI of the interfering channels, i.e. TX_1 would have to know the channel $\mathrm{TX}_1 \rightarrow \mathrm{RX}_2$ and vice versa. This requires a coordinated approach to training, and schemes that facilitate overhearing of training sequences. Therefore, for non-orthogonal inter-operator sharing to have much practical potential, the gains in communication performance must be substantial.

The objective of this section is to examine, fundamentally, and assuming the CSI transfer problem can be solved, under what conditions non-orthogonal sharing can provide gains as compared to conventional operations. Specifically, 1) we model non-orthogonal spectrum sharing via a MISO IC, and the reference scenario as a MISO broadcast channel (BC); 2) we summarize known upper and achievable bounds on the sum-rate for these models in Secs. 2.5.3 and 2.5.4, respectively; 3) we evaluate the bounds for flat and frequency selective fading in Sec. 2.5.5; 4) we draw conclusions on what operating points where non-orthogonal spectrum sharing is likely to work at all. Sec. 2.5.6 summarizes these conclusions.

While most modeling techniques and algorithms used in this section are known, to our knowledge their use in the context in question is new and provides considerable new insight. The fast method we use to compute achievable sum-rates for the MISO BC using linear transmitter processing (Sec. 2.5.4) extends the work for the MISO IC in [39] and represents a new algorithmic contribution; it is substantially faster than the method developed specifically for the same purpose in [43].

2.5.2 Models

The system consists of a cell with two coexisting TXs belonging to different operators. The total spectrum is split into $2N_s$ subchannels. The bandwidth of each subchannel is the coherence bandwidth W_c. Hence, the total bandwidth for the system is $2B = 2W_cN_s$. For the non-sharing case, each operator owns a spectrum of bandwidth B, i.e., N_s subchannels. For the sharing case, both operators use the entire $2B$ band, see Fig. 2.8. We assume that each TX is equipped with $n_t = 2$ antennas. Hence, for the non-sharing and sharing scenarios, we can serve two users and one user, respectively, per TX.[1]

[1] As a variation, in the sharing scenario, four users in total could be served (like in the non-sharing setup), one in the first B band and one in the second B band. This however would not change

For the spectrum sharing scenario, we assume that the operators have one RX (user) each to serve. These have different channels. Summing rates over the subchannels has the interpretation of ergodic capacity (coding over the subchannels) and summing over the users has the interpretation of sum-rate. Also, each TX can spend power P. Hence, the total power spent in the system is $2P$. Hence the average power per served user is P, i.e., $P/2N_s$ per user per subchannel. In order to meet the power constraint, we must have

$$\sum_{k=1}^{2N_s} P_{i,k} \leq P \tag{2.47}$$

for each TX_i where $P_{i,k}$ is the power sent by TX_i on subchannel k.

For the non-sharing scenario, each operator serves two users. Each operator can spend power P over the N_s subchannels. Hence, the average power per user and subchannel is $P/2N_s$.[2] In order to meet the power constraint for the non-sharing scenario, we must have

$$\sum_{i=1}^{2} \sum_{k=1}^{N_s} P_{i,k} \leq P, \tag{2.48}$$

where $P_{i,k}$ is the power spent on user i on subchannel k.

As performance measure we use the average rate over users and subchannels. Maximizing the average rate is the same as maximizing the sum-rate. The motivation for this choice of performance measure is that it gives the highest possible throughput of the operators.

The analysis that follows will use information theoretic results for the MISO IC [38, 44] and BC [43, 45, 46]. For the MISO IC, we define $\boldsymbol{h}_{ij,k} \in \mathbb{C}^{n_t}$ to be the (conjugated) channel vector for the link $\text{TX}_i \to \text{RX}_j$ for $i, j \in \{1, 2\}$ on subchannel k. The channels for the MISO BC model can be obtained from the MISO IC model by setting $\boldsymbol{h}_{ij,k} = \boldsymbol{h}_{j,k}$, $i, j = 1, 2$ where $\boldsymbol{h}_{i,k}$ is the channel between the TX and RX_i [38]. For both scenarios we assume that the TXs have instantaneous CSI.

2.5.3 Non-Orthogonal Sharing: The MISO IC

The problem of finding the capacity region of the general IC is still open. For the single-antenna case, it was shown that interference does not reduce the capacity when interference is strong [36]. One good known achievable rate region for the

the conclusion of our study, since the metric we will use is an average rate over all users and subchannels.

[2] We have chosen to keep the total emitted power per cell the same in the non-sharing and sharing scenarios. By contrast, in [35], it was assumed that the total emitted power per cell in the sharing scenario was twice that of the non-sharing scenario. It is not clear what future regulatory requirements would look like if non-orthogonal spectrum sharing becomes reality.

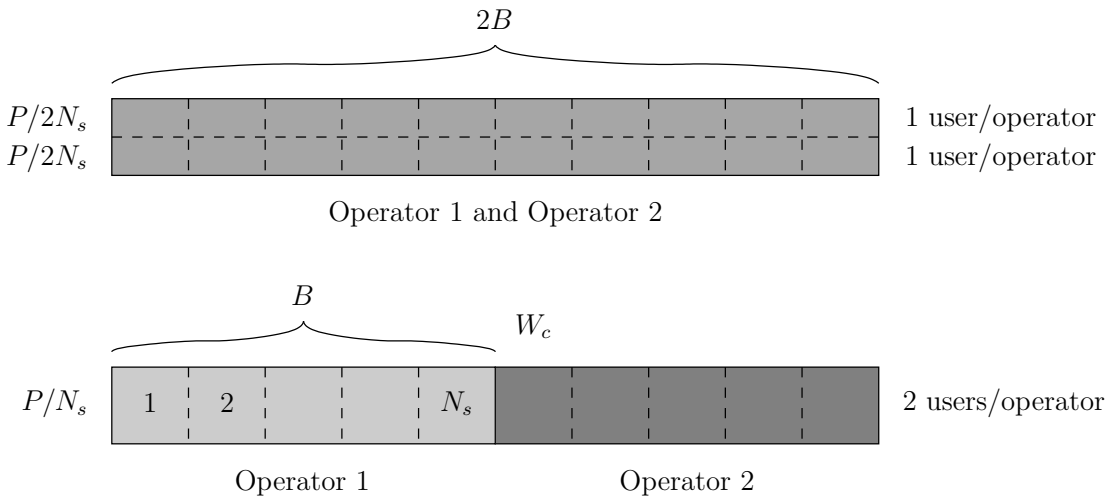

Figure 2.8: Illustration of the spectrum sharing scenarios. The upper and lower parts of the figure show the non-orthogonal sharing and non-sharing scenarios, respectively.

general IC is given in [47]. Outer bounds of the capacity region were provided in [48]. During the last decade, the multiple antenna IC has gained a lot of interest. The so-called vector Gaussian IC was introduced in [49]. Many of the existing achievable and upper bounds on the capacity region of the multiple-antenna IC are extensions from the single-antenna case. Recent results on the capacity region of the multiple-antenna IC are reported in [50, 44]. In this section, we summarize some lower and upper bounds on the sum-rate of the MISO IC.

Lower (Achievable) Bounds Using Linear Beamforming

Here, we first give the system model for the MISO IC using linear beamforming. Then, by using such a transmission scheme we obtain lower (achievable) bounds on the sum-capacity of the MISO IC. The matched-filtered symbol-sampled complex baseband data received by the RXs on subchannel k for the MISO IC is modeled as

$$\begin{aligned} y_{1,k} &= \sqrt{P_{1,k}}\boldsymbol{h}_{11,k}^H \boldsymbol{w}_{1,k} s_{1,k} + \sqrt{P_{2,k}}\boldsymbol{h}_{21,k}^H \boldsymbol{w}_{2,k} s_{2,k} + e_{1,k} \\ y_{2,k} &= \sqrt{P_{2,k}}\boldsymbol{h}_{22,k}^H \boldsymbol{w}_{2,k} s_{2,k} + \sqrt{P_{1,k}}\boldsymbol{h}_{12,k}^H \boldsymbol{w}_{1,k} s_{1,k} + e_{2,k}. \end{aligned} \tag{2.49}$$

Also, $P_{i,k}$, $\boldsymbol{w}_{i,k} \in \mathbb{C}^{n_t}$, $\|\boldsymbol{w}_{i,k}\| = 1$ are the power and beamforming vector allocated by TX_i, respectively, and $s_{i,k} \sim \mathcal{CN}(0,1)$ is the transmitted symbol for RX_i. By $e_{i,k} \sim \mathcal{CN}(0,1)$ we model the noise at RX_i.

Assuming linear beamforming using the beamforming vectors $\boldsymbol{w}_{i,k}$ and power allocation $P_{i,k}$, $i = 1, 2$, $k = 1, \ldots, N_s$, the average rate in bits per channel use (bpcu)

per served user is

$$\bar{R}^{\mathrm{IC}} = \frac{1}{2}\sum_{i=1}^{2}\frac{1}{2N_s}\sum_{k=1}^{2N_s} R_i^{\mathrm{IC}}(P_{1,k}, P_{2,k}, \boldsymbol{w}_{1,k}, \boldsymbol{w}_{2,k}), \tag{2.50}$$

where[3] [38]

$$R_1^{\mathrm{IC}}(P_{1,k}, P_{2,k}, \boldsymbol{w}_{1,k}, \boldsymbol{w}_{2,k}) \triangleq \log\left(1 + \frac{P_{1,k}|\boldsymbol{h}_{11,k}^H \boldsymbol{w}_{1,k}|^2}{P_{2,k}|\boldsymbol{h}_{21,k}^H \boldsymbol{w}_{2,k}|^2 + 1}\right). \tag{2.51}$$

The inner sum of (2.50) is the ergodic rate for the ith user while the outer sum yields the average rate of the two users.

Zero-forcing (ZF) beamforming: ZF is a linear transmit beamforming strategy that cancels out the interference to the unintended receiver. The ZF beamforming vectors are [38],

$$\boldsymbol{w}_{1,k}^{\mathrm{ZF}} = \frac{\boldsymbol{\Pi}_{\boldsymbol{h}_{12,k}}^{\perp}\boldsymbol{h}_{11,k}}{\left\|\boldsymbol{\Pi}_{\boldsymbol{h}_{12,k}}^{\perp}\boldsymbol{h}_{11,k}\right\|}, \quad \boldsymbol{w}_{2,k}^{\mathrm{ZF}} = \frac{\boldsymbol{\Pi}_{\boldsymbol{h}_{21,k}}^{\perp}\boldsymbol{h}_{22,k}}{\left\|\boldsymbol{\Pi}_{\boldsymbol{h}_{21,k}}^{\perp}\boldsymbol{h}_{22,k}\right\|}, \tag{2.52}$$

where $\boldsymbol{\Pi}_{\mathbf{x}}^{\perp} \triangleq \mathbf{I} - \mathbf{x}\mathbf{x}^H/\left\|\mathbf{x}\right\|^2$ is the orthogonal projection onto the orthogonal complement of the vector $\mathbf{x}$. Using the ZF beamforming vectors in (2.50), we get

$$\bar{R}^{\mathrm{ICZF}} = \frac{1}{4N_s}\sum_{i=1}^{2}\sum_{k=1}^{2N_s}\log\left(1 + P_{i,k}\left\|\boldsymbol{\Pi}_{\boldsymbol{h}_{ij,k}}^{\perp}\boldsymbol{h}_{ii,k}\right\|^2\right). \tag{2.53}$$

We will consider two possible power allocations. The first is equal power allocation, i.e., $P_{i,k} = P/2N_s$. The second is to maximize (2.53) with respect to $P_{i,k}$, $i = 1, 2$ and $k = 1, \ldots, 2N_s$ using water-filling.

Clearly, these schemes yield achievable bounds for the capacity. However, as we will see next, we can obtain better achievable bounds by also optimizing the beamforming vectors.

Maximum sum-rate using linear beamforming: Here, we maximize (2.50)–(2.51) with respect to the beamforming vectors, assuming equal power allocation

[3] Whenever an expression is given for only one user, the expression for the other is obtained by interchanging the indices. In this paper, we use the base-2 logarithm.

over the subchannels. That is, for each subchannel, we solve[4]

$$\max_{\boldsymbol{w}_1,\boldsymbol{w}_2} \quad \sum_{i=1}^{2} R_i^{\mathrm{IC}}(P/2N_s, P/2N_s, \boldsymbol{w}_1, \boldsymbol{w}_2) \tag{2.54}$$

$$\text{s. t.} \quad \|\boldsymbol{w}_i\|^2 = 1, \quad i = 1, 2. \tag{2.55}$$

We can equivalently write (2.54)–(2.55) as

$$\max_{\boldsymbol{w}_1,\boldsymbol{w}_2} \quad \log\left(1+\frac{|\boldsymbol{h}_{11}^H\boldsymbol{w}_1|^2}{|\boldsymbol{h}_{21}^H\boldsymbol{w}_2|^2+\frac{2N_s}{P}}\right)+\log\left(1+\frac{|\boldsymbol{h}_{22}^H\boldsymbol{w}_2|^2}{|\boldsymbol{h}_{12}^H\boldsymbol{w}_1|^2+\frac{2N_s}{P}}\right) \tag{2.56}$$

$$\text{s. t.} \quad \|\boldsymbol{w}_i\|^2 = 1, \quad i = 1, 2. \tag{2.57}$$

The problem (2.56)–(2.57) is non-convex. However, by using our result from [39], we find the optimum of (2.56)–(2.57) in an efficient way. Specifically, we find the Pareto boundary of the two-user MISO IC in closed-form using the algorithm in [39]. In order to find the maximum sum-rate point, we then perform a one-dimensional search over the Pareto boundary.

Upper Bounds

Here, we give two upper bounds on the MISO IC sum-capacity. The first bound is a trivial bound, where interference is ignored. The second bound is more sophisticated and hence tighter.

Trivial upper bound assuming no interference: In order to find a trivial upper (TU) bound on the MISO IC capacity, we neglect the interference terms in (2.49). For this case, it is optimal to use the maximum-ratio transmission (MRT) beamforming vectors, i.e. $\boldsymbol{w}_{1,k}^{\mathrm{MRT}} = \boldsymbol{h}_{11,k}/\left\|\boldsymbol{h}_{11,k}\right\|$. Inserting these in (2.50), we get

$$\bar{R}^{\mathrm{ICTU}} = \frac{1}{4N_s}\sum_{i=1}^{2}\sum_{k=1}^{2N_s}\log\left(1+P_{i,k}\left\|\boldsymbol{h}_{ii,k}\right\|^2\right). \tag{2.58}$$

To obtain an upper bound, we optimize the power using water-filling.

Non-trivial upper bound: As an improvement of the trivial upper bound given

[4] In order to simplify notation, we omit the subchannel index when we focus on a single subchannel.

above, we give an upper bound based on [44]. From there, we have

$$\begin{aligned} R_1 + R_2 \leq \min \big\{ & \log(1 + P_1 \|\boldsymbol{h}_{11}\|^2) + \log(1 + P_2 \|\boldsymbol{h}_{22}\|^2), \\ & \log(1 + P_1 \|\boldsymbol{h}_{12}\|^2 + P_2 \|\boldsymbol{h}_{22}\|^2) + \log(1 + P_1 K_1), \\ & \log(1 + P_2 \|\boldsymbol{h}_{21}\|^2 + P_1 \|\boldsymbol{h}_{11}\|^2) + \log(1 + P_2 K_2), \\ & \log(1 + P_2 \|\boldsymbol{h}_{21}\|^2 + P_1 K_1) \\ & + \log(1 + P_1 \|\boldsymbol{h}_{12}\|^2 + P_2 K_2) \big\} \end{aligned} \tag{2.59}$$

where

$$K_1 \triangleq \|\boldsymbol{h}_{11}\|^2 - P_1 |\boldsymbol{h}_{12}^H \boldsymbol{h}_{11}|^2 / (1 + P_1 \|\boldsymbol{h}_{12}\|^2) \tag{2.60}$$

$$K_2 \triangleq \|\boldsymbol{h}_{22}\|^2 - P_2 |\boldsymbol{h}_{21}^H \boldsymbol{h}_{22}|^2 / (1 + P_2 \|\boldsymbol{h}_{21}\|^2). \tag{2.61}$$

We see that the first term in (2.59) corresponds to the trivial upper bound given above.

The bounds in [44] are derived for a single-channel MIMO IC. By formulating the multi-channel system as a single-channel MIMO system with block-diagonal channel matrices, we can extend (2.59) to also include optimal power allocation. However, this is not done herein. Hence, the bound in (2.59) is only valid for a given power allocation. As we will see in Sec. 2.5.5, power control appears to yield only a marginal difference for the conclusions of the paper.

2.5.4 No Sharing: The MISO BC

The MISO BC models the scenario without sharing and there is no interference between the operators. Here, no inter-operator CSI transfer is needed. The capacity region of the general BC is still an open problem. Nevertheless, the capacity region of the Gaussian BC is known. For the two-user MISO BC, the sum-capacity was derived in closed form in [45]. This result was later extended to the entire capacity region of the multiple-input multiple-output (MIMO) BC in [46]. Here, we give lower and upper bounds for the sum-capacity of the MISO BC.

Lower (Achievable) Bounds Using Linear Beamforming

Assuming linear beamforming using the beamforming vectors $\boldsymbol{w}_{i,k}$, and power allocation $P_{i,k}$, $i = 1, 2$, $k = 1, \ldots, N_s$, the average rate over the users per subchannel is

$$\bar{R}^{\mathrm{BC}} = \frac{1}{2} \sum_{i=1}^{2} \frac{1}{N_s} \sum_{k=1}^{N_s} R_i^{\mathrm{BC}}(P_{1,k}, P_{2,k}, \boldsymbol{w}_{1,k}, \boldsymbol{w}_{2,k}), \tag{2.62}$$

where [38]

$$R_1^{\mathrm{BC}}(P_{1,k}, P_{2,k}, \boldsymbol{w}_{1,k}, \boldsymbol{w}_{2,k}) \triangleq \log\left(1 + \frac{P_{1,k}|\boldsymbol{h}_{1,k}^H \boldsymbol{w}_{1,k}|^2}{P_{2,k}|\boldsymbol{h}_{1,k}^H \boldsymbol{w}_{2,k}|^2 + 1}\right). \tag{2.63}$$

Zero-forcing beamforming: The ZF beamforming vectors for the MISO BC are similar to those of the MISO IC, namely [43],

$$\boldsymbol{w}_{1,k}^{\mathrm{ZF}} = \frac{\boldsymbol{\Pi}_{\boldsymbol{h}_{2,k}}^{\perp} \boldsymbol{h}_{1,k}}{\left\|\boldsymbol{\Pi}_{\boldsymbol{h}_{2,k}}^{\perp} \boldsymbol{h}_{1,k}\right\|}, \quad \boldsymbol{w}_{2,k}^{\mathrm{ZF}} = \frac{\boldsymbol{\Pi}_{\boldsymbol{h}_{1,k}}^{\perp} \boldsymbol{h}_{2,k}}{\left\|\boldsymbol{\Pi}_{\boldsymbol{h}_{1,k}}^{\perp} \boldsymbol{h}_{2,k}\right\|} \tag{2.64}$$

Using the ZF beamforming vectors, we get

$$\bar{R}^{\mathrm{BCZF}} = \frac{1}{2N_s} \sum_{i=1}^{2} \sum_{k=1}^{N_s} \log\left(1 + P_{i,k} \left\|\boldsymbol{\Pi}_{\boldsymbol{h}_{j,k}}^{\perp} \boldsymbol{h}_{i,k}\right\|^2\right). \tag{2.65}$$

We consider two possible power allocations; either equal power allocation, i.e., $P_{i,k} = P/2N_s$ or maximizing (2.65) with respect to $P_{i,k}$, $i = 1, 2$, $k = 1, \ldots, N_s$ using water-filling.

Maximum sum-rate using linear beamforming: We provide an algorithm for finding the maximum sum-rate of the MISO BC when equal power allocation over the subchannels is used. This method is an alternative to [43] where monotonic optimization using polyblocks was used. For each subchannel we solve

$$\max_{\boldsymbol{w}_1, \boldsymbol{w}_2} \quad \sum_{i=1}^{2} R_i^{\mathrm{BC}}(P_1, P_2, \boldsymbol{w}_1, \boldsymbol{w}_2) \tag{2.66}$$

$$\text{s. t.} \quad \|\boldsymbol{w}_i\|^2 = 1, \quad i = 1, 2, \tag{2.67}$$

$$P_1 + P_2 = P/N_s. \tag{2.68}$$

For a given power allocation (P_1, P_2) that meets (2.68), we solve

$$\max_{\boldsymbol{w}_1, \boldsymbol{w}_2} \quad \log\left(1 + \frac{P_1|\boldsymbol{h}_1^H \boldsymbol{w}_1|^2}{P_2|\boldsymbol{h}_1^H \boldsymbol{w}_2|^2 + 1}\right) + \log\left(1 + \frac{P_2|\boldsymbol{h}_2^H \boldsymbol{w}_2|^2}{P_1|\boldsymbol{h}_2^H \boldsymbol{w}_1|^2 + 1}\right) \tag{2.69}$$

$$\text{s. t.} \quad \|\boldsymbol{w}_i\|^2 = 1, \quad i = 1, 2 \tag{2.70}$$

If we use the effective channels $\tilde{\mathbf{h}}_{ij} \triangleq \sqrt{P_i}\boldsymbol{h}_j$, $i, j = 1, 2$, we can use the fast method of [39], to find the optimum of (2.69)–(2.70) for fixed P_1, P_2. This requires a one-dimensional search. By traversing all feasible power allocations (P_1, P_2) with $P_2 = P/N_s - P_1$, we will find the optimum of (2.66)–(2.68). For example, we can search over P_1, which also is a one-dimensional search. Hence, in order to solve (2.66)–(2.68), we have to perform a two-dimensional search, which is faster than

the algorithm in [43].

Upper Bounds

As for the MISO IC in Sec. 2.5.3, we give two upper bounds; a trivial bound and the sum-capacity.

Trivial Upper Bound Assuming No Interference: We obtain a trivial upper bound by ignoring the interference and using MRT, i.e. $\boldsymbol{w}_{i,k}^{\mathrm{MRT}} = \boldsymbol{h}_{i,k}/\left\|\boldsymbol{h}_{i,k}\right\|$. Then the upper bound on (2.62) is

$$\bar{R}^{\mathrm{BCTU}} = \frac{1}{2N_s}\sum_{i=1}^{2}\sum_{k=1}^{N_s}\log\left(1+P_{i,k}\left\|\boldsymbol{h}_{i,k}\right\|^2\right). \tag{2.71}$$

We obtain the upper bound by performing power allocation using water-filling. We note that if $\boldsymbol{h}_{1,k}$ and $\boldsymbol{h}_{2,k}$ are orthogonal, then these trivial upper bounds will coincide with the achievable ZF bounds.

Sum-capacity of the MISO BC: The sum-capacity per subchannel for the two-user MISO BC under the sum-power constraint P/N_s is found on closed form to be [45]

$$C_{\mathrm{sum}}^{\mathrm{BC}} = \begin{cases} \log\left(1+\frac{P\|\boldsymbol{h}_1\|^2}{N_s}\right), & \frac{P}{N_s} \le A, \\ \log\left(\frac{\left(\frac{P}{N_s}\det(\mathbf{H}\mathbf{H}^H)+\mathrm{trace}(\mathbf{H}\mathbf{H}^H)\right)^2-4|\boldsymbol{h}_2^H\boldsymbol{h}_1|^2}{4\det(\mathbf{H}\mathbf{H}^H)}\right), & \frac{P}{N_s} > A, \end{cases} \tag{2.72}$$

where $A \triangleq (\|\boldsymbol{h}_1\|^2 - \|\boldsymbol{h}_2\|^2)/\det(\mathbf{H}\mathbf{H}^H)$ and $\mathbf{H} \triangleq [\boldsymbol{h}_1 \ \ \boldsymbol{h}_2]^T$. Without loss of generality, we have assumed that $\|\boldsymbol{h}_1\|^2 \ge \|\boldsymbol{h}_2\|^2$. In order to achieve the capacity (2.72), we need dirty-paper coding.

By using the duality property of the MIMO BC and MIMO multiple access channel (MAC) [51], we can include power control across the subchannels. The trick is to write the multi-channel system as an equivalent MIMO system. However, for finding the capacity for this case, numerical methods are needed.

2.5.5 Numerical Comparisons

In this section we provide numerical evaluations of the bounds provided in Secs. 2.5.3 and 2.5.4. We assume unit-variance Rayleigh-fading, i.e., $\boldsymbol{h}_{ij} \sim \mathcal{CN}(\mathbf{0},\mathbf{I})$. This corresponds to the scenario where the TXs are approximately co-located. We provide numerical results for the cases of $P/N_s = 7$ dB and $P/N_s = 17$ dB and $N_s = 4$ (the main conclusions seem to be insensitive of N_s). For each bound, we perform 10000 Monte Carlo runs and plot the cumulative density function (cdf)

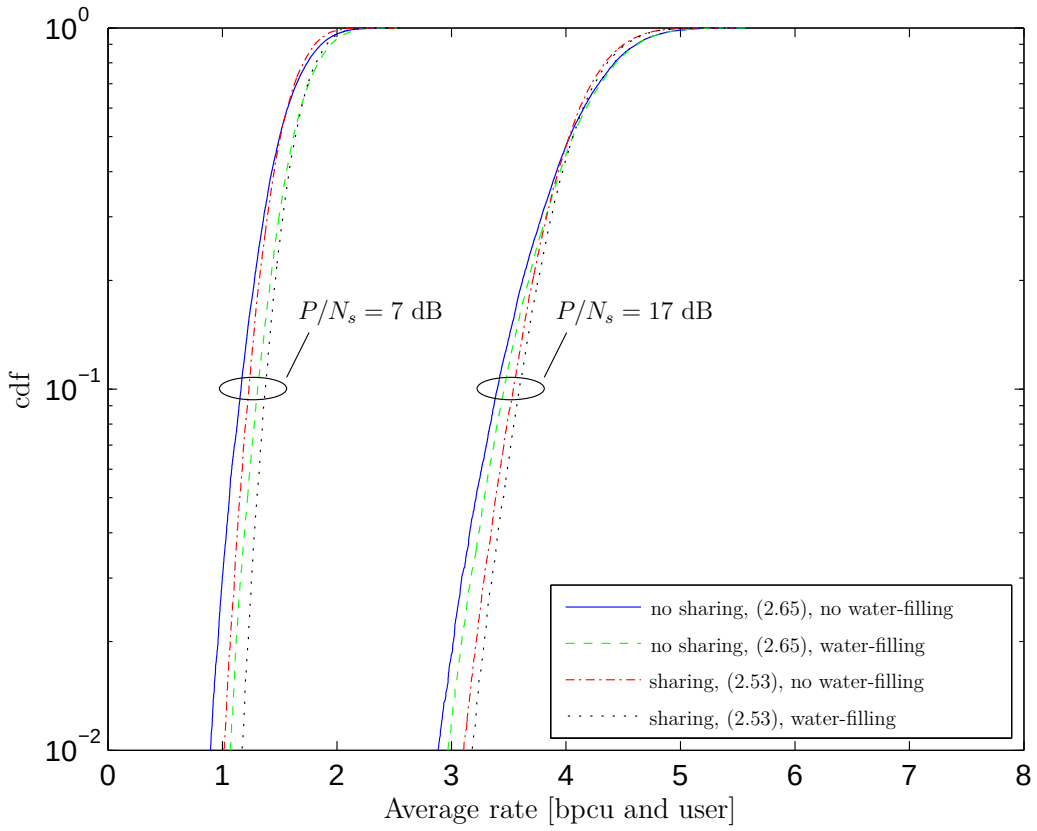

Figure 2.9: Achievable sum-rate bounds using ZF beamforming, with and without water-filling.

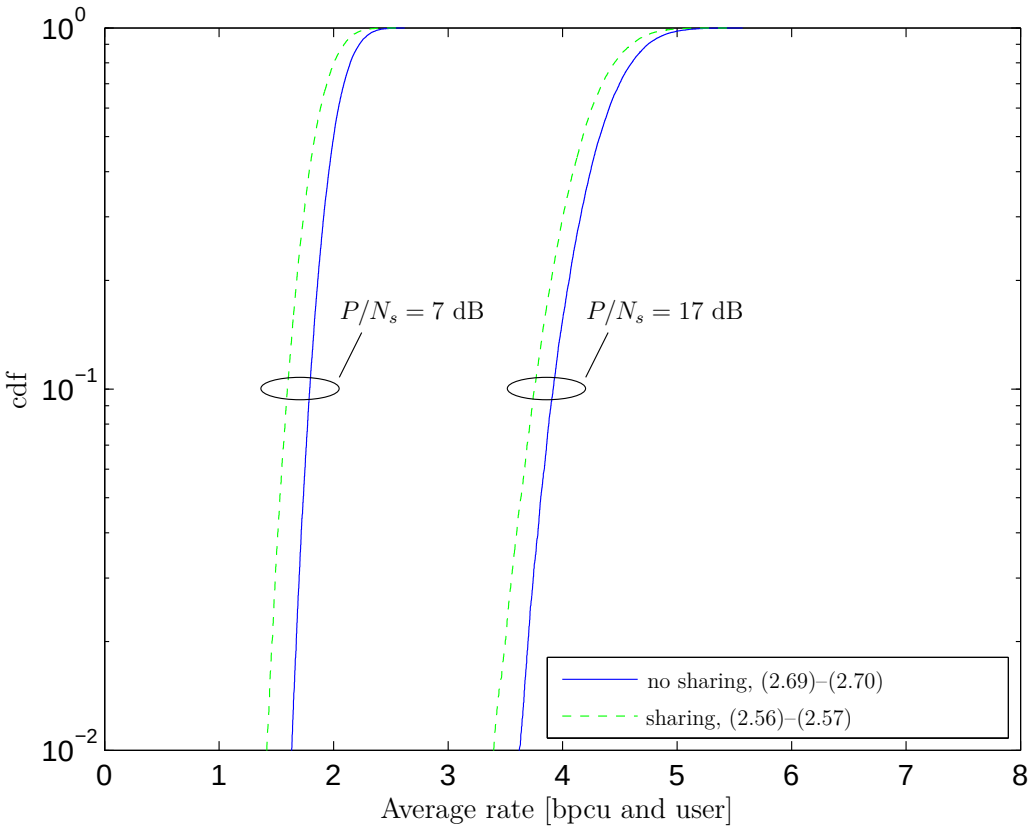

Figure 2.10: Achievable sum-rate bounds using linear beamforming and equal power allocation across the subchannels.

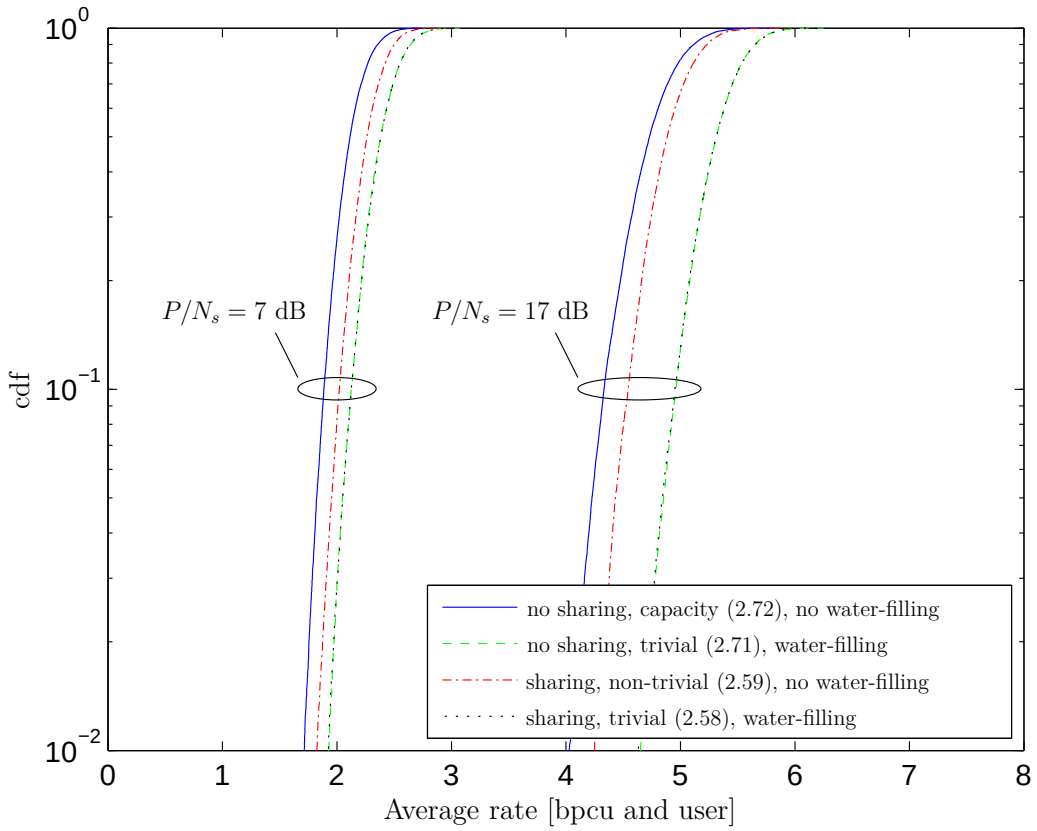

Figure 2.11: Upper sum-rate bounds for sharing and no sharing.

of the rate. Compared to time-average, the cdf gives us a better insight about extreme-case performance. As a general note, we see that the lower and higher choices of transmit power gives rates of approximately 1-3 and 3-6 bpcu and user, respectively.

In Fig. 2.9, we plot the cdfs of the bounds achievable using ZF. As expected, we get slightly higher rates with water-filling than without. Also, the spectrum sharing yields slightly higher rates than the non-sharing baseline. This observation holds for both choices of power.

For the achievable bounds using per subchannel sum-rate maximization and linear beamforming, we see in Fig. 2.10 that the non-sharing case yields rates that are approximately 0.2 bpcu and user higher than in the sharing case. This holds for both the high and low power. This difference could be explained by that the fact that we for the MISO BC do power control among the users in one subchannel.

Fig. 2.11 shows the upper bounds. There, we can make a number of interesting observations. First, the trivial bounds for no-sharing and non-orthogonal sharing coincide. Second, we observe that the non-trivial upper bound (2.59) for the IC yields higher rates than the sum-capacity for the BC. The difference is approximately 0.1 bpcu and user for $P/N_s = 7$ dB and slightly more fore $P/N_s = 17$ dB. Probably, the reason for this gap is the fact that (2.59) is an upper bound. However, we cannot for sure say that we can achieve higher rates with spectrum sharing than without, or vice versa. Third, for high transmit power, we notice that the trivial upper bounds yield rates that are approximately 0.7 bpcu and user higher than the sum-capacity bound for the MISO BC.

2.5.6 Conclusions

We have analyzed the potential gains of non-orthogonal spectrum sharing by using first principles based information theoretic models. In conclusion, the gain of non-orthogonal sharing appears to be very limited. The intuition behind this result is that without sharing, each operator has a bandwidth of B and two spatial degrees of freedom (DoF) per bandwidth unit. By contrast, with sharing each operator has a bandwidth of $2B$ and two spatial DoF per bandwidth unit of which one can be used for transmission and the other must be used to suppress interference.

The potential gain might be larger if, in the non-sharing scenario, highly suboptimal transmission schemes are used (not fully utilizing all spatial DoF); however, in this case, better utilization of spatial DoF per operator appears to be more attractive than non-orthogonal sharing between operators. Taking into account the extra CSI needed for non-orthogonal sharing, it is questionable whether non-orthogonal sharing can give any gain in practice.

In this study, channels were randomly drawn but given. This corresponds to the case of delay constrained traffic. For future studies, multi-user diversity, i.e., the

possibility of selecting two users from a larger pool of users per subchannel, should be incorporated. However, results not shown herein indicate that this does not change the main conclusion.

3 Achievable Rate Region of the MISO IC with SUD and imperfect CSI

3.1 Achievable Rate region with incomplete Channel State Information

We consider two transmitter-receiver pairs sharing the same spectral band. Each transmitter is equipped with multiple antennas while each receiver uses a single antenna. This setting corresponds to the MISO IC [52]. We assume that the receivers treat the interference from unintended transmitters as additive Gaussian noise. The achievable rate region, of this setting is in general not a convex set. The outermost boundary of this region is called the Pareto boundary and consists of Pareto optimal points. At these points, it is impossible to increase the rate of one user without reducing the rate of the other.

In the case of perfect CSI, the beamforming vectors that are relevant for Pareto optimal operation are proven in [11] to be a linear combination of MRT and ZF. For the general K-user case, real-valued parametrization of the efficient beamforming vectors is provided recently in [53, 54]. In [55], Pareto optimal beamforming for partial CSI at the transmitters is considered in the two-user MISO IFC.

The parametrization of the Pareto optimal beamforming vectors requires that the transmitters know the channels to all receivers. We consider the case where the transmitters have imperfect CSI and the uncertainty of the channel information is bounded by a spherical region. In [56], channel mismatches are modeled by spherical uncertainty, while in [57] by ellipsoidal uncertainty. The latter work encompasses the spherical uncertainty model as a special case. Different robust adaptive beamforming techniques are found in [58] and robust beamforming using convex optimization is discussed in [19].

We investigate robust Pareto optimal transmission in which the transmitters have imperfect CSI. We adopt the spherical uncertainty model from [56]. Considering the worst case achievable rate of the links, we characterize the beamforming vectors that achieve points on the Pareto boundary of the robust rate region. In addition, we investigate the gain in spectrum sharing under channel information uncertainty compared to time division multiple access (TDMA). The spectral efficiency gain with spectrum sharing is larger in the mid SNR regime. We provide analytical results for asymptotic cases on the SNR for optimal sum rate transmission.

3.1.1 Preliminaries

System and Channel model

The quasi-static block flat-fading channel vector from transmitter k to receiver ℓ is denoted by $\hat{\boldsymbol{h}}_{k\ell} \in \mathbb{C}^N$. We assume that transmission consists of scalar coding followed by beamforming. The beamforming vector used by transmitter k is $\boldsymbol{w}_k \in \mathbb{C}^N$. The matched-filtered, symbol-sampled complex baseband data received at receiver k is

$$y_k = \hat{\boldsymbol{h}}_{kk}^H \mathbf{w}_k s_k + \hat{\boldsymbol{h}}_{\ell k}^H \mathbf{w}_\ell s_\ell + n_k, \quad k \neq \ell, \tag{3.1}$$

where s_k is the symbol transmitted by transmitter k. The random variables n_k are noise terms which are independent and identically distributed (i.i.d.) complex Gaussian with zero mean and variance σ^2. Each transmitter has a total power constraint of $P := 1$ such that $\|\boldsymbol{w}_k\|^2 \leq 1$. Define SNR as $\rho = 1/\sigma^2$.

Spherical Uncertainty model

We assume a transmitter k does not know the channels $\hat{\boldsymbol{h}}_{kk}$ and $\hat{\boldsymbol{h}}_{k\ell}$ perfectly. In the spherical uncertainty model, the channel estimation errors are defined as

$$\boldsymbol{\delta}_{k\ell} = \hat{\boldsymbol{h}}_{k\ell} - \mathbf{h}_{k\ell}, \quad \boldsymbol{\delta}_{k\ell} \in D(\epsilon_{k\ell}), \tag{3.2}$$

where $\mathbf{h}_{k\ell}$ is the estimate of $\hat{\boldsymbol{h}}_{k\ell}$ and

$$D(\epsilon) = \{\boldsymbol{\delta} : \|\boldsymbol{\delta}\| \leq \epsilon_{kk}\}. \tag{3.3}$$

The worst case power gain at intended receiver k is the squared of

$$x_{kk}(\mathbf{w}_k) = \min_{\boldsymbol{\delta}_{kk} \in D(\epsilon_{kk})} |\mathbf{w}_k^H \hat{\boldsymbol{h}}_{kk}|. \tag{3.4}$$

The error vector as a function of the used beamforming vector which realizes the worst case intended power gain in (3.4) is determined in [56], and the worst case intended power gain can be written as [56, 59].

$$x_{kk}(\mathbf{w}_k)^2 = \left((|\mathbf{w}_k^H \mathbf{h}_{kk}| - \|\mathbf{w}_k\| \, \epsilon_{kk})^+\right)^2, \tag{3.5}$$

where $(x)^+ := \max(0, x)$. Define the worst case interference gain as the squared of

$$x_{k\ell}(\mathbf{w}_k) = \max_{\boldsymbol{\delta}_{k\ell} \in D(\epsilon_{k\ell})} |\mathbf{w}_k^H \hat{\boldsymbol{h}}_{k\ell}|. \tag{3.6}$$

Similarly, the error vector as a function of the used beamforming vector which realizes the worst case interference power gain can be calculated and the interference

power gain at receiver ℓ is

$$x_{k\ell}(\mathbf{w}_k)^2 = \left(|\mathbf{w}_k^H \mathbf{h}_{k\ell}| + \|\mathbf{w}_k\| \, \epsilon_{k\ell}\right)^2. \tag{3.7}$$

Thus, the worst case SINR at receiver k can be written as

$$\phi_k(\mathbf{w}_1, \mathbf{w}_2) = \frac{\left((|\mathbf{h}_{kk}^H \mathbf{w}_k| - \epsilon_{kk} \, \|\mathbf{w}_k\|)^+\right)^2}{\left(|\mathbf{h}_{\ell k}^H \mathbf{w}_\ell| + \epsilon_{\ell k} \, \|\mathbf{w}_\ell\|\right)^2 + \sigma^2}, \quad k \neq \ell. \tag{3.8}$$

Robust Rate Region

The achievable rate for link k is

$$r_k(\mathbf{w}_1, \mathbf{w}_2) = \log_2(1 + \phi_k(\mathbf{w}_1, \mathbf{w}_2)), \tag{3.9}$$

where single-user decoding is performed at the receiver. The *rate region* is the set of all achievable rate tuples:

$$R := \left\{(r_1(\boldsymbol{w}_1, \boldsymbol{w}_2), r_2(\boldsymbol{w}_1, \boldsymbol{w}_2)) : \|\boldsymbol{w}_k\|^2 \leq 1\right\}. \tag{3.10}$$

Definition 3.1. An operating point $(r_1, r_2) \in R$ is *Pareto optimal* if there is no other operating point $(r_1', r_2') \in R$ such that $(r_1', r_2') \geq (r_1, r_2)$, where the inequality is componentwise and strict for at least one component. ■

The set of all Pareto optimal operating points makes up the *Pareto boundary* of the rate region. We are interested in operating points which are on the Pareto boundary of the rate region.

3.1.2 Pareto Optimal Beamforming

In this section, we will first review the results for Pareto optimal beamforming for perfect CSI. Then we provide the parametrization for the imperfect CSI case.

3.1.3 Perfect CSI case

For the two-user MISO IFC with perfect CSI at the transmitters and receivers, the set of beamforming vectors for each transmitter that are relevant for Pareto optimal operation are parameterized by a single real-valued parameter $\lambda_k \in [0, 1]$ as [11, Corollary 1]

$$\mathbf{w}_k(\lambda_k) = \sqrt{\lambda_k} \frac{\mathbf{\Pi}_{\hat{\boldsymbol{h}}_{k\ell}} \hat{\boldsymbol{h}}_{kk}}{\left\|\mathbf{\Pi}_{\hat{\boldsymbol{h}}_{k\ell}} \hat{\boldsymbol{h}}_{kk}\right\|} + \sqrt{1 - \lambda_k} \frac{\mathbf{\Pi}_{\hat{\boldsymbol{h}}_{k\ell}}^{\perp} \hat{\boldsymbol{h}}_{kk}}{\left\|\mathbf{\Pi}_{\hat{\boldsymbol{h}}_{k\ell}}^{\perp} \hat{\boldsymbol{h}}_{kk}\right\|}, \tag{3.11}$$

where $k \neq \ell$. This parametrization is valuable for designing efficient low complexity distributed resource allocation schemes [9]. The set of beamforming vector in (3.11) includes maximum ratio transmission (MRT) ($\lambda_k^{\mathrm{MRT}} = \left\|\Pi_{\hat{\boldsymbol{h}}_{k\ell}} \hat{\boldsymbol{h}}_{kk}\right\|^2 / \left\|\hat{\boldsymbol{h}}_{kk}\right\|^2$) and zero forcing transmission (ZF) ($\lambda_k^{\mathrm{ZF}} = 0$). According to [11, Corollary 2], it suffices that the parameters λ_k only be from the set $[0, \lambda_k^{\mathrm{MRT}}]$ for Pareto optimal operation.

Imperfect CSI case

In case the channel knowledge at the transmitters is not perfect but lies within the uncertainty region, robust transmission can be modeled with worst case analysis. According to the SINR expression in (3.8), worst case signal power and interference powers include additive terms influenced only by the norm of the beamforming vectors. It is thus expected that robust Pareto optimal beamforming includes additionally varying transmission power.

Proposition 3.1. *The Pareto boundary of the rate region R in* (3.10) *is achieved by the beamforming vectors*

$$\mathbf{w}_k(p_k, \lambda_k) = p_k \sqrt{\lambda_k} \frac{\Pi_{\mathbf{h}_{k\ell}} \mathbf{h}_{kk}}{\|\Pi_{\mathbf{h}_{k\ell}} \mathbf{h}_{kk}\|} + p_k \sqrt{1-\lambda_k} \frac{\Pi^{\perp}_{\mathbf{h}_{k\ell}} \mathbf{h}_{kk}}{\left\|\Pi^{\perp}_{\mathbf{h}_{k\ell}} \mathbf{h}_{kk}\right\|}, \tag{3.12}$$

where $k \neq \ell, p_k \in [0,1]$, and $\lambda_k \in [0, \lambda_k^{MRT}]$, with $\lambda_k^{MRT} = \|\Pi_{\mathbf{h}_{k\ell}} \mathbf{h}_{kk}\|^2 / \|\mathbf{h}_{kk}\|^2$.

Proof: The proof is provided in [60]. ■

The result in Proposition Proposition 3.1 differs to the case with perfect CSI in (3.11) in the additional parameter which controls the power allocation. Otherwise, the estimated channels $\hat{\boldsymbol{h}}_{kk}$ and $\hat{\boldsymbol{h}}_{k\ell}$ replace the true channels from (3.11).

The beamforming vectors corresponding to MRT and ZF represent extreme strategies which have the objective of either maximizing the power at the intended receiver or minimizing the interference power gain. Robust MRT is the solution of the following problem

$$\max_{\|\mathbf{w}_k\| \leq 1} \quad |\hat{\boldsymbol{h}}_{kk}^H \mathbf{w}_k| = |\mathbf{h}_{kk}^H \mathbf{w}_k| - \|\mathbf{w}_k\| \epsilon_{kk}, \tag{3.13}$$

which is $\mathbf{w}_k^{\text{R-MRT}} = \mathbf{h}_{kk} / \|\mathbf{h}_{kk}\|$. In other words, to maximize the power gain at the intended receiver in the worst case of spherical uncertainty, the transmitter chooses full power transmission in the direction of the estimated channel. Robust ZF transmission is achieved only by allocating zero power. This is observed in the expression in (3.7) which can only be zero for $\|\mathbf{w}_k\| = 0$.

3.1.4 Efficiency in High and Low SNR

Efficiency at High SNR

The quantitative performance is analyzed using the high-SNR offset concept in [61, Section II]. Denote as $C(\rho)$ the sum rate as a function of the SNR. The high-SNR slope is

$$S_\infty = \lim_{\rho\to\infty} \frac{C(\rho)}{\log_2(\rho)} \quad \text{and} \tag{3.14}$$

which corresponds to the multiplexing gain, i.e. the slope of the sum rate curve at high SNR. The maximum sum rate for the case of perfect CSI is

$$\begin{aligned}\hat{C}(\rho) = &\max_{\lambda_1,\lambda_2} \log_2\left(1+\frac{\rho|\hat{\boldsymbol{h}}_{11}^H \mathbf{w}_1(\lambda_1)|^2}{1+\rho|\hat{\boldsymbol{h}}_{21}^H \mathbf{w}_2(\lambda_2)|^2}\right)\\ &+\log_2\left(1+\frac{\rho|\hat{\boldsymbol{h}}_{22}^H \mathbf{w}_2(\lambda_2)|^2}{1+\rho|\hat{\boldsymbol{h}}_{12}^H \mathbf{w}_1(\lambda_1)|^2}\right).\end{aligned} \tag{3.15}$$

In the high SNR regime, the maximum sum rate is achieved with ZF transmissions:

$$\begin{aligned}\hat{C}(\rho) = &\log_2\left(1+\rho|\hat{\boldsymbol{h}}_{11}^H \mathbf{w}_1(\lambda_1^{\mathrm{ZF}})|^2\right)\\ &+\log_2\left(1+\rho|\hat{\boldsymbol{h}}_{22}^H \mathbf{w}_2(\lambda_2^{\mathrm{ZF}})|^2\right),\end{aligned} \tag{3.16}$$

which gives the maximum high-SNR slope of

$$\hat{S}_\infty = \lim_{\rho\to\infty} \frac{\hat{C}(\rho)}{\log_2(\rho)} = 2. \tag{3.17}$$

The maximum sum rate for the case of imperfect CSI is

$$\begin{aligned}C(\rho) = &\max_{p_1,\lambda_1,p_2,\lambda_2} \log_2\left(1+\frac{\rho\left((|\mathbf{h}_{11}^H \mathbf{w}_1(p_1,\lambda_1)|-\epsilon_{11}p_1)^+\right)^2}{\rho(|\mathbf{h}_{21}^H \mathbf{w}_2(p_2,\lambda_2)|+\epsilon_{21}p_2)^2+1}\right)\\ &+\log_2\left(1+\frac{\rho\left((|\mathbf{h}_{22}^H \mathbf{w}_2(p_2,\lambda_2)|-\epsilon_{22}p_2)^+\right)^2}{\rho(|\mathbf{h}_{12}^H \mathbf{w}_1(p_1,\lambda_1)|+\epsilon_{12}p_1)^2+1}\right),\end{aligned} \tag{3.18}$$

where $\epsilon_{12}>0, \epsilon_{21}>0$ and $0\le\epsilon_{11}\le\|\mathbf{h}_{11}\|$ and $0\le\epsilon_{22}\le\|\mathbf{h}_{22}\|$. In the high-SNR regime single-user transmission is optimal achieving the largest high-SNR slope of $S_\infty = 1$. The maximum sum rate is

$$C(\rho) = \log_2\left(1+\rho\max_{k=1,2}\left((\|\mathbf{h}_{kk}\|^2-\epsilon_{kk})^+\right)\right), \tag{3.19}$$

where only one user operates using MRT and full power transmission. Note that the condition that determines the dominant user does not only depend on the channel gains but also on the amount of uncertainty present at the transmitter.

Efficiency at Low SNR

In [62], the low-SNR regime has been analyzed and two performance measures namely the $(E_b/N_0)_{min}$ and the wideband slope S_0 were introduced. The system parameters bandwidth B, transmission rate R, transmit power P and spectral efficiency $C(E_b/N_0)$ satisfy the fundamental limit $\frac{R}{B} \leq C\left(\frac{E_b}{N_0}\right)$. The function $C(E_b/N_0)$ is directly related to the common capacity expression $\mathcal{C}(\text{SNR})$, i.e. $C(E_b/N_0) = \mathcal{C}(\text{SNR})$ for the SNR which solves $(E_b/N_0)\mathcal{C}(\text{SNR}) = \text{SNR}$. At low SNR, the function $C(E_b/N_0)$ can be expressed as [62]

$$C\left(\frac{E_b}{N_0}\right) \approx \frac{S_0}{3dB}\left(\left(\frac{E_b}{N_0}\right)\Big|_{dB} - \left(\frac{E_b}{N_0}\right)_{min}\Big|_{dB}\right), \tag{3.20}$$

with $(E_b/N_0)_{min} = \frac{\log_e 2}{\dot{\mathcal{C}}(0)}$ and $S_0 = \frac{2\left[\dot{\mathcal{C}}(0)\right]^2}{-\ddot{\mathcal{C}}(0)}$. The closer (E_b/N_0) gets to $(E_b/N_0)_{min}$ the better is the approximation in (3.20).

For the sum spectral efficiency for perfect CSI we obtain

$$\left(\frac{E_b}{N_0}\right)_{\min}^{pCSI} = \frac{\log_e 2}{|\hat{\boldsymbol{h}}_{11}^H \mathbf{w}_1(\lambda_1)|^2 + |\hat{\boldsymbol{h}}_{22}^H \mathbf{w}_2(\lambda_2)|^2}, \tag{3.21}$$

where the minimum is achieved with $\frac{\log_e 2}{\|\hat{\boldsymbol{h}}_{11}\|^2 + \|\hat{\boldsymbol{h}}_{22}\|^2}$ corresponding to MRT transmission. For the case of imperfect CSI, we obtain

$$\left(\frac{E_b}{N_0}\right)_{\min}^{iCSI} = \frac{\log_e 2}{(\left\|\hat{\boldsymbol{h}}_{11}\right\| - \epsilon_{11})^2 + (\left\|\hat{\boldsymbol{h}}_{22}\right\| - \epsilon_{22})^2}, \tag{3.22}$$

which clearly shows the loss due to channel uncertainty.

3.1.5 Illustrations

In Figure 3.1, three rate regions are plotted. The largest region corresponds to the case of perfect CSI where the Pareto boundary is attained from (3.11). The second largest region corresponds to the case of imperfect CSI. For this case, we fix $\epsilon_{kk} = \epsilon_{k\ell} = 0.1$ and generate the beamforming vectors characterized in Proposition Proposition 3.1. We choose for the parameters p_k 10 samples uniformly in $[0, 1]$. For the parameters λ_k we chose 20 samples uniformly in the range $[0, \lambda_k^{\text{MRT}}]$. The

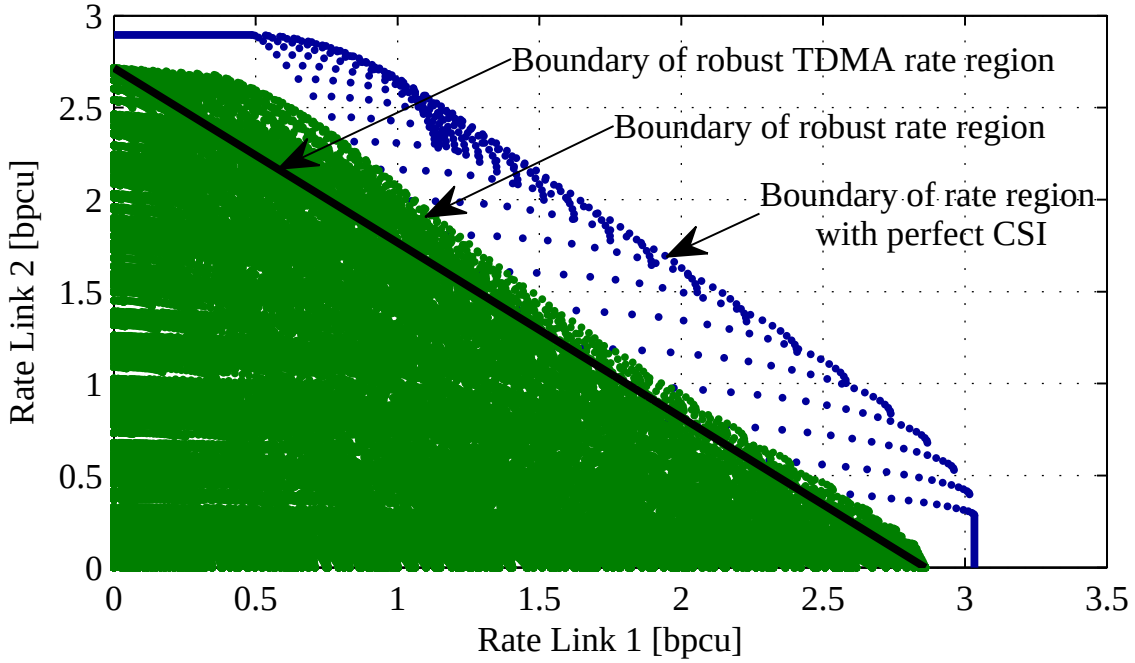

Figure 3.1: Comparison of rate regions for perfect CSI, imperfect CSI and TDMA with imperfect CSI. Two antennas are used at the transmitters, with 5 dB SNR and $\epsilon_{kk} = \epsilon_{k\ell} = 0.1$

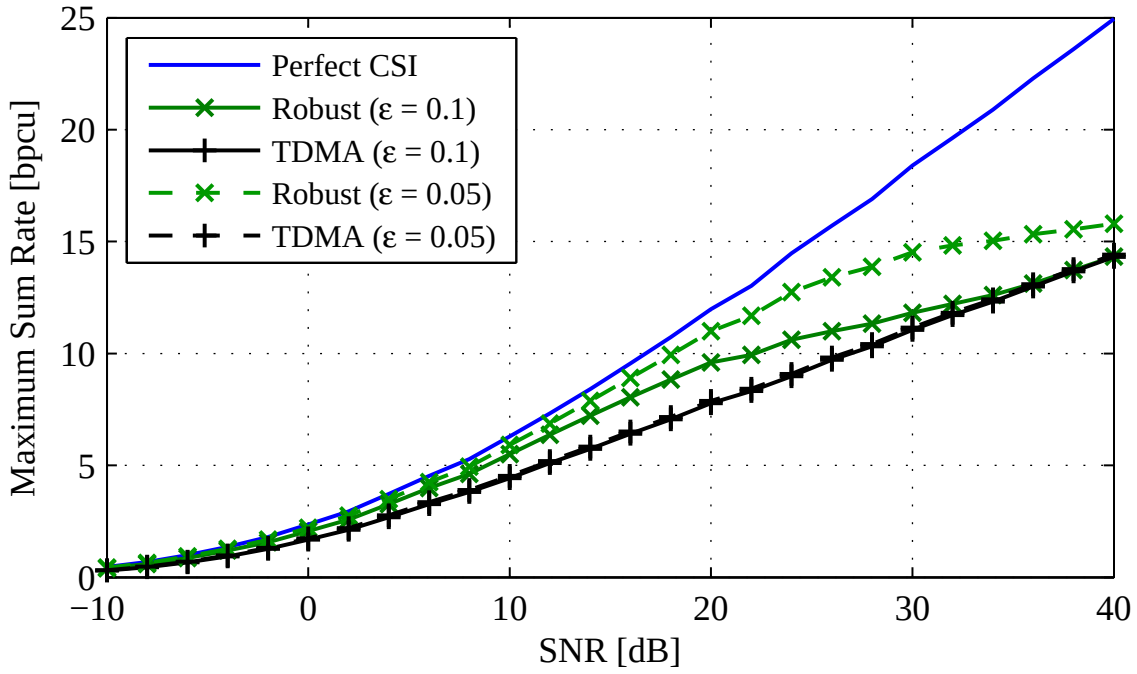

Figure 3.2: Comparison of maximum sum rates ($\epsilon = \epsilon_{kk} = \epsilon_{k\ell}$). Two antennas are used at the transmitters.

smallest region corresponds to TDMA with imperfect CSI. The region is a triangle with two corners at the axes corresponding to the single-user points.

In Figure 3.2, maximum sum rate is plotted for different SNR levels. We compare the cases of perfect CSI, imperfect CSI, and TDMA with imperfect CSI. We generate 1000 random channel realizations and average over achievable sum rates. For each channel realization, the maximum sum rate point is found by a grid search over the rate samples corresponding to the parameterized beamforming vectors. In the case of perfect CSI, we used the parametrization in (3.11), and for the imperfect CSI case we used the parametrization in Proposition Proposition 3.1. For each parametrization, we generate 100 samples uniformly in the ranges of the parameters. The estimation error amplitude is equally chosen for all channels such that $\epsilon = \epsilon_{kk} = \epsilon_{k\ell}$. The plots are generated for two values of ϵ, 0.1 and 0.5. The sum rate in TDMA is determined as the maximum of the single-user rates. The gain in spectrum sharing for the case of imperfect CSI to that of TDMA is observed as the distance between the two curves. This distance is highest in the mid SNR regime and increases for smaller ϵ, i.e., less channel uncertainty. The performance of spectrum sharing and TDMA is the same for low and high SNRs. The high-SNR slope for the imperfect CSI is 1 and for the perfect CSI case is 2 as calculated in Section 3.1.4. In the high SNR regime, ZF transmission is optimal to achieve maximum sum rate. In the low SNR regime, MRT is sum rate optimal and all curves in Figure 3.2 overlap.

3.1.6 Conclusions

In this work, we studied robust Pareto optimal beamforming in a two-user multiple-input single-output interference channel. It turns out that a similar beamforming parametrization can be used as in the perfect CSI case. However, additional power allocation is necessary. Since ZF beamforming is not possible due to uncertainty, the achievable high SNR sum rate converges to the TDMA case with slope one.

For future work, we plan to extend the setting to the K-user scenario and include also ellipsoidal uncertainty regions. Furthermore, an important question is related to strategic bargaining in interference channels with imperfect channel state information.

3.2 Outage Rate Regions for the MISO Interference Channel

We consider the two-user MISO IC, consisting of two transmitter (TX) - receiver (RX) pairs (or else links). The TXs employ multiple antennas and the RXs a single antenna. The transmissions are concurrent and cochannel; hence, they interfere with each other. We assume that the channels are flat and slow fading. The latter means that the coherence time of the channels is longer than the codeword length. We assume that TX_i encodes data at rate R_i. If the channels are in fading states that cannot support this rate, the decoding error probability cannot be arbitrarily small and the link is in *outage* [32, Ch. 5]. The fundamental question raised is which rates can be achieved for given specifications on the outage probabilities of the links, i.e. how to define the *outage* rate region?

Previous work on the MISO IC rate regions has focused on scenarios without the possibility of allowing the links to be in outage; specifically, on the achievable *instantaneous* and *ergodic* rate regions. In [38], the authors characterized the transmit strategies, which yield operating points on the outer boundary of the instantaneous rate region. This refers to the scenario that the TXs have instantaneous CSI, i.e. they perfectly know the realizations of the channel vectors. In [63], the characterization in [38] was extended to the ergodic rate region. There, the TXs have statistical CSI, i.e, they assume that the channels are zero-mean complex Gaussian random variables with known covariance matrices. The ergodic rate is a long-term achievable rate, averaged over the time-varying channel and requires coding across an infinite number of channel realizations. However, for some applications (e.g. real-time), we cannot tolerate these coding delays. If we accept that the transmission is in outage during severe fading, then we can achieve higher rates when the channel conditions are good. For some applications, e.g. voice or video communications, we can tolerate some data loss without appreciably degrading the call quality.

The outage probability for a single-user multi-antenna link with statistical CSI was

studied in [64]. For the scenario of spatially white channel vectors and very low SNR, it was shown that it is optimal for the TX to use only some of its antennas. Also, a scheme was proposed to find locally-optimal power allocations when the channel vectors are correlated.

In multi-user systems, such as those modeled via the IC, broadcast channel (BC), and multiple-access channel (MAC), one can consider *individual* or *common* outage. By individual outage we refer to the event that a specific user is unable to communicate with its desired rate. For this scenario, there is an outage probability specification for each link. That is, one link might be declared in outage when others support their desired rates. Common outage is declared if the rate of at least one link cannot be supported (see, e.g. [65] for the MAC). Therefore, the common outage probability is specified for the entire multi-user system. Common outage might be of interest in applications where the transmitted information is useful only when all RXs can obtain it simultaneously [66], e.g., multicast channels [67].

All studies so far of the outage rate regions have been restricted to the single-antenna BC and MAC [66, 65, 68, 69]. The outage capacity regions for the BC were studied in [66] for the case of instantaneous CSI and bounded time-averaged total transmit power. First, outage regions were determined for superposition coding (with and without successive decoding) and time division (TD). Superposition coding implies simultaneous and cochannel transmissions, whereas TD means that transmissions are separated in time. Second, outage capacity regions were determined for both individual and common outage probability specifications. It was shown that the outage capacity regions are implicitly obtained from the outage probability regions for a given rate vector. For different spectrum sharing methods and given rate points, power allocations that bound the outage probabilities were found.

Outage capacity regions for the MAC were studied in [65], again for instantaneous CSI. Given a required rate and an average power constraint, a successive decoding strategy and an optimal power allocation policy for achieving points on the boundary were determined. Both common and individual outage were discussed. In [69], outage capacity regions were studied for a cognitive radio network that constitutes a MAC operating on the same spectrum with an existing primary network. Under an interference power constraint together with the individual transmit power constraint of each user, the outage capacity regions for the cognitive MAC were defined for individual and common outage specifications. The optimal power allocation strategies that achieve the boundary points of the regions were derived by maximizing the usage (i.e. non-outage) probability for given rate vectors. The case of statistical TX CSI, with channels modeled as i.i.d. zero-mean Gaussian with unit variance, was treated in [68].

Up to our knowledge, there are no published results on definitions and characterizations of the outage rate regions for the IC. However, various methods have been proposed to find specific operating points and the enabling transmission schemes. For example, in [70], the optimal power allocations were found, given transmission

rates and outage probability specifications. Also, in [71], for given rates, the outage probabilities were minimized taking into account the cost of power consumption. The results of [70] were derived under the assumption of statistical CSI at the TXs with channels modeled as zero-mean Gaussian with general variance. The same channel model was considered in [72], where it was assumed that the RXs can decode interference and rate splitting was used. The asymptotic behavior of the outage probability in the interference-limited regime was studied. Upper and lower bounds on the exponent of the outage probability for the IC were derived. The two-user SISO IC with mixed channel knowledge was studied in [71], where it was assumed that each TX has perfect knowledge of the direct channel and statistical knowledge of the forward crosstalk channel. The power and rate allocation problem was considered based on the throughput accounting for the outage event. The proposed algorithms were based on either Bayesian games or optimization. In [73], the results in [74] were used to solve the weighted sum-rate maximization under outage constraints for the MISO IC. It was assumed that the TXs have statistical CSI and the problem was solved via a convex optimization approach.

Contributions and Organization

In this section, we propose a two-fold generalization of the outage rate regions definitions for multiuser systems. Not only we consider the IC, which is a generalization of the BC and MAC, but we do so for multi-antenna transmitters. In Section 3.2.1, we describe the system model. Our contributions are organized as follows:

- In Sections 3.2.2 and 3.2.2, we consider the statistical CSI case and propose definitions for the common and individual outage rate regions, respectively. We discuss the interpretations of the regions. Compared to [74], we extend the single-stream transmission scheme to multi-stream.
- In Section 3.2.2, we show how the outage probability can be obtained in closed-form.
- In Sections 3.2.3 and 3.2.3, we consider the instantaneous CSI case and propose definitions for the common and individual outage rate regions, respectively. We discuss the interpretations of the regions. Compared to [74], we propose a definition for the individual outage region.
- In Section 3.2.4, we give a numerical example and observe a number of relations between the regions. We formalize and prove these relations.

Finally, in Section 3.2.5, we summarize the conclusions of this study.

For the ease of notations, by $\mathbf{x} \sim \mathcal{CN}(\mathbf{0}, \boldsymbol{Q})$ we say that $\mathbf{x}$ is a zero-mean complex-symmetric Gaussian random vector with covariance matrix $\boldsymbol{Q}$. We define the index set $\mathcal{I} \triangleq \{(1,2),(2,1)\}$.

3.2.1 System Model

We consider the two-user MISO IC, where the receivers treat the interference as additive Gaussian noise, the transmit power is bounded, the channels experience slow fading and a non-zero probability of outage is allowed. We assume that each TX employs n antenna elements. TX_i transmits a vector $\mathbf{x}_i \in \mathbb{C}^n \sim \mathcal{CN}(\mathbf{0}, \mathbf{\Psi}_i)$, with covariance matrix $\mathbf{\Psi}_i = \mathrm{E}\{\mathbf{x}_i \mathbf{x}_i^H\}$. The matched-filtered symbol-sampled complex baseband data received by RX_i is modeled as

$$y_i = \mathbf{h}_{ii}^H \mathbf{x}_i + \mathbf{h}_{ji}^H \mathbf{x}_j + e_i, \qquad (i,j) \in \mathcal{I}, \tag{3.23}$$

where e_i is i.i.d. zero-mean Gaussian noise with variance σ_i^2. The conjugated[1] channel vector $\mathbf{h}_{ij} \in \mathbb{C}^n$ between TX_i and RX_j is modeled as $\mathbf{h}_{ij} \sim \mathcal{CN}(\mathbf{0}, \boldsymbol{Q}_{ij})$. We assume that the channel vectors $\{\mathbf{h}_{ij}\}_{i,j=1}^2$ are statistically independent.

Due to regulatory and hardware constraints, the transmit power is constrained. Without loss of generality we set this bound to

$$\mathrm{E}\{\|\mathbf{x}_i\|^2\} = \mathrm{E}\{\mathrm{trace}\{\mathbf{x}_i \mathbf{x}_i^H\}\} = \mathrm{trace}\{\mathbf{\Psi}_i\} \leq 1. \tag{3.24}$$

Hence, the set of feasible transmit covariance matrices $\mathcal{W}_{\mathbf{\Psi}}$ consists of all positive semi-definite $n \times n$ matrices whose trace is at most one, i.e.

$$\mathcal{W}_{\mathbf{\Psi}} \triangleq \{\mathbf{\Psi} \in \mathbb{C}^{n \times n} : \mathbf{\Psi} \succeq \mathbf{0}, \ \mathrm{trace}\{\mathbf{\Psi}\} \leq 1\}. \tag{3.25}$$

The transmit covariance matrix $\mathbf{\Psi}_i$ can potentially be of any $\mathrm{rank}\{\mathbf{\Psi}_i\} \leq n$. The optimal choice of number N_i of transmitted streams depends on the CSI available at TX_i. For instantaneous CSI, single-stream transmission, i.e. $N_i = 1$, is optimal [75] and this means that $\mathbf{\Psi}_i$ is rank-one. However, for statistical CSI, multi-stream transmission, i.e. $N_i \geq 1$, is in general optimal [76]. In principle, the number of transmitted streams may be any positive integer. Without loss of generality, we can assume that $N_i \leq n$. If we have more than n streams, then stream $n+1$ must be a linear combination of streams $1, \ldots, n$. Hence, equivalently to transmitting stream $n+1$, streams $1, \ldots, n$ could be modified. The notation of the rate expression differs somewhat between the multi-stream and single-stream scenarios; therefore, we present them separately.

Multi-Stream Transmission

In this section, we illustrate how the symbol vector $\mathbf{x}_i \sim \mathcal{CN}(\mathbf{0}, \mathbf{\Psi}_i)$ is constructed [64]. TX_i splits the incoming data stream s_i into N_i parallel data streams $s_{i,1}, \ldots, s_{i,N_i}$. Data stream l of TX_i, $s_{i,l}$, is then scaled by a factor $\sqrt{p_{i,l}}$ and a unit-norm beam-shaping vector $\mathbf{u}_{i,l}$. We assume that the vectors $\mathbf{u}_{i,1}, \ldots, \mathbf{u}_{i,N_i}$ are orthogonal. This

[1] We incorporate conjugation in definition to simplify subsequent notation.

scheme is depicted in Fig. 3.3. We define $\mathbf{w}_{i,l} \triangleq \sqrt{p_{i,l}}\mathbf{u}_{i,l}$ to be the effective beamforming vector of stream l of TX_i. Summing up the parallel weighted streams, we get the transmitted vector

$$\mathbf{x}_i = \sum_{l=1}^{N_i} \sqrt{p_{i,l}}\mathbf{u}_{i,l}s_{i,l} = \boldsymbol{P}_i^{1/2}\boldsymbol{U}_i\boldsymbol{s}_i, = \boldsymbol{W}_i\boldsymbol{s}_i = \sum_{l=1}^{N_i} \mathbf{w}_{i,l}s_{i,l}, \tag{3.26}$$

where $\boldsymbol{P}_i = \mathrm{diag}\{p_{i,1}, \ldots, p_{i,N_i}\}$, $\boldsymbol{U}_i = [\mathbf{u}_{i,1}, \ldots, \mathbf{u}_{i,N_i}]$ is a semi-unitary matrix, $\boldsymbol{s}_i = [s_{i,1}, \ldots, s_{i,N_i}]^T$ is the vector of transmitted symbols, and $\boldsymbol{W} = [\mathbf{w}_{i,1}, \ldots, \mathbf{w}_{i,N_i}]$. Assuming that $\mathrm{E}\{\boldsymbol{s}_i\boldsymbol{s}_i^H\} = \mathbf{I}$, i.e. the streams are statistically independent with unit average power, we have

$$\boldsymbol{\Psi}_i = \mathrm{E}\{\mathbf{x}_i\mathbf{x}_i^H\} = \mathrm{E}\{\boldsymbol{W}_i\boldsymbol{s}_i\boldsymbol{s}_i^H\boldsymbol{W}_i^H\} = \boldsymbol{W}_i\boldsymbol{W}_i^H = \boldsymbol{U}_i\boldsymbol{P}_i\boldsymbol{U}_i^H. \tag{3.27}$$

The power constraint (3.24) can be rewritten as

$$\mathrm{E}\{\|\mathbf{x}_i\|^2\} = \mathrm{trace}\{\boldsymbol{\Psi}_i\} = \mathrm{trace}\{\boldsymbol{U}_i\boldsymbol{P}_i\boldsymbol{U}_i^H\} = \mathrm{trace}\{\boldsymbol{P}_i\} = \sum_{l=1}^{N_i} p_{i,l} \leq 1. \tag{3.28}$$

Assuming that RX_i treats the signal from TX_j as additive noise, the achievable rate, in bits per channel use, of link i as a function of the channel vectors and transmit covariance matrices is given by

$$R_i(\mathbf{h}_{ii}, \mathbf{h}_{ji}, \boldsymbol{\Psi}_i, \boldsymbol{\Psi}_j) = \log_2\left(1 + \frac{\mathbf{h}_{ii}^H\boldsymbol{\Psi}_i\mathbf{h}_{ii}}{\mathbf{h}_{ji}^H\boldsymbol{\Psi}_j\mathbf{h}_{ji} + \sigma_i^2}\right). \tag{3.29}$$

The rate in (3.29) is achieved when RX_i uses multiuser detection to decode the streams intended for it and treats the interfering streams (from TX_j) as noise. It is further assumed that TX_i performs an appropriate rate and power allocation over the streams $s_{i,1}, \ldots, s_{i,N_i}$. In order to illustrate this point, we sum up interference and noise into a new variable $z_i \triangleq \mathbf{h}_{ji}^H\mathbf{x}_j + e_i$ and get

$$y_i = \mathbf{h}_{ii}^H\mathbf{x}_i + z_i = \sum_{l=1}^{N_i} \mathbf{h}_{ii}^H\mathbf{w}_{i,l}s_{i,l} + z_i = \sum_{l=1}^{N_i} \alpha_{i,l}s_{i,l} + z_i, \tag{3.30}$$

where $\alpha_{i,l} \triangleq \mathbf{h}_{ii}^H\mathbf{w}_{i,l}$. We can interpret (3.30) as the received signal in a MAC of N_i TXs, each transmitting a single stream, where $s_{i,l}$ is the symbol from TX_l and $\alpha_{i,l}$ is the gain of the channel between TX_l and the receiver. By performing multiuser detection, we can achieve the sum-capacity [32, Ch. 6]

$$C_{\mathrm{sum}} = \log_2\left(1 + \frac{\sum_{l=1}^{N_i}|\alpha_{i,l}|^2}{\mathrm{E}\{|z_i|^2\}}\right). \tag{3.31}$$

Single-Stream Transmission

When single-stream transmission is used, the transmitted symbol vector can be written as $\mathbf{x}_i = \mathbf{w}_i s_i$, which gives us $\mathbf{\Psi}_i = \mathbf{w}_i \mathbf{w}_i^H$. In this case, the power constraint (3.28) reads

$$\mathrm{E}\{\|\mathbf{x}_i\|^2\} = \mathrm{E}\{|s_i|^2\}\,\|\mathbf{w}_i\|^2 = \|\mathbf{w}_i\|^2 \leq 1. \tag{3.32}$$

Hence, we get the feasible set of beamforming vectors

$$\mathcal{W}_{\mathbf{w}} \triangleq \{\mathbf{w} \in \mathbb{C}^n : \|\mathbf{w}\|^2 \leq 1\}. \tag{3.33}$$

Then, the maximum achievable rate of link i in bits per channel use, (3.29), can be written as

$$R_i(\mathbf{h}_{ii}, \mathbf{h}_{ji}, \mathbf{w}_i, \mathbf{w}_j) = \log_2\left(1 + \frac{\mathbf{h}_{ii}^H\,\mathrm{E}\{\mathbf{x}_i\mathbf{x}_i^H\}\,\mathbf{h}_{ii}}{\mathbf{h}_{ji}^H\,\mathrm{E}\{\mathbf{x}_j\mathbf{x}_j^H\}\,\mathbf{h}_{ji} + \sigma_i^2}\right) = \log_2\left(1 + \frac{|\mathbf{h}_{ii}^H\mathbf{w}_i|^2}{|\mathbf{h}_{ji}^H\mathbf{w}_j|^2 + \sigma_i^2}\right). \tag{3.34}$$

3.2.2 Outage Rate Regions for Statistical CSI

In this section, we assume that the TXs have statistical CSI; hence, they can only adapt their transmit covariance matrices to the statistical distributions of the channels. When a TX chooses a rate, it continues transmitting with this rate as if the RX is able to correctly decode it, no matter if the communication is actually in outage or not. Under these assumptions, we would like to find the outage rate region, which consists of all the rate pairs that can be achieved given common or individual outage specifications.

We determine the outage rate region in two steps. Given a pair of transmit covariance matrices, the rates in (3.29) are functions of the random channels; hence, they are random variables. Using these transmit covariance matrices, we find the set of rate points which are achievable for a specific outage probability specification. It is apparent that each choice of transmit covariance matrices yields a different rate region, that we denote $\mathcal{R}_{\mathbf{\Psi}}$. Second, we define the outage rate region as the union of all these regions $\mathcal{R}_{\mathbf{\Psi}}$. In the following, we consider the cases of common and individual outage probabilities, in Sections 3.2.2 and 3.2.2, respectively.

Common Outage Rate Region for Statistical CSI

We denote by $\mathcal{R}_{\text{stat}}^{\text{com}}(\epsilon)$ the sought common outage rate region for statistical CSI, where $\epsilon > 0$ is the common outage probability specification. We say that a rate point (r_1, r_2) is in $\mathcal{R}_{\text{stat}}^{\text{com}}(\epsilon)$ if there exists a pair of transmit covariance matrices $(\mathbf{\Psi}_1, \mathbf{\Psi}_2)$, such that r_1 and r_2 are achieved with probability at least $1 - \epsilon$. That is, the chance is at least $1 - \epsilon$ that the channels are in fading states which enable

the links to operate simultaneously at rates r_1 and r_2. In this case, an outage is declared when either (or both) RX(s) cannot correctly decode the received data.

Let us assume a specific choice of transmit covariance matrices $(\mathbf{\Psi}_1, \mathbf{\Psi}_2)$. Then, using these matrices, the common usage (i.e. non-outage) probability of rate point (r_1, r_2) is

$$U_{\text{com}}^{\text{stat}}(r_1, r_2, \mathbf{\Psi}_1, \mathbf{\Psi}_2) \triangleq \Pr\left\{ \bigcap_{(i,j)\in\mathcal{J}} \{R_i(\mathbf{h}_{ii}, \mathbf{h}_{ji}, \mathbf{\Psi}_1, \mathbf{\Psi}_2) > r_i\} \middle| \mathbf{\Psi}_1, \mathbf{\Psi}_2 \right\}. \tag{3.35}$$

With this specific $(\mathbf{\Psi}_1, \mathbf{\Psi}_2)$, a common outage rate region is achieved, consisting of the rate points that have common usage probability at least $1-\epsilon$, i.e.

$$\mathcal{R}_{\mathbf{\Psi}}^{\text{com}}(\epsilon, \mathbf{\Psi}_1, \mathbf{\Psi}_2) = \left\{(r_1, r_2) : U_{\text{com}}^{\text{stat}}(r_1, r_2, \mathbf{\Psi}_1, \mathbf{\Psi}_2) \geq 1-\epsilon\right\}. \tag{3.36}$$

Considering all possible choices for $(\mathbf{\Psi}_1, \mathbf{\Psi}_2)$, the *overall* common outage rate region for statistical CSI is the union of the regions in (3.36).

Definition 1. Let $\epsilon > 0$ denote the *common* outage probability specification. The common outage rate region for statistical CSI is the set of rate points (r_1, r_2) that can be achieved with probability at least $1-\epsilon$, using a pair of feasible transmit covariance matrices $(\mathbf{\Psi}_1, \mathbf{\Psi}_2)$, i.e.

$$\mathcal{R}_{\text{stat}}^{\text{com}}(\epsilon) = \bigcup_{(\mathbf{\Psi}_1, \mathbf{\Psi}_2)\in\mathcal{W}_{\mathbf{\Psi}}^2} \left\{(r_1, r_2) : U_{\text{com}}^{\text{stat}}(r_1, r_2, \mathbf{\Psi}_1, \mathbf{\Psi}_2) \geq 1-\epsilon\right\}. \tag{3.37}$$

Individual Outage Rate Region for Statistical CSI

We denote by $\mathcal{R}_{\text{stat}}^{\text{ind}}(\epsilon_1, \epsilon_2)$ the sought individual outage rate region for statistical CSI, where $\epsilon_1 > 0$ and $\epsilon_2 > 0$ are the individual outage probability specifications for links 1 and 2, respectively. A rate point (r_1, r_2) is in $\mathcal{R}_{\text{stat}}^{\text{ind}}(\epsilon_1, \epsilon_2)$, if there exists a pair of transmit covariance matrices such that r_1 and r_2 are achieved with probabilities at least $1-\epsilon_1$ and $1-\epsilon_2$, respectively.

Let us denote the individual usage probability of link i, for a specific rate value r_i and pair of transmit covariance matrices $(\mathbf{\Psi}_1, \mathbf{\Psi}_2)$, as

$$U_i^{\text{stat}}(r_i, \mathbf{\Psi}_1, \mathbf{\Psi}_2) \triangleq \Pr\{R_i(\mathbf{h}_{ii}, \mathbf{h}_{ji}, \mathbf{\Psi}_1, \mathbf{\Psi}_2) \geq r_i | \mathbf{\Psi}_1, \mathbf{\Psi}_2\}, \quad (i,j) \in \mathcal{J}. \tag{3.38}$$

With this specific $(\mathbf{\Psi}_1, \mathbf{\Psi}_2)$, an individual outage rate region is achieved, consisting of the rate points that have individual usage probabilities at least $1-\epsilon_i$,

$$\mathcal{R}_{\mathbf{\Psi}}^{\text{ind}}(\epsilon_1, \epsilon_2, \mathbf{\Psi}_1, \mathbf{\Psi}_2) = \{(r_1, r_2) : U_1^{\text{stat}}(r_1, \mathbf{\Psi}_1, \mathbf{\Psi}_2) \geq 1-\epsilon_1,\ U_2^{\text{stat}}(r_2, \mathbf{\Psi}_1, \mathbf{\Psi}_2) \geq 1-\epsilon_2\}. \tag{3.39}$$

Considering all possible choices for $(\mathbf{\Psi}_1, \mathbf{\Psi}_2)$, the *overall* individual outage rate region for statistical CSI is the union of the regions in (3.39). Note that the region

$\mathcal{R}^{\text{ind}}_{\mathbf{\Psi}}$ defined in (3.39) has a rectangular shape. Its north-east corner is the point (r_1, r_2) where the usage probabilities in (3.39) are exactly $1-\epsilon_1$ and $1-\epsilon_2$. On the contrary, the common outage rate region $\mathcal{R}^{\text{com}}_{\mathbf{\Psi}}$ defined in (3.36) is not rectangular.

Definition 2. Let $\epsilon_1 > 0$ and $\epsilon_2 > 0$ denote the *individual* outage probability specifications. The individual outage rate region for statistical CSI is the set of rate points (r_1, r_2) such that r_1 and r_2 are achieved with probabilities at least $1-\epsilon_1$ and $1-\epsilon_2$, respectively, using a pair of feasible transmit covariance matrices $(\mathbf{\Psi}_1, \mathbf{\Psi}_2)$, i.e.

$$\mathcal{R}^{\text{ind}}_{\text{stat}}(\epsilon_1, \epsilon_2) = \bigcup_{(\mathbf{\Psi}_1, \mathbf{\Psi}_2) \in \mathcal{W}^2_{\mathbf{\Psi}}} \{(r_1, r_2) : U^{\text{stat}}_1(r_1, \mathbf{\Psi}_1, \mathbf{\Psi}_2) \geq 1-\epsilon_1,\ \ U^{\text{stat}}_2(r_2, \mathbf{\Psi}_1, \mathbf{\Psi}_2) \geq 1-\epsilon_2\}. \tag{3.40}$$

Usage Probabilities for Statistical CSI

In this section, we discuss how to to find the usage probabilities in closed-form. We begin by showing that the common usage probability is equal to the product of the individual ones. We see from (3.29) that, for a specific $(\mathbf{\Psi}_1, \mathbf{\Psi}_2)$, the rates of links 1 and 2 depend on different pairs of channel vectors. Since the channel vectors are independent, the rates are independent too. Hence, the events intersected in the probability term of (3.35) are independent and we can use (3.38) to rewrite (3.35) as a product of the individual usage probabilities, i.e,

$$U^{\text{stat}}_{\text{com}}(r_1, r_2, \mathbf{\Psi}_1, \mathbf{\Psi}_2) = U^{\text{stat}}_1(r_1, \mathbf{\Psi}_1, \mathbf{\Psi}_2) U^{\text{stat}}_2(r_2, \mathbf{\Psi}_1, \mathbf{\Psi}_2). \tag{3.41}$$

Note that (3.41) holds for any distribution of the channels, provided they are independent.

Due to (3.41), we can focus on the individual usage probability for link i. We use (3.29) and exploit the knowledge of channels' distributions to elaborate (3.38) as

$$\begin{aligned} U^{\text{stat}}_i(r_i, \mathbf{\Psi}_1, \mathbf{\Psi}_2) &= \Pr\left\{ \log_2\left(1 + \frac{\mathbf{h}^H_{ii} \mathbf{\Psi}_i \mathbf{h}_{ii}}{\mathbf{h}^H_{ji} \mathbf{\Psi}_j \mathbf{h}_{ji} + \sigma^2_i}\right) > r_i \right\} \\ &= \Pr\left\{ \mathbf{h}^H_{ii} \mathbf{\Psi}_i \mathbf{h}_{ii} - (2^{r_i} - 1) \mathbf{h}^H_{ji} \mathbf{\Psi}_j \mathbf{h}_{ji} > (2^{r_i} - 1)\sigma^2_i \right\} \\ &= \Pr\left\{ \mathbf{h}^H_{ii} \mathbf{\Psi}_i \mathbf{h}_{ii} - \gamma_i \mathbf{h}^H_{ji} \mathbf{\Psi}_j \mathbf{h}_{ji} > \gamma_i \sigma^2_i \right\}. \end{aligned} \tag{3.42}$$

In (3.42), we defined $\gamma_i \triangleq 2^{r_i} - 1$ to be the signal-to-interference-plus-noise ratio (SINR) that yields, due to (3.29), rate r_i. In Appendix 3.2.6, we explain how one can derive the closed-form expression of (3.42). Using that result, we can write (3.42) as

$$U^{\text{stat}}_i(\gamma_i, \mathbf{\Psi}_1, \mathbf{\Psi}_2) = \sum_{k=1}^{N_i} \sum_{l=1}^{N_j} \frac{\chi_{ii,k} \chi_{ji,l} \lambda_{ii,k}}{\lambda_{ii,k} + \gamma_i \lambda_{ji,l}} \exp\left(-\frac{\gamma_i \sigma^2_i}{\lambda_{ii,k}}\right), \tag{3.43}$$

where $\lambda_{ji,k}$ is the kth eigenvalue of $\boldsymbol{Q}_{ji}^{1/2}\boldsymbol{\Psi}_j\boldsymbol{Q}_{ji}^{1/2}$ and

$$\chi_{ji,k} \triangleq \prod_{n=1,n\neq k}^{N_j} \frac{\lambda_{ji,k}}{\lambda_{ji,k}-\lambda_{ji,n}}. \tag{3.44}$$

The result in (3.43) holds under the assumption that the non-zero eigenvalues of the matrices of the form $\boldsymbol{Q}^{1/2}\boldsymbol{\Psi}\boldsymbol{Q}^{1/2}$ are distinct. The derivation of (3.43) capitalizes on the fact that the random variables of the form $\mathbf{h}^H\boldsymbol{\Psi}\mathbf{h}$ are hypoexponentially distributed. For the single-stream transmission case, (3.43) can be written as

$$U_i^{\text{stat}}(\gamma_i,\mathbf{w}_1,\mathbf{w}_2) = \frac{\mathbf{w}_i^H\boldsymbol{Q}_{ii}\mathbf{w}_i}{\mathbf{w}_i^H\boldsymbol{Q}_{ii}\mathbf{w}_i+\gamma_i\mathbf{w}_j^H\boldsymbol{Q}_{ji}\mathbf{w}_j}e^{-\frac{\gamma_i\sigma_i^2}{\mathbf{w}_i^H\boldsymbol{Q}_{ii}\mathbf{w}_i}}. \tag{3.45}$$

The quadratic terms of the form $\mathbf{w}^H\boldsymbol{Q}\mathbf{w}$ are the mean of the random variables of the form $\mathbf{h}^H\boldsymbol{\Psi}\mathbf{h}$. For single-stream beamforming, we write this as $\mathbf{h}^H\mathbf{w}\mathbf{w}^H\mathbf{h}$, which is exponentially distributed with mean $\mathbf{w}^H\boldsymbol{Q}\mathbf{w}$.

3.2.3 Outage Rate Region for Instantaneous CSI

In this section, we assume that the TXs have instantaneous CSI so that they can adapt their beamforming vectors to the current fading state. Based on this, we provide two definitions for the outage rate region of the two-user MISO IC with instantaneous CSI. We consider the cases of common and individual outage probabilities, in Sections 3.2.3 and 3.2.3, respectively.

We again follow a two-step approach, but now we first consider a given realization of the channels; thus, the rates in (3.34) are functions only of the beamforming vectors. Then, for this realization, we define the region $\mathcal{R}_{\mathbf{h}}$ consisting of the rate points that can be achieved using all possible pairs of beamforming vectors, i.e.

$$\mathcal{R}_{\mathbf{h}}(\mathbf{h}_{11},\mathbf{h}_{21},\mathbf{h}_{22},\mathbf{h}_{12}) = \bigcup_{(\mathbf{w}_1,\mathbf{w}_2)\in\mathcal{W}_{\mathbf{w}}^2} \left(R_1(\mathbf{h}_{11},\mathbf{h}_{21},\mathbf{w}_1,\mathbf{w}_2), R_2(\mathbf{h}_{22},\mathbf{h}_{12},\mathbf{w}_1,\mathbf{w}_2)\right). \tag{3.46}$$

The instantaneous rate region of (3.46) has been the topic of many previous studies; see, e.g. [38] and references therein. We denote the maximum rate for link i as

$$S_i(\mathbf{h}_{ii}) \triangleq \log_2\left(1+\|\mathbf{h}_{ii}\|^2/\sigma_i^2\right). \tag{3.47}$$

This is the rate that corresponds to the point where the outer boundary of $\mathcal{R}_{\mathbf{h}}$ meets the ith rate axis. It is achieved when TX_i uses the maximum-ratio beamforming vector, i.e. $\mathbf{w}_i = \mathbf{h}_{ii}/\|\mathbf{h}_{ii}\|$, and TX_j creates no interference to RX_i, either by not transmitting or by transmitting into the nullspace of $\mathbf{h}_{ji}$; see, e.g. [38].

Common Outage Rate Region for Instantaneous CSI

We denote by $\mathcal{R}_{\text{inst}}^{\text{com}}(\epsilon)$ the sought common outage rate region for instantaneous CSI. We say that a rate point (r_1, r_2) is in $\mathcal{R}_{\text{inst}}^{\text{com}}(\epsilon)$, if the chance is at least $1-\epsilon$, that the fading state is such that operation at this rate point is possible. Here, being able to operate means that we can find a pair of feasible beamforming vectors that yields the rate point in question.

Contrary to in Section 3.2.2, we define the usage probabilities for instantaneous CSI taking into account all feasible pairs of beamforming vectors. It is apparent that each fading state yields a different achievable instantaneous rate region $\mathcal{R}_{\mathbf{h}}$, defined in (3.46). Since $\mathcal{R}_{\mathbf{h}}$ is a function of the random channels, it may be seen as a random variable. Drawing an arbitrary realization of $\mathcal{R}_{\mathbf{h}}$, the common usage probability of a rate point (r_1, r_2) is the probability that this point lies within this realization, i.e.

$$U_{\text{com}}^{\text{inst}}(r_1, r_2) \triangleq \Pr\{(r_1, r_2) \in \mathcal{R}_{\mathbf{h}}\}. \tag{3.48}$$

Definition 3. Let $\epsilon > 0$ denote the common outage probability specification. The common outage rate region for instantaneous CSI is the set of all rate points (r_1, r_2) that can be achieved with probability at least $1-\epsilon$, using a pair of feasible beamforming vectors $(\mathbf{w}_1, \mathbf{w}_2)$, i.e.

$$\mathcal{R}_{\text{inst}}^{\text{com}}(\epsilon) = \left\{(r_1, r_2) : U_{\text{com}}^{\text{inst}}(r_1, r_2) \geq 1-\epsilon\right\}. \tag{3.49}$$

Individual Outage Rate Region for Instantaneous CSI

We denote by $\mathcal{R}_{\text{inst}}^{\text{ind}}(\epsilon_1, \epsilon_2)$ the sought individual outage rate region for instantaneous CSI. At first glance, one might be misled to give the following straightforward definition for the individual rate region: "A point (r_1, r_2) is in the region, if there is a chance of at least $1-\epsilon_1$ that channels are in a fading state such that $r_1 \leq S_1$, and there is a chance of at least $1-\epsilon_2$ that $r_2 \leq S_2$." This definition results in a rectangular region, whose north-east corner point is given by $\Pr\{r_i \leq S_i\} = 1-\epsilon_i$, $i = 1, 2$. This definition is flawed because it does not take into account the coupling of the links and looks at them as being parallel rather than constituting an interference channel.

Contrary to in Section 3.2.2, we assume that when the rate of one link cannot be achieved, the corresponding TX is turned off. This is now possible due to the availability of instantaneous CSI at the TXs. In such an occasion, the other link experiences an interference-free environment and hence has increased chances of achieving its rate. In this context, the problem of interest is to determine how probable it is to achieve r_1 and r_2, i.e. how to define the individual usage probabilities for instantaneous CSI.

In the following, we focus on a given rate pair (r_1, r_2) and a realization of the region

$\mathcal{R}_{\mathbf{h}}$. We need to determine whether the rates r_1 and r_2 are achievable. It can be either that none of them is achievable, or both of them are achievable, or only one of them is achievable. In order to formalize the answer, we introduce the flowchart in Fig. 3.4 and perform the following checks:

1. Is $r_1 > S_1$ and $r_2 > S_2$? If yes, we have case $\mathbb{A}$: none of r_1 and r_2 is achievable. That is, both links will be in outage, so both TXs are turned off.
2. Is $(r_1, r_2) \in \mathcal{R}_{\mathbf{h}}$? If yes, we have case $\mathbb{B}$: both r_1 and r_2 are achievable. That is, there exists a pair of beamforming vectors that enables operation at the desired rate point.
3. Is $r_1 > S_1$ or $r_2 > S_2$? If $r_2 > S_2$, we have case $\mathbb{C}_1$: r_1 is achievable and TX_2 is turned off. If $r_1 > S_1$, we have case $\mathbb{C}_2$: r_2 is achievable and TX_1 is turned off. If neither $r_1 > S_1$ nor $r_2 > S_2$, we have case $\mathbb{D}$: both rates can be achieved, but not simultaneously. In this case, there is ambiguity; the channels are in fading states that can support any of the two rates, provided that only one link operates. Therefore, in this case the TX that would be on has to be chosen. In order to later define a region which is as large as possible, we make this binary choice at random. Otherwise, we can e.g. always decide in favor of link 1. The binary choice can be seen as the outcome of a coin flip.
4. What is the outcome of the coin flip? If heads, we have case $\mathbb{D}_1$: r_1 is achievable and TX_2 is turned off. If tails, we have case $\mathbb{D}_2$: r_2 is achievable and TX_1 is turned off.

The previous discussion reveals that link 1 can operate at rate r_1 if the fading states and coin outcome are such that they give either of the cases $\mathbb{B}$, $\mathbb{C}_1$, or $\mathbb{D}_1$. Similarly, link 2 can operate at rate r_2 in the cases $\mathbb{B}$, $\mathbb{C}_2$, or $\mathbb{D}_2$. Hence, the usage probabilities of link 1 and link 2 for instantaneous CSI are defined as

$$U_1^{\mathrm{inst}}(r_1, r_2) \triangleq \Pr\{\mathbb{B}\} + \Pr\{\mathbb{C}_1\} + \Pr\{\mathbb{D}_1\} \quad \text{and} \tag{3.50}$$

$$U_2^{\mathrm{inst}}(r_1, r_2) \triangleq \Pr\{\mathbb{B}\} + \Pr\{\mathbb{C}_2\} + \Pr\{\mathbb{D}_2\}. \tag{3.51}$$

In order to elaborate the usage probabilities, we express the probabilities of the cases $\mathbb{A}$–$\mathbb{D}$ as

$$\Pr\{\mathbb{A}\} \triangleq \Pr\{r_1 > S_1, r_2 > S_2\} = \Pr\{r_1 > S_1\} \Pr\{r_2 > S_2\}, \tag{3.52}$$

$$\Pr\{\mathbb{B}\} \triangleq \Pr\{(r_1, r_2) \in \mathcal{R}_{\mathbf{h}}\}, \tag{3.53}$$

$$\Pr\{\mathbb{C}_1\} \triangleq \Pr\{r_1 \leq S_1, r_2 > S_2\} = \Pr\{r_1 \leq S_1\} \Pr\{r_2 > S_2\}, \tag{3.54}$$

$$\Pr\{\mathbb{C}_2\} \triangleq \Pr\{r_1 > S_1, r_2 \leq S_2\} = \Pr\{r_1 > S_1\} \Pr\{r_2 \leq S_2\}, \tag{3.55}$$

$$\Pr\{\mathbb{D}\} \triangleq \Pr\{r_1 \leq S_1, r_2 \leq S_2, (r_1, r_2) \notin \mathcal{R}_{\mathbf{h}}\}. \tag{3.56}$$

Note that in (3.52), (3.54), and (3.55), the equalities are true since the random variables S_1 and S_2 are independent. This is due to (3.47) and the assumption that

the channels $\mathbf{h}_{11}$ and $\mathbf{h}_{22}$ are independent. The probabilities of the form $\Pr\{r_i \leq S_i(\mathbf{h}_{ii})\}$ can be computed in closed form, based on the results in Appendix 3.2.6. This is because they can be rewritten, due to (3.47), as $\Pr\{\|\mathbf{h}_{ii}\|^2 \geq \gamma_i\sigma_i^2\}$ and $\|\mathbf{h}_{ii}\|^2$ is hypoexponentially distributed. The probability $\Pr\{(r_1, r_2) \in \mathcal{R}_\mathbf{h}\}$ can be numerically approximated by drawing a large number of regions $\mathcal{R}_\mathbf{h}$ and counting how many times the point (r_1, r_2) lies in them. In the following, we express (3.56) with respect to $\Pr\{r_i \leq S_i\}$ and $\Pr\{(r_1, r_2) \in \mathcal{R}_\mathbf{h}\}$. We note that if a point lies in $\mathcal{R}_\mathbf{h}$, then it also lies in the rectangle rate region with north-east point (S_1, S_2). Hence, we can write

$$\begin{aligned}\Pr\{r_1 \leq S_1, r_2 \leq S_2\} =& \Pr\{r_1 \leq S_1, r_2 \leq S_2 | (r_1, r_2) \in \mathcal{R}_\mathbf{h}\} \Pr\{(r_1, r_2) \in \mathcal{R}_\mathbf{h}\} \\ &+ \Pr\{r_1 \leq S_1, r_2 \leq S_2 | (r_1, r_2) \notin \mathcal{R}_\mathbf{h}\} \Pr\{(r_1, r_2) \notin \mathcal{R}_\mathbf{h}\} \\ =& \Pr\{(r_1, r_2) \in \mathcal{R}_\mathbf{h}\} + \Pr\{\mathbb{D}\} \Leftrightarrow \\ \Pr\{\mathbb{D}\} =& \Pr\{r_1 \leq S_1\} \Pr\{r_2 \leq S_2\} - \Pr\{(r_1, r_2) \in \mathcal{R}_\mathbf{h}\}. \end{aligned} \tag{3.57}$$

While traversing the flowchart, if we happen to be in $\mathbb{D}$, then we will terminate in either $\mathbb{D}_1$ or $\mathbb{D}_2$, depending on the outcome of the coin. The coin outcome depends on the bias that we define as $t \triangleq \Pr\{\text{heads}\}$. So, the probability of case $\mathbb{D}_1$ and $\mathbb{D}_2$ is

$$\Pr\{\mathbb{D}_1\} \triangleq t \Pr\{\mathbb{D}\} \quad \text{and} \tag{3.58}$$

$$\Pr\{\mathbb{D}_2\} \triangleq (1-t) \Pr\{\mathbb{D}\}. \tag{3.59}$$

It is apparent that, by construction, the cases $\mathbb{A}$, $\mathbb{B}$, $\mathbb{C}_1$, $\mathbb{C}_2$, $\mathbb{D}_1$, and $\mathbb{D}_2$, to which the flowchart terminates, are *mutually exclusive*. Using (3.52)–(3.55) and (3.57)–(3.59), one can easily verify that their probabilities sum up to one.

The usage probability of link 1 in (3.50) is expressed, due to (3.53), (3.54), (3.57), (3.58), and (3.59), as

$$U_1^{\text{inst}}(r_1, r_2, t) = \Pr\{r_1 \leq S_1\} - (1-t)\big(\Pr\{r_1 \leq S_1\} \Pr\{r_2 \leq S_2\} - \Pr\{(r_1, r_2) \in \mathcal{R}_\mathbf{h}\}\big) \tag{3.60}$$

$$= \Pr\{r_1 \leq S_1\} - \Pr\{\mathbb{D}_2\}. \tag{3.61}$$

As mentioned in the beginning of this section, it is flawed to consider the usage probability of link 1 being equal to $\Pr\{r_1 \leq S_1\}$. This would only hold if links 1 and 2 were parallel. Due to the coupling, the usage probability is actually lower by, as seen in (3.61), the probability that TX_2 is on, when either one of r_1 and r_2 can be achieved. By the same token, the usage probability of link 2 in (3.51) is expressed,

due to (3.53), (3.55), (3.57), (3.58), and (3.59), as

$$U_2^{\text{inst}}(r_1, r_2, t) = \Pr\{r_2 \leq S_2\} - t\big(\Pr\{r_1 \leq S_1\}\Pr\{r_2 \leq S_2\} - \Pr\{(r_1, r_2) \in \mathcal{R}_{\mathbf{h}}\}\big) \tag{3.62}$$

$$= \Pr\{r_2 \leq S_2\} - \Pr\{\mathbb{D}_1\}. \tag{3.63}$$

Using the usage probabilities in (3.60) and (3.62), we can formalize the definition of the individual outage rate region for instantaneous CSI. Note that the expressions of the usage probabilities depend on the coin bias t. By increasing the value of t, link 1 is prioritized over link 2. So, if there exists a $t \in [0, 1]$ such that $U_1^{\text{inst}}(r_1, r_2, t) \geq 1-\epsilon_1$ and $U_2^{\text{inst}}(r_1, r_2, t) \geq 1-\epsilon_2$, then (r_1, r_2) belongs to the individual outage rate region.

Definition 4. Let $\epsilon_1 > 0$ and $\epsilon_2 > 0$ denote the individual outage probability specifications. Then, the individual outage rate region for instantaneous CSI is the set of all rate points (r_1, r_2) that yield usage probabilities for links 1 and 2, defined in (3.60) and (3.62), at least $1-\epsilon_1$ and $1-\epsilon_2$, respectively. Considering all possible values for the coin bias $t \in [0, 1]$, it is

$$\mathcal{R}_{\text{inst}}^{\text{ind}}(\epsilon_1, \epsilon_2) = \bigcup_{0 \leq t \leq 1} \left\{(r_1, r_2) : U_1^{\text{inst}}(r_1, r_2, t) \geq 1 - \epsilon_1,\ \ U_2^{\text{inst}}(r_1, r_2, t) \geq 1 - \epsilon_2\right\}. \tag{3.64}$$

Computing the Outage Rate Regions for Instantaneous CSI

Here, we sketch a method to determine numerically whether a rate point (r_1, r_2) is within an outage rate region for instantaneous CSI. The core ingredient of the method is the approximate calculation of the usage probabilities as sums of frequencies of occurrence for the cases $\mathbb{B}$–$\mathbb{D}$. We draw a large number of channel realizations. For each of them, we use the flowchart in Fig. 3.4 to determine which of the mutually exclusive cases occurs. For each of the cases, we have a counter that we increase according to the termination of the flowchart. We normalize the counters with the total number of trials to approximately obtain $\Pr\{\mathbb{B}\}$, $\Pr\{\mathbb{C}_1\}$, $\Pr\{\mathbb{C}_2\}$, and $\Pr\{\mathbb{D}\}$. Obviously, the accuracy of the approximation increases with the number of realizations. We use (3.58) and (3.59) to obtain $\Pr\{\mathbb{D}_1\}$ and $\Pr\{\mathbb{D}_2\}$, respectively, as functions of t. Then, due to (3.48), the common usage probability is given by $\Pr\{\mathbb{B}\}$ and comparing it with the common outage specification, we determine whether the rate point is in the common outage rate region. The individual usage probabilities are given by the sums in (3.50) and (3.51). If there exists a $t \in [0, 1]$ that meets the individual outage specifications, we determine that the rate point is in the individual outage rate region.

We now illustrate with the anecdotal example in Fig. 3.5 the approximation of (3.50) and (3.51) by the frequencies of occurrence for the cases $\mathbb{B}$–$\mathbb{D}$. For three different channel realizations, we plot the respective instantaneous rate regions, $\mathcal{R}_{\mathbf{h}}^1$,

$\mathcal{R}_{\mathbf{h}}^2$, and $\mathcal{R}_{\mathbf{h}}^3$. Also, we show four different rate points, $\boldsymbol{a}$, $\boldsymbol{b}$, $\boldsymbol{c}$, and $\boldsymbol{d}$ for which we would like to find the usage probabilities. The results are summarized in Table 3.1. For point $\boldsymbol{a}$, the flowchart of Fig. 3.4 terminates at $\mathbb{B}$ for all three trial regions. Hence, the common and individual usage probabilities of $\boldsymbol{a}$ are equal to 1. For point $\boldsymbol{b}$, the flowchart terminates at $\mathbb{B}$ in the first and third trial and at $\mathbb{C}_2$ in the second trial. Therefore, the common usage probability of $\boldsymbol{b}$ is 2/3 and the individual ones are 2/3 and 1 for link 1 and 2, respectively. For point $\boldsymbol{c}$ and either of $\mathcal{R}_{\mathbf{h}}^1$ and $\mathcal{R}_{\mathbf{h}}^2$, we have case $\mathbb{D}$. That is, the flowchart terminates at $\mathbb{D}_1$ with probability t and at $\mathbb{D}_2$ with probability $1-t$. For $\mathcal{R}_{\mathbf{h}}^3$, the flowchart terminates at $\mathbb{B}$. Hence, the common usage probability of $\boldsymbol{c}$ is 1/3 and the individual ones are $(1+2t)/3$ for link 1 and $(1+2(1-t))/3 = 1-2t/3$ for link 2. For point $\boldsymbol{d}$, the flowchart terminates at $\mathbb{A}$. Hence, the common and individual usage probabilities of $\boldsymbol{d}$ are zero.

3.2.4 Comparison of Regions

In this section we compare the outage rate regions of Definitions 1–4. In Fig. 3.6, we depict the four regions for a set of randomly drawn full-rank channel covariance matrices. In the example, both TXs have $n = 5$ antennas and employ single-stream beamforming, even for the scenario of statistical CSI. The noise variance is $\sigma_i^2 = 0.5$ for both RXs and the outage specifications are set to $\epsilon = \epsilon_1 = \epsilon_2 = 0.1$. First, we discuss the methods we used to generate the regions in Fig. 3.6. Second, we make some observations from the graphical comparison of the regions. Third, we formalize these observations on the relations between the regions into two propositions.

We use exhaustive-search methods to generate the regions in Fig. 3.6. For statistical CSI we draw beamforming vectors randomly. For each pair of beamforming vectors, we determine the rate points that meet the outage specifications using (3.45). Then, we find the boundary via a brute-force search of the north-eastern rate points. For instantaneous CSI, we make a grid of rate points. Then, for each rate point, we use the method sketched in Section 3.2.3 to determine whether the rate pair is in the outage rate region or not. We use the closed-form method in [39] to compute the outer boundary of the instantaneous rate region $\mathcal{R}_{\mathbf{h}}$ for each channel realization.

In the anecdotal example of Fig. 3.6, we see that the individual outage regions are larger than the common outage regions. Also, the instantaneous CSI regions are larger than the corresponding statistical CSI regions. As stated in the following propositions, these relations are true in general.

Proposition 1. *When $\epsilon_1 = \epsilon_2 = \epsilon$, the individual outage regions are larger that the common outage regions, i.e.,*

a) $\mathcal{R}_{stat}^{com}(\epsilon) \subseteq \mathcal{R}_{stat}^{ind}(\epsilon_1, \epsilon_2)$ *and*

b) $\mathcal{R}_{inst}^{com}(\epsilon) \subseteq \mathcal{R}_{inst}^{ind}(\epsilon_1, \epsilon_2)$.

Proof of Prop. 1a): Due to Definition 1, for any rate point $(r_1, r_2) \in \mathcal{R}_{\text{stat}}^{\text{com}}(\epsilon)$, there

is a pair of transmit covariance matrices $(\mathbf{\Psi}_1, \mathbf{\Psi}_2)$ such that

$$U_{\text{com}}^{\text{stat}}(r_1, r_2, \mathbf{\Psi}_1, \mathbf{\Psi}_2) \geq 1 - \epsilon. \tag{3.65}$$

This implies that $U_i^{\text{stat}}(r_i, \mathbf{\Psi}_1, \mathbf{\Psi}_2) \geq 1 - \epsilon$, $i = 1, 2$. Hence, $(r_1, r_2) \in \mathcal{R}_{\text{stat}}^{\text{ind}}(\epsilon_1, \epsilon_2)$. ■

Proof of Prop. 1b): For any rate point $(r_1, r_2) \in \mathcal{R}_{\text{inst}}^{\text{com}}(\epsilon)$, we have $U_{\text{com}}^{\text{inst}}(r_1, r_2) = \Pr\{\mathbb{B}\} \geq 1 - \epsilon$. From (3.50) and (3.51), we get that $U_i^{\text{inst}}(r_1, r_2, t) \geq 1 - \epsilon = 1 - \epsilon_i$, since $\Pr\{\mathbb{C}_i\} \geq 0$ and $\Pr\{\mathbb{D}_i\} \geq 0$. Hence, it follows that $(r_1, r_2) \in \mathcal{R}_{\text{inst}}^{\text{ind}}(\epsilon_1, \epsilon_2)$. ■

This statement is quite intuitive; the definition of common outage says that the entire IC is in outage when at least one of the links is in outage. Individual outage is less restrictive since it allows one link to be in outage while the other is not.

Proposition 2. *For given ϵ, ϵ_1, and ϵ_2, the instantaneous CSI regions are larger than the statistical CSI regions, i.e.,*

a) $\mathcal{R}_{stat}^{com}(\epsilon) \subseteq \mathcal{R}_{inst}^{com}(\epsilon)$ *and*

b) $\mathcal{R}_{stat}^{ind}(\epsilon_1, \epsilon_2) \subseteq \mathcal{R}_{inst}^{ind}(\epsilon_1, \epsilon_2)$.

Proof of Prop. 2a): If $(r_1, r_2) \in \mathcal{R}_{\text{stat}}^{\text{com}}(\epsilon)$, then there is a pair of transmit covariance matrices $(\mathbf{\Psi}_1, \mathbf{\Psi}_2)$ such that the common usage probability of (r_1, r_2) is at least $1 - \epsilon$. So, the probability is at least $1 - \epsilon$ that we get channel realizations for which there exists a pair $(\mathbf{\Psi}_1, \mathbf{\Psi}_2)$ yielding the rate pair (r_1, r_2). Hence, we have $(r_1, r_2) \in \mathcal{R}_{\text{inst}}^{\text{com}}(\epsilon)$. ■

Proof of Prop. 2b): First, we simplify notation by using R_i instead of $R_i(\mathbf{h}_{ii}, \mathbf{h}_{ji}, \mathbf{\Psi}_i, \mathbf{\Psi}_j)$. For all pairs of transmit covariance matrices $(\mathbf{\Psi}_1, \mathbf{\Psi}_2)$, we note that $\Pr\{r_i \leq R_i\} \leq \Pr\{r_i \leq S_i\}$, since S_i is the maximum rate we can achieve for a given realization of the channels.

We assume that $U_i^{\text{stat}}(r_i, \mathbf{\Psi}_1, \mathbf{\Psi}_2) = \Pr\{r_i \leq R_i\} = 1 - \epsilon_i$, $i = 1, 2$, for a rate point (r_1, r_2) and a pair of transmit covariance matrices $(\mathbf{\Psi}_1, \mathbf{\Psi}_2)$. Hence, $(r_1, r_2) \in \mathcal{R}_{\text{stat}}^{\text{ind}}(\epsilon_1, \epsilon_2)$. We note that

$$\begin{aligned} 1 - \epsilon_1 &= \Pr\{r_1 \leq R_1\} \\ &= \Pr\{r_1 \leq R_1 | r_1 \leq S_1\} \Pr\{r_1 \leq S_1\} + \Pr\{r_1 \leq R_1 | r_1 > S_1\} \Pr\{r_1 > S_1\} \\ &= \Pr\{r_1 \leq R_1 | r_1 \leq S_1\} \Pr\{r_1 \leq S_1\} \end{aligned} \tag{3.66}$$

since $\Pr\{r_1 \leq R_1 | r_1 > S_1\} = 0$. Also, we can write (3.60) as

$$U_1^{\text{inst}}(r_1, r_2, t) = \Pr\{r_1 \leq S_1\} \left(1 - (1 - t) \Pr\{r_2 \leq S_2\} \left(1 - \frac{\Pr\{(r_1, r_2) \in \mathcal{R}_{\mathbf{h}}\}}{\Pr\{r_1 \leq S_1\} \Pr\{r_2 \leq S_2\}}\right)\right). \tag{3.67}$$

For r_2, we have expressions similar to (3.66) and (3.67).

We have to show that there exists a $t \in [0, 1]$ such that $U_i^{\text{inst}}(r_1, r_2, t) \geq 1 - \epsilon_i$,

$i = 1, 2$. Then it follows that $(r_1, r_2) \in \mathcal{R}_{\text{inst}}^{\text{ind}}(\epsilon_1, \epsilon_2)$. Comparing (3.66) and (3.67), we see that they have the factor $\Pr\{r_1 \leq S_1\}$ in common. So, we show that there exists a $t \in [0, 1]$ such that

$$\Pr\{r_1 \leq R_1 | r_1 \leq S_1\} \leq 1 - (1-t)\Pr\{r_2 \leq S_2\}\left(1 - \frac{\Pr\{(r_1, r_2) \in \mathcal{R}_{\mathbf{h}}\}}{\Pr\{r_1 \leq S_1\}\Pr\{r_2 \leq S_2\}}\right), \tag{3.68}$$

$$\Pr\{r_2 \leq R_2 | r_2 \leq S_2\} \leq 1 - t\Pr\{r_1 \leq S_1\}\left(1 - \frac{\Pr\{(r_1, r_2) \in \mathcal{R}_{\mathbf{h}}\}}{\Pr\{r_1 \leq S_1\}\Pr\{r_2 \leq S_2\}}\right). \tag{3.69}$$

In order to simplify notation, we define $\alpha_i \triangleq \Pr\{r_i \leq R_i | r_i \leq S_i\}$, $\beta_i \triangleq \Pr\{r_i \leq S_i\}$, $i = 1, 2$, and $\eta \triangleq 1 - \Pr\{(r_1, r_2) \in \mathcal{R}_{\mathbf{h}}\}/(\Pr\{r_1 \leq S_1\}\Pr\{r_2 \leq S_2\})$. Now, we write (3.68) and (3.69) as

$$t \geq t_L \triangleq \frac{\beta_2\eta - 1 + \alpha_1}{\beta_2\eta}, \quad t \leq t_U \triangleq \frac{1 - \alpha_2}{\beta_1\eta}. \tag{3.70}$$

Since $\alpha_i \leq 1$, we have $t_U \geq 0$ and $t_L \leq 1$. So, there exists a feasible t if we can verify that $t_L \leq t_U$. From (3.70) we have

$$t_L \leq t_U \;\Leftrightarrow\; \beta_1\beta_2\eta \leq \beta_1(1-\alpha_1) + \beta_2(1-\alpha_2). \tag{3.71}$$

From the definitions of β_1, β_2, and η, we have $\beta_1\beta_2\eta = \beta_1\beta_2 - \Pr\{(r_1, r_2) \in \mathcal{R}_{\mathbf{h}}\}$. Also, we know that $\alpha_i\beta_i = 1 - \epsilon_i$. Hence, we write (3.71) as

$$\beta_1\beta_2 \leq \Pr\{(r_1, r_2) \in \mathcal{R}_{\mathbf{h}}\} + \beta_1 + \beta_2 + \epsilon_1 + \epsilon_2 - 2. \tag{3.72}$$

From (3.41) and Definition 1 we note that since $(r_1, r_2) \in \mathcal{R}_{\text{stat}}^{\text{ind}}(\epsilon_1, \epsilon_2)$ implies $(r_1, r_2) \in \mathcal{R}_{\text{stat}}^{\text{com}}(\epsilon_1 + \epsilon_2 - \epsilon_1\epsilon_2)$. Using Proposition 2 a), we know that $(r_1, r_2) \in \mathcal{R}_{\text{inst}}^{\text{com}}(\epsilon_1 + \epsilon_2 - \epsilon_1\epsilon_2)$. Hence, $\Pr\{(r_1, r_2) \in \mathcal{R}_{\mathbf{h}}\} \geq 1 - \epsilon_1 - \epsilon_2 + \epsilon_1\epsilon_2$. Therefore, it is sufficient to prove that

$$\beta_1\beta_2 - \beta_1 - \beta_2 \leq \epsilon_1\epsilon_2 - 1. \tag{3.73}$$

Since $\Pr\{r_i \leq S_i\} \geq \Pr\{r_i \leq R_i\} = 1 - \epsilon_i$, one can verify that $\beta_1\beta_2 - \beta_1 - \beta_2$ cannot be larger than $\epsilon_1\epsilon_2 - 1$. Hence, there exists a $t \in [0, 1]$ such that (3.68) and (3.69) are satisfied. Then, it follows that $(r_1, r_2) \in \mathcal{R}_{\text{stat}}^{\text{ind}}$ implies $(r_1, r_2) \in \mathcal{R}_{\text{inst}}^{\text{ind}}$. ■

Also, the results of this proposition are quite intuitive. When the TXs only have statistical CSI, they will spread their power in many directions in order to get some good channel. For the scenario of instantaneous CSI, the TXs know the good directions and transmit along them.

3.2.5 Conclusions

We defined four outage rate regions for the MISO IC. The different definitions correspond to different scenarios of channel knowledge and outage specification. Comparing the definitions, we saw that regions for individual outage are larger than those for common. Also, we proved that the regions become larger when the TXs have instantaneous CSI instead of statistical CSI.

3.2.6 Appendix: Derivation of the Individual Usage Probability for Statistical CSI

In order to find a closed form expression of the usage probability (3.42), we have to find the pdfs of a random variable of the form $X \triangleq \mathbf{h}^H \mathbf{\Psi} \mathbf{h}$, where $\mathbf{h} \sim \mathcal{CN}(\mathbf{0}, \boldsymbol{Q})$. We let $\boldsymbol{T}\mathbf{\Delta}\boldsymbol{T}^H$, where $\mathbf{\Delta} = \mathrm{diag}\{\lambda_1, \ldots, \lambda_n\}$, be the eigenvalue decomposition of $\boldsymbol{Q}^{1/2}\mathbf{\Psi}\boldsymbol{Q}^{1/2}$. Also, we define $\tilde{\mathbf{h}}, \bar{\mathbf{h}} \sim \mathcal{CN}(\mathbf{0}, \mathbf{I})$. Then, we get

$$X = \mathbf{h}^H \mathbf{\Psi} \mathbf{h} = \tilde{\mathbf{h}}^H \boldsymbol{Q}^{1/2} \mathbf{\Psi} \boldsymbol{Q}^{1/2} \tilde{\mathbf{h}} = \tilde{\mathbf{h}}^H \boldsymbol{T} \mathbf{\Delta} \boldsymbol{T}^H \tilde{\mathbf{h}} = \bar{\mathbf{h}}^H \mathbf{\Delta} \bar{\mathbf{h}}. \tag{3.74}$$

We define $\bar{h}_k$ to be the kth element of $\bar{\mathbf{h}}$. Now we can write (3.74) as

$$X = \mathbf{h}^H \mathbf{\Psi} \mathbf{h} = \sum_{k=1}^{K} \lambda_k |\bar{h}_k|^2, \tag{3.75}$$

where $K = \mathrm{rank}\left\{\boldsymbol{Q}^{1/2}\mathbf{\Psi}\boldsymbol{Q}^{1/2}\right\} \leq n$. Also $|\bar{h}_k|^2 \sim \exp(1)$, that is $|\bar{h}_k|^2$ is exponentially distributed with parameter 1. Note that all $|\bar{h}_k|^2$ are statistically independent. Without loss of generality we can assume that $\lambda_1 \geq \lambda_2 \geq \ldots \geq \lambda_n$. We define $\rho(\mathbf{\Delta})$ to be the number of distinct eigenvalues of $\mathbf{\Delta}$, $\lambda_{\langle 1 \rangle} > \lambda_{\langle 2 \rangle} > \ldots > \lambda_{\langle \rho(\mathbf{\Delta}) \rangle}$. Also, we define $\tau_k(\mathbf{\Delta})$ to be the multiplicity of $\lambda_{\langle k \rangle}$. Then, $\mathbf{h}^H \mathbf{\Psi} \mathbf{h}$ is hypoexponentially distributed with pdf [77, Ch. 5], [78]

$$f(x) = \sum_{k=1}^{\rho(\mathbf{\Delta})} \sum_{l=1}^{\tau_k(\mathbf{\Delta})} \chi_{kl}(\mathbf{\Delta}) \frac{\lambda_{\langle k \rangle}^{-l}}{(l-1)!} x^{l-l} e^{-x/\lambda_{\langle k \rangle}}, \quad x \geq 0. \tag{3.76}$$

For the general case of non-distinct eigenvalues, the derivation of the coefficients $\chi_{kl}(\mathbf{\Delta})$ in (3.76) can be found in [79]. Assuming that $\tau_k(\mathbf{\Delta}) = 1, \ \forall k$, i.e. all eigenvalues of $\boldsymbol{Q}^{1/2}\mathbf{\Psi}\boldsymbol{Q}^{1/2}$ are distinct, we can write (3.76) as

$$f(x) = \sum_{k=1}^{K} \frac{\chi_{k1}(\mathbf{\Delta})}{\lambda_k} e^{-x/\lambda_k}, \quad x \geq 0 \tag{3.77}$$

with

$$\chi_{k1}(\mathbf{\Delta}) = \prod_{n=1,n\neq k}^{K} \frac{\lambda_k}{\lambda_k - \lambda_n}. \tag{3.78}$$

Now, we define $f_{ii}(x)$ and $f_{ji}(x)$ to be the pdf of $\mathbf{h}_{ii}^H \mathbf{\Psi}_i \mathbf{h}_{ii}$ and $\mathbf{h}_{ji}^H \mathbf{\Psi}_j \mathbf{h}_{ji}$, respectively. Combining (3.42) and (3.75), we have

$$\Pr\left\{\mathbf{h}_{ii}^H \mathbf{\Psi}_i \mathbf{h}_{ii} - \gamma_i \mathbf{h}_{ji}^H \mathbf{\Psi}_j \mathbf{h}_{ji} > \gamma_i \sigma_i^2\right\} = \Pr\left\{X_{ii} - \gamma_i X_{ji} > \gamma_i \sigma_i^2\right\} = \Pr\left\{X_{ii} + \tilde{X}_{ji} > \gamma_i \sigma_i^2\right\}, \tag{3.79}$$

where $\tilde{X}_{ji} \triangleq -\gamma_i X_{ji}$. We note that the pdf of $\tilde{X}_{ji}$ is $f_{ji}(-x/\gamma_i)/\gamma_i$. To get the pdf $f_i(x)$ of $X_{ii} + \tilde{X}_{ji}$, we convolve $f_{ii}(x)$ and $f_{ji}(-x/\gamma_i)/\gamma_i$. Then we get (3.79) by computing

$$U_i^{\text{stat}}(\mathbf{\Psi}_i, \mathbf{\Psi}_j, r_i) = \int_{\gamma_i \sigma_i^2}^{\infty} \int_{-\infty}^{\infty} \frac{1}{\gamma_i} f_{ji}(-y/\gamma_i) f_{ii}(x-y) dy dx. \tag{3.80}$$

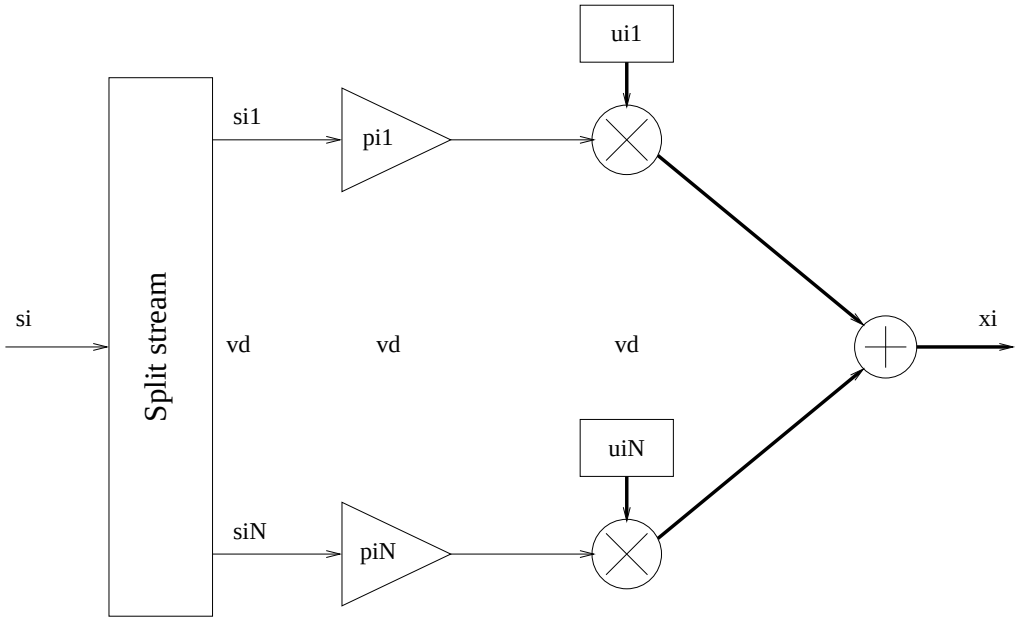

Figure 3.3: Implementation of the multi-stream transmission.

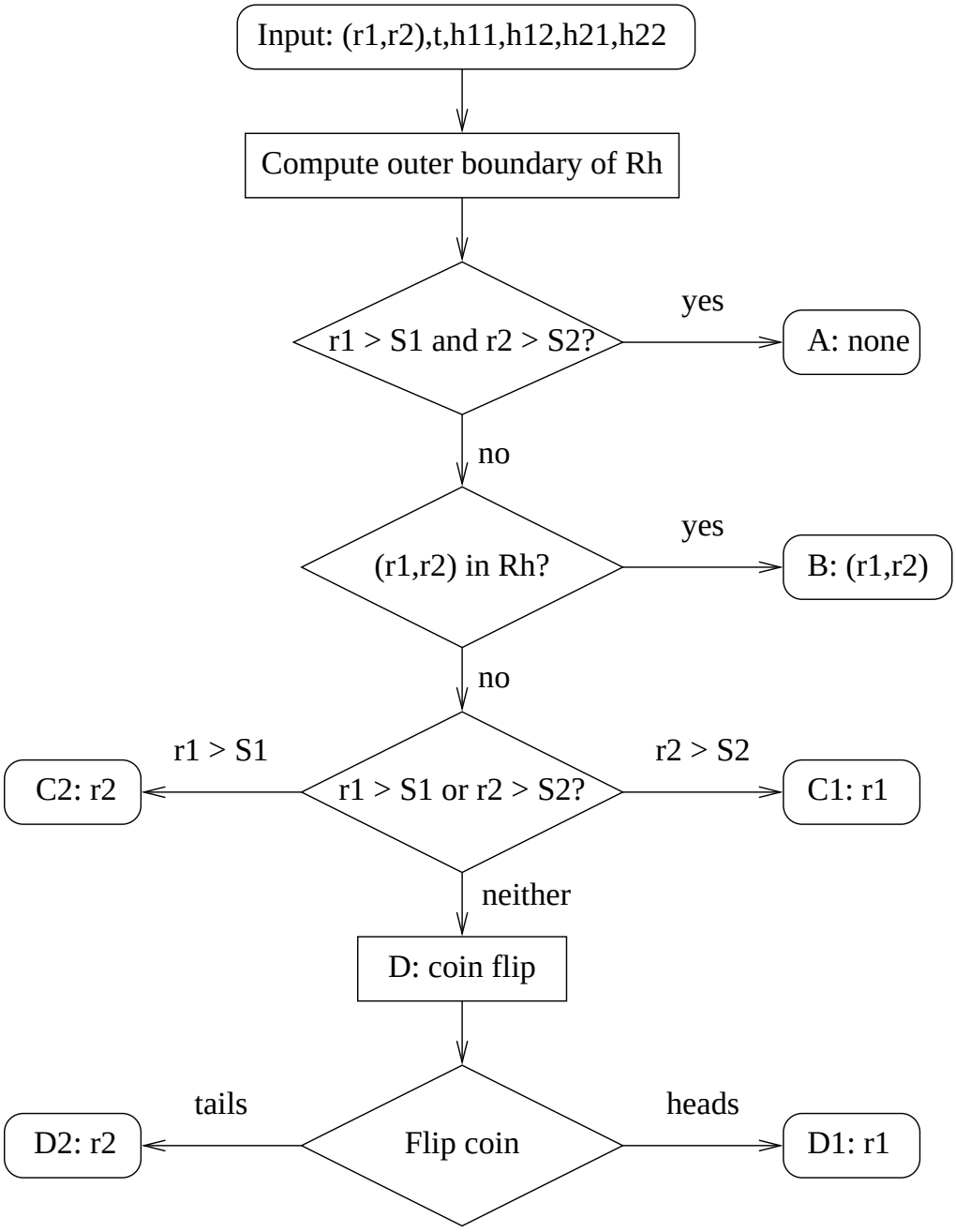

Figure 3.4: Flowchart determining achievability of rates r_1 and r_2 for given channel realizations and coin bias.

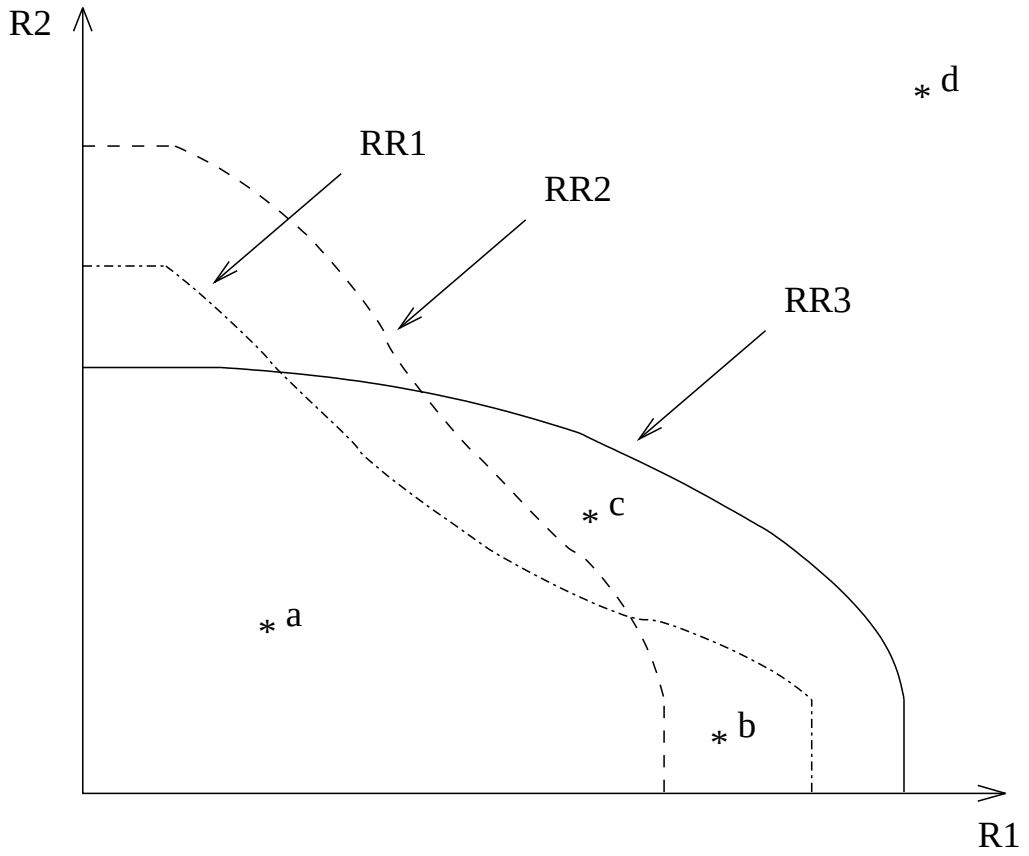

Figure 3.5: Three examples of instantaneous rate regions and rate points.

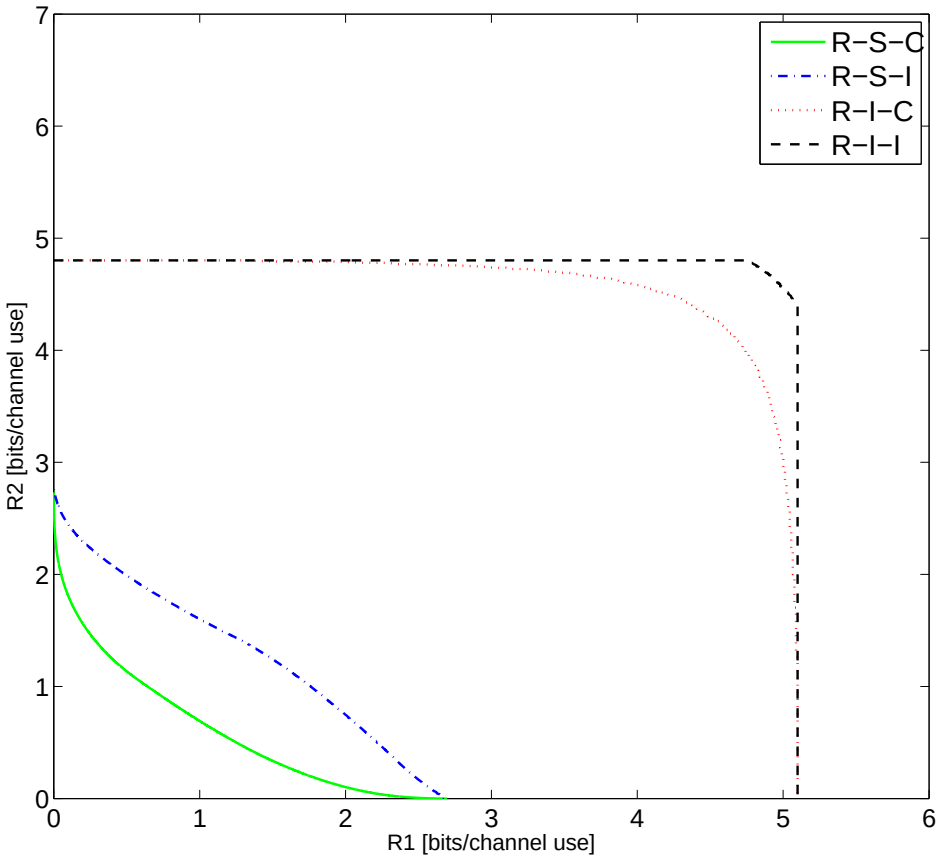

Figure 3.6: Outer boundaries of the outage rate region for the MISO IC.

Table 3.1: Example of approximating usage probabilities for three realizations.

	$\mathcal{R}_{\mathbf{h}}^1$	$\mathcal{R}_{\mathbf{h}}^2$	$\mathcal{R}_{\mathbf{h}}^3$	$U_{\text{com}}^{\text{inst}}$	U_1^{inst}	U_2^{inst}
$\boldsymbol{a}$	$\mathbb{B}$	$\mathbb{B}$	$\mathbb{B}$	1	1	1
$\boldsymbol{b}$	$\mathbb{B}$	$\mathbb{C}_2$	$\mathbb{B}$	$2/3$	$2/3$	1
$\boldsymbol{c}$	$\mathbb{D}$	$\mathbb{D}$	$\mathbb{B}$	$1/3$	$(1+2t)/3$	$1-2t/3$
$\boldsymbol{d}$	$\mathbb{A}$	$\mathbb{A}$	$\mathbb{A}$	0	0	0

4 Achievable Rate Regions of the MISO IC with MUD Capability

4.1 Achievable Rate Regions of the two user MISO IC with IDC

In this chapter the Multiple-Input-Single-Output Interference Channel (MISO IC) is considers in which transmitters and receivers are in a spectrum sharing environment. We consider receivers with interference decoding capability (IDC) so that the interference signal can be decoded and subtracted from the received signal. On the MISO IC with single user decoding, transmit beamforming vectors are designed to mitigate interference at the receivers. With IDC, receivers can potentially decode interference which yields a higher data rate. However, decoding interference poses a rate constraint on the interferer and in turn on the sum rate of the system. This brings some interesting questions: when should the transmitters (Txs) mitigate interference and when should Txs amplify interference? Under what situations should Txs change from mitigating interference to amplifying interference? We answer these questions in this chapter.

4.2 Introduction

The capacity region of the two-user SISO IC has been studied extensively [80, 81, 82, 83, 84, 85, 86], although the general capacity region is not fully known, except for special cases, e.g. the low and strong interference regime.

To extend the above results, the authors [87, 52] study the capacity region of the vector Gaussian interference channel in the weak interference regime. Results show that treating interference as noise in the weak interference regime achieves capacity. Apart from the capacity of the IC, the frontier of the achievable rate region assuming linear precoders, also known as the Pareto boundary, holds importance to the understanding of the IC. Any rate points on the Pareto boundary are operating points such that it is impossible to increase one user's rate without decreasing the others. Assuming perfect channel state information at transmitters (CSIT), the Pareto boundary of the SISO IC and MISO IC with single user detection (SUD) are characterized in [88, 11] respectively. In [7], the authors extended the results to partial CSIT. In this chapter, we assume simple single user encoding transmitters and interference decoding capability at receivers, which yield a simpler achievable rate

region comparing to the Han-Kobayashi scheme [89]. This allows us to study the effects of transmit beamforming on the achievable rate region and to characterize the Pareto boundary. We limit ourselves to the two transmitter-receiver (Tx-Rx) pairs interference channel with interference decoding capability (IDC), each receiver can choose to decode interference or treat interference as noise. The main contributions of this chapter are the followin.g

We formulate the achievable rate region of the 2-user MISO IC IDC which is a region achieved by varying transmit powers and beamforming vectors in Section 4.4. Then, we show that the achievable rate region of the MISO IC IDC is a union of four rate regions of different decoding structures (e.g. Rx 1, 2 decode interference or treat interference as noise). In Section 4.6, we characterize the boundaries of rate regions of each decoding structures and therefore characterize the Pareto boundary of the MISO IC IDC. As an application of the Pareto boundary characterization, we characterize the maximum sum rate points and the conditions in which MRT strategies are sum rate optimal [90]. Due to space limit, we do not include the results here, for details please refer to [90]. In Section 4.7, we use these results to develop a simple suboptimal algorithm that performs close to the maximum sum rate point, whose computation is NP-hard [91].

4.3 Channel Model

We assume a simple system of two transmitter-receiver (Tx-Rx) pairs in which each Tx has N antennas and each Rx has only one antenna. This results in a two-user MISO IC, which is illustrated in Figure 4.1 as an example with $N = 3$. We assume linear pre-coders and the Txs use the same Gaussian codebooks and therefore the Rxs, if the channel qualities allow, can decode the interference and subtract it from the received signal. Also, we assume that the interference is successfully decoded if the rate of the interference signal is smaller than the Shannon capacity of the interference channel.

Denote the transmit beamforming vector of Tx i by $\mathbf{w}_i$ and the channel from Tx i to Rx $\bar{i}$, where $i, \bar{i} \in \{1, 2\}, \bar{i} \neq i$, $\mathbf{h}_{\bar{i}i} \in \mathbb{C}^{N\times 1}$. Note that the channel gains are i.i.d complex Gaussian coefficients with zero mean and unit variance. The received signal at Rx i is therefore

$$y_i = \mathbf{h}_{ii}^H \mathbf{w}_i x_i \sqrt{P_i} + \mathbf{h}_{i\bar{i}}^H \mathbf{w}_{\bar{i}} x_{\bar{i}} \sqrt{P_{\bar{i}}} + n_i. \tag{4.1}$$

The noise n_i is a complex Gaussian random variable with zero mean and unit variance. P_i is the transmit power at each Tx and we assume the same power constraint for both Txs, $P_i \leq P^*$. The symbol x_i is the transmit symbol at Tx i with unit power. The transmit beamformer has unit norm $\|\mathbf{w}_i\| = 1$. Denote the hypersphere of dimension N in the complex space with unit radius by $\mathcal{S}$: $\mathcal{S} = \left\{\mathbf{w} \in \mathbb{C}^{N\times 1} : \|\mathbf{w}\| = 1\right\}$, $\mathbf{w}_i \in \mathcal{S}$. We define here the projector matrices which will

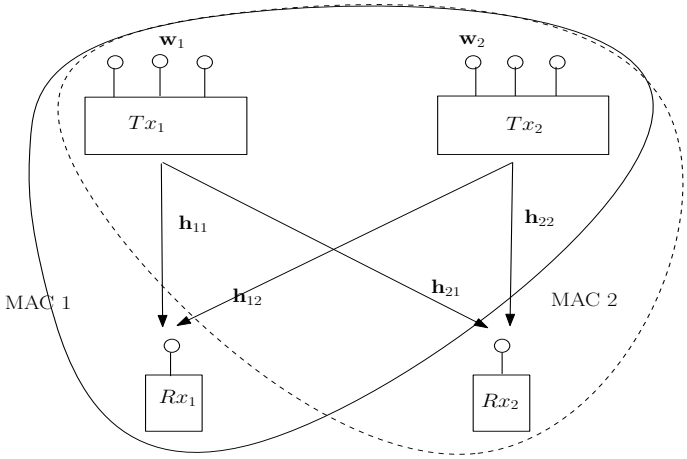

Figure 4.1: The 2-user MISO IC where Txs are quipped with 3 antennas.

be referenced to later:

$$\mathbf{\Pi}_{ij} = \frac{\mathbf{h}_{ij}\mathbf{h}_{ij}^H}{\|\mathbf{h}_{ij}\|^2} \tag{4.2}$$

$$\mathbf{\Pi}_{ij}^{\perp} = \mathbf{I} - \mathbf{\Pi}_{ij}. \tag{4.3}$$

4.4 Achievable Rate Region

We assume simple matched filter decoders and propose the following four decoding schemes, similar to the SISO case [80]. We define the following important quantities:

$$\begin{aligned}
C_1 \triangleq C_1(\mathbf{w}_1, P_1) &\triangleq \log_2\left(1 + |\mathbf{h}_{11}^H\mathbf{w}_1|^2 P_1\right), \\
C_2 \triangleq C_2(\mathbf{w}_2, P_2) &\triangleq \log_2\left(1 + |\mathbf{h}_{22}^H\mathbf{w}_2|^2 P_2\right), \\
D_1 \triangleq D_1(\mathbf{w}_1, \mathbf{w}_2, P_1, P_2) &\triangleq \log_2\left(1 + \frac{|\mathbf{h}_{11}^H\mathbf{w}_1|^2 P_1}{|\mathbf{h}_{12}^H\mathbf{w}_2|^2 P_2 + 1}\right), \\
D_2 \triangleq D_2(\mathbf{w}_1, \mathbf{w}_2, P_1, P_2) &\triangleq \log_2\left(1 + \frac{|\mathbf{h}_{22}^H\mathbf{w}_2|^2 P_2}{|\mathbf{h}_{21}^H\mathbf{w}_1|^2 P_1 + 1}\right), \\
T_2 \triangleq T_2(\mathbf{w}_1, \mathbf{w}_2, P_1, P_2) &\triangleq \log_2\left(1 + \frac{|\mathbf{h}_{12}^H\mathbf{w}_2|^2 P_2}{|\mathbf{h}_{11}^H\mathbf{w}_1|^2 P_1 + 1}\right), \\
T_1 \triangleq T_1(\mathbf{w}_1, \mathbf{w}_2, P_1, P_2) &\triangleq \log_2\left(1 + \frac{|\mathbf{h}_{21}^H\mathbf{w}_1|^2 P_1}{|\mathbf{h}_{22}^H\mathbf{w}_2|^2 P_2 + 1}\right).
\end{aligned}$$

C_1 and C_2 are the *single user rates*, the largest rate user 1 and 2 can achieve without the influence of interference. D_1 and D_2 are the rates of decoding desired signal while treating interference as thermal noise and T_1 and T_2 are the rate of decoding interference while treating desired signals as noise.

If both receivers decode interference, user i must transmit at a rate that ensures interference decoding at Rx $\bar{i}$, thus we have the following:

$$\begin{aligned} R_1 &\leq \min\{C_1, T_1\} \\ R_2 &\leq \min\{C_2, T_2\}. \end{aligned} \tag{4.4}$$

Denote the rate region with interference decoding at both receivers by (4.5) (shown at the top of the page).

$$\mathcal{R}^{dd} = \bigcup_{\substack{\mathbf{w}_1,\mathbf{w}_2\in\mathcal{S} \\ 0\leq P_1,P_2\leq P^*}} \Big\{(R_1,R_2) \leq \big(\min\{C_1,T_1\}, \min\{C_2,T_2\}\big)\Big\} \tag{4.5}$$

$$\mathcal{R}^{nn} = \bigcup_{\substack{\mathbf{w}_1,\mathbf{w}_2\in\mathcal{S} \\ 0\leq P_1,P_2\leq P^*}} \Big\{(R_1,R_2) \leq \big(D_1, D_2\big)\Big\} \tag{4.6}$$

$$\mathcal{R}^{dn} = \bigcup_{\substack{\mathbf{w}_1,\mathbf{w}_2\in\mathcal{S} \\ 0\leq P_1,P_2\leq P^*}} \Big\{(R_1,R_2) \leq \big(C_1, \min\{D_2,T_2\}\big)\Big\} \tag{4.7}$$

$$\mathcal{R}^{nd} = \bigcup_{\substack{\mathbf{w}_1,\mathbf{w}_2\in\mathcal{S} \\ 0\leq P_1,P_2\leq P^*}} \Big\{(R_1,R_2) \leq \big(\min\{D_1,T_1\}, C_2\big)\Big\} \tag{4.8}$$

Remark 4.1. For each selected pair of transmit beamformers, a corresponding rate region which satisfies the inequalities (4.5) is obtained. The achievable rate region $\mathcal{R}^{dd}$ is defined as the union of all regions achieved by all possible transmit beamformers.

On the other hand, if both Rxs choose to treat interference as noise, we obtain (4.6). If Rx 1 decodes interference but Rx 2 treats interference as noise, Tx 2 transmits a rate that ensure interference decoding at Rx 1 as described in (4.7). Similarly, exchanging the role of Tx 1 and 2, we have (4.8).

The achievable rate region of the MISO IC with interference decoding capability is therefore the union of the above regions:

$$\mathcal{R} = \mathcal{R}^{nn} \cup \mathcal{R}^{dd} \cup \mathcal{R}^{dn} \cup \mathcal{R}^{nd}. \tag{4.9}$$

Definition 4.1. Denote the set of points on the Pareto boundary by $\mathcal{B}(\mathcal{R})$. If the rate pair $(r_1, r_2) \in \mathcal{R}$ is on the boundary, $(r_1, r_2) \in \mathcal{B}(\mathcal{R})$, then there does not exist a rate pair $(r_1', r_2') \geq (r_1, r_2)$, with one strict inequality. By (4.9),

$$\mathcal{B}(\mathcal{R}) \subset \mathcal{B}(\mathcal{R}^{nn}) \cup \mathcal{B}(\mathcal{R}^{dd}) \cup \mathcal{B}(\mathcal{R}^{dn}) \cup \mathcal{B}(\mathcal{R}^{nd}). \tag{4.10}$$

Definition 4.2. Denote the set of beamforming vectors and power allocations that achieve the rate boundaries $\mathcal{B}(\mathcal{R}^{xy})$ for $x, y = \{n, d\}$, the solution set of $\mathcal{B}(\mathcal{R}^{xy})$,

termed as Ω^{xy}.

$$\Omega^{xy} = \left\{(\mathbf{w}_1, \mathbf{w}_2, P_1, P_2) : \left(R_1, R_2\right) \in \mathcal{B}(\mathcal{R}^{xy})\right\} \tag{4.11}$$

Similarly, the solution set of $\mathcal{B}(\mathcal{R})$ is Ω.

$$\Omega = \left\{(\mathbf{w}_1, \mathbf{w}_2, P_1, P_2) : \left(R_1, R_2\right) \in \mathcal{B}(\mathcal{R})\right\} \tag{4.12}$$

In the following sections, we study the Pareto boundary in terms of power allocation and transmit beamforming vectors in different decoding structure namely $\mathbf{R}^{nd}$ and $\mathbf{R}^{dd}$. $\mathbf{R}^{dn}$ is symmetric to $\mathbf{R}^{nd}$ and is therefore omitted here. $\mathbf{R}^{nn}$ is treated in [11].

4.5 The Pareto Boundary Characterization

In this section, we characterize the Pareto boundary by characterizing the boundaries of different decoding structures. In Section 4.5.1, we compute the solution sets of the boundary $\mathcal{B}(\mathcal{R}^{nd})$ whereas in Section 4.5.2, we compute the solution sets of the boundary $\mathcal{B}(\mathcal{R}^{dd})$.

4.5.1 The Pareto Boundary Characterization in $\mathbf{R}^{nd}$

With decoding structure $\mathbf{R}^{nd}$, Rx 1 treats interference as noise and Rx 2 decodes and subtracts the interference signal from the received signal before decoding the desired signal. By the definition of rate pair (R_1, R_2) in Eqt. (4.8), the Pareto boundary is the solution of the following optimization problem

$$\begin{aligned} &\max_{\mathbf{w}_1, \mathbf{w}_2, P_1, P_2} \min\{T_1, D_1\} \\ \text{s.t.} \quad &C_2 = r_2, \quad \|\mathbf{w}_1\| = 1, \quad \|\mathbf{w}_2\| = 1, \quad P_1 \leq P^*, \quad P_2 \leq P^*. \end{aligned} \tag{4.13}$$

Lemma 4.1. *The optimization problem* (4.13) *has the solution* Ω^1,

$$\Omega^1 = \{\mathbf{w}_1 \in \mathcal{W}_1, P_1 = P^*\} \tag{4.14}$$

where $\mathcal{W}_1$ *is defined in* (4.19).

Proof. see [90]. □

If we reverse the optimization order, we have

$$\begin{aligned} &\max_{\mathbf{w}_2, P_2} C_2, \\ \text{s.t.} \quad &T_1 \geq r_1, \quad D_1 \geq r_1, \quad \mathbf{w}_1 \in \mathcal{W}_1, \quad \|\mathbf{w}_2\| \leq 1, \quad P_1 = P^*, \quad P_2 \leq P^*, \end{aligned} \tag{4.15}$$

for some positive value r_1.

Lemma 4.2. *The optimization problem* (4.15) *has the solution* Ω^2*,*

$$\Omega^2 = \{\mathbf{w}_2 \in \mathcal{W}_2, 0 \leq P_2 \leq P^*\} \tag{4.16}$$

where $\mathcal{W}_2$ *is defined in* (4.20)*.*

Proof. see [90]. □

Lemma 4.1 gives the solution set of $\mathbf{w}_1$, for arbitrary fixed $\mathbf{w}_2$, which attain the Pareto boundary of $\mathcal{R}^{nd}$. On the other hand, Lemma 4.2 gives the solution set of $\mathbf{w}_2$ for arbitrary fixed $\mathbf{w}_1$. We combine both results and obtain the following theorem.

Theorem 4.1. *The Pareto boundary* $\mathcal{B}(\mathcal{R}^{nd})$ *is attained by the solution set* Ω^{nd}

$$\Omega^{nd} = \{\mathbf{w}_1 \in \mathcal{W}_1, \mathbf{w}_2 \in \mathcal{W}_2, P_1 = P^*, 0 \leq P_2 \leq P^*\} \tag{4.17}$$

where $\mathcal{W}_1, \mathcal{W}_2$ *are defined in* (4.19) *and* (4.20)*.*

Proof. Note that $\Omega^1 \bigcup \Omega^2 \subset \Omega^{nd}$. From Lemma 4.1 and Lemma 4.2, $\Omega^1 \bigcup \Omega^2$ attains Pareto boundary $\mathcal{Q}^1 \bigcup \mathcal{Q}^2 \supset \mathcal{B}(\mathcal{R}^{nd})$. Thus, solution set Ω^{nd} attains Pareto boundary $\mathcal{B}(\mathcal{R}^{nd})$. □

Note that in Theorem 4.1 we computed the set of beamformers that attain the Pareto boundary in $\mathbf{R}^{nd}$. This parameterization allows us to represent the beamforming vectors with positive real scalars $0 \leq \lambda_1, \lambda_2 \leq 1$. By varying λ_1, λ_2 from zero to one and P_2 from zero to P^*, we obtain all beamforming vectors that may attain the Pareto boundary. Intuitively, it means that the Pareto boundary attaining beamforming vectors exist only in a two-dimensional subspace, spanned by the direct channel and the interference channel, in a N-dimensional signal space.

In the next section, we investigate the Pareto boundary attaining beamforming vectors in decoding structure $\mathbf{R}^{dd}$.

4.5.2 The Pareto Boundary Characterization in $\mathbf{R}^{dd}$

Theorem 4.2. *The pareto boundary* $\mathcal{B}(\mathcal{R}^{dd})$ *is attained by solution set*

$$\Omega^{dd} = \{0 \leq P_1, P_2 \leq P^*, \mathbf{w}_1 \in \mathcal{V}_1, \mathbf{w}_2 \in \mathcal{V}_2\}. \tag{4.18}$$

where $\mathcal{V}_1, \mathcal{V}_2$ *are defined in* (4.21) *and* (4.22)*.*

Proof. see [90]. □

Note that the solution sets $\mathcal{W}_i$ and $\mathcal{V}_i$ are different as $\mathcal{W}_i$ is a set of beamforming vectors spanned by $\frac{\Pi_{ji}\mathbf{h}_{ii}}{\|\Pi_{ji}\mathbf{h}_{ii}\|}$ and $\frac{\Pi_{ji}^{\perp}\mathbf{h}_{ii}}{\|\Pi_{ji}^{\perp}\mathbf{h}_{ii}\|}$ whereas $\mathcal{V}_i$ is a set of beamforming vectors spanned by $\frac{\Pi_{ii}\mathbf{h}_{ji}}{\|\Pi_{ii}\mathbf{h}_{ji}\|}$ and $\frac{\Pi_{ii}^{\perp}\mathbf{h}_{ji}}{\|\Pi_{ii}^{\perp}\mathbf{h}_{ji}\|}$.

$$\mathcal{W}_1 = \left\{ \mathbf{w}_1 : \mathbf{w}_1 = \sqrt{\lambda_1}\frac{\Pi_{21}\mathbf{h}_{11}}{\|\Pi_{21}\mathbf{h}_{11}\|} + \sqrt{1-\lambda_1}\frac{\Pi_{21}^{\perp}\mathbf{h}_{11}}{\|\Pi_{21}^{\perp}\mathbf{h}_{11}\|} \; ; \; 0 \leq \lambda_1 \leq 1 \right\} \tag{4.19}$$

$$\mathcal{W}_2 = \left\{ \mathbf{w}_2 : \mathbf{w}_2 = \sqrt{\lambda_2}\frac{\Pi_{12}\mathbf{h}_{22}}{\|\Pi_{12}\mathbf{h}_{22}\|} + \sqrt{1-\lambda_2}\frac{\Pi_{12}^{\perp}\mathbf{h}_{22}}{\|\Pi_{12}^{\perp}\mathbf{h}_{22}\|} \; ; \; 0 \leq \lambda_2 \leq 1 \right\} \tag{4.20}$$

$$\mathcal{V}_1 = \left\{ \mathbf{w}_1 : \mathbf{w}_1 = \sqrt{\lambda_1}\frac{\Pi_{11}\mathbf{h}_{21}}{||\Pi_{11}\mathbf{h}_{21}||} + \sqrt{1-\lambda_1}\frac{\Pi_{11}^{\perp}\mathbf{h}_{21}}{||\Pi_{11}^{\perp}\mathbf{h}_{21}||} \; ; \; 0 \leq \lambda_1 \leq 1 \right\} \tag{4.21}$$

$$\mathcal{V}_2 = \left\{ \mathbf{w}_2 : \mathbf{w}_2 = \sqrt{\lambda_2}\frac{\Pi_{22}\mathbf{h}_{12}}{||\Pi_{22}\mathbf{h}_{12}||} + \sqrt{1-\lambda_2}\frac{\Pi_{22}^{\perp}\mathbf{h}_{12}}{||\Pi_{22}^{\perp}\mathbf{h}_{12}||} \; ; \; 0 \leq \lambda_2 \leq 1 \right\} \tag{4.22}$$

4.6 The Pareto Boundary of MISO IC IDC

The Pareto Boundary is attained if at least one of the boundaries of the decoding structures is attained. Thus, we have the following solutions sets that attain the Pareto boundary.

$$\Omega = \Omega^{nd} \bigcup \Omega^{dd}. \tag{4.23}$$

Note that the solution set of $\mathbf{R}^{nn}$ is a subset of Ω^{nd} [11]. By reversing the role of Tx 1 and 2, we see that the solution set of $\mathbf{R}^{dn}$ is Ω^{nd} except with $0 \leq P_1 \leq P^*$ which is included in Ω^{dd}.

4.7 A Simple Transmit Strategy

In this section, we propose a simple suboptimal transmission strategy. This transmission strategy is inspired by the parameterizaiton of each decoding structure. We propose to select only one beamforming vector in each solution set. Given the channel states information, we compare the sum rate performance of these four beamforming vectors and choose the beamforming vector and the corresponding decoding structure which achieves the highest sum rate.

- $\mathbf{R}^{nn}$: $\mathbf{w}_1 = \frac{\Pi_{21}^{\perp}\mathbf{h}_{11}}{\|\Pi_{21}^{\perp}\mathbf{h}_{11}\|}, \mathbf{w}_2 = \frac{\Pi_{12}^{\perp}\mathbf{h}_{22}}{\|\Pi_{12}^{\perp}\mathbf{h}_{22}\|}$.
- $\mathbf{R}^{nd}$: $\mathbf{w}_1 = \frac{\mathbf{h}_{21}}{\|\mathbf{h}_{21}\|}, \mathbf{w}_2 = \frac{\mathbf{h}_{22}}{\|\mathbf{h}_{22}\|}$.
- $\mathbf{R}^{dn}$: $\mathbf{w}_1 = \frac{\mathbf{h}_{11}}{\|\mathbf{h}_{11}\|}, \mathbf{w}_2 = \frac{\mathbf{h}_{12}}{\|\mathbf{h}_{12}\|}$.

- $\mathbf{R}^{dd}$: $\mathbf{w}_1 = \frac{\mathbf{h}_{21}}{\|\mathbf{h}_{21}\|}, \mathbf{w}_2 = \frac{\mathbf{h}_{12}}{\|\mathbf{h}_{12}\|}$.
- TDMA: time sharing between single user points and therefore $\mathbf{w}_i = \frac{\mathbf{h}_{ii}}{\|\mathbf{h}_{ii}\|}$.

4.8 Simulation Results

In this section, we demonstrate that the proposed parameterization allows us to design beamforming vectors which attain the Pareto boundaries. We also plotted the corresponding MRT strategies and maximum sum rate points, in Section 4.8.1. In Section 4.8.2, we observe the change of sum rate optimal decoding structure when the strength of the interference channel increases. We compare the sum rate performance between the optimal sum rate and the proposed simple algorithm.

4.8.1 The Pareto Boundary in Different Decoding Structure

In Figures 4.2 and 4.3 we plot the achievable rate region of the decoding structure $\mathbf{R}^{nd}$ and $\mathbf{R}^{dd}$ respectively. The number of transmit antennas is three and the SNR is set at 0dB. The channel coefficients for this particular channel realization are:

$$\begin{aligned}
\mathbf{h}_{11} &= [0.3776 + 0.8444i, -1.0265 + 0.3100i, 0.2292 + 0.6424i]^T, \\
\mathbf{h}_{22} &= [-0.1445 - 0.0385i, -1.2045 - 0.1070i, 0.9119 - 0.3682i]^T, \\
\mathbf{h}_{12} &= [1.0156 + 0.6832i, 0.6064 - 0.2969i, 0.1510 + 0.8155i]^T, \\
\mathbf{h}_{21} &= [-0.1735 + 0.5270i, 0.6659 + 0.3887i, -1.6426 - 0.4348i]^T.
\end{aligned}$$

We vary the parameters λ_1, λ_2 and the transmit power from zero to P^* in order to generate the beamforming vectors in the proposed solution sets.

4.8.2 The Simple Algorithm

In this section, we assume a symmetric channel [92] in which the direct channels, $\mathbf{h}_{ii}$, are i.i.d complex Gaussian vector channels. The interference channel $\mathbf{h}_{ji}$ has a projection angle θ_i with the direct channel $\mathbf{h}_{ii}$: $|\mathbf{h}_{ji}^H \mathbf{h}_{ii}| = \|\mathbf{h}_{ii}\| \|\mathbf{h}_{ji}\| \cos(\theta_i)$. Moreover, we assume that the strength of the interference channel is α times of that of the direct channel: $\|\mathbf{h}_{ji}\|^2 = \alpha \|\mathbf{h}_{ii}\|^2$ where $\alpha \in \mathbb{R}^+$. In Figures 4.4 and 4.5, we plotted the maximum sum rate achieved by different decoding structure and compare it with the proposed simple algorithm when the strength of interference channel, $\sqrt{\alpha}$, increases. In both figures, we see that when the interference is weak, it is sum rate optimal to treat interference as noise and when the interference strength increases, sum rate can be increased by allowing one of the Rx to decode interference and in the strong interference regime, both Rxs. decoding interference achieves the highest sum rate. Depending on the channel coefficients, TDMA may outperform

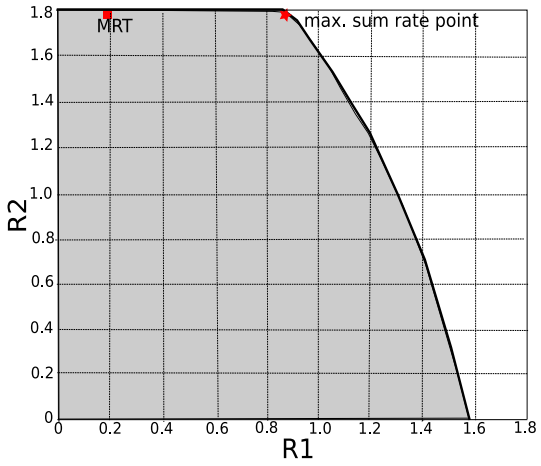

Figure 4.2: Achievable rate region of $\mathbf{R}^{nd}$: proposed parameterization achieves the Pareto Boundary at SNR 0dB.

$\mathbf{R}^{nn}$ and $\mathbf{R}^{dd}$ in the medium interference regime. Note that the computation of the maximum sum rate point is NP-hard. However, we see the the proposed simple algorithm achieves nice sum rate performance with only five choices of beamforming vectors.

4.8.3 The SAPHYRE Gain

We define here the SAPHYRE gain to be the performance gain of the proposed low complexity algorithm over the TDMA schemes where no cooperation is performed. As shown in Figures 4.4 and 4.5, we see a big difference between the sum rate performance of the proposed algorithm over the TDMA scheme in medium and high SNR regime.

4.9 Conclusion

We proposed and formulated the achievable rate region and the Pareto boundary of the MISO IC IDC. We characterized the Pareto boundary in terms of beamforming vectors and power allocation. The Pareto boundary attaining beamforming vectors are parameterized by two real valued scalars that take values from zero to one. As an application of this parameterization, we compute the maximum sum rate point and compare with a simple suboptimal algorithm that takes only five beamforming vectors of choice. In symmetric channels, we show that the sum rate optimal decoding structures changes from treating interference as noise to TDMA to decoding interference when the strength of interference increases. The suboptimal algorithm performs nicely according to simulations.

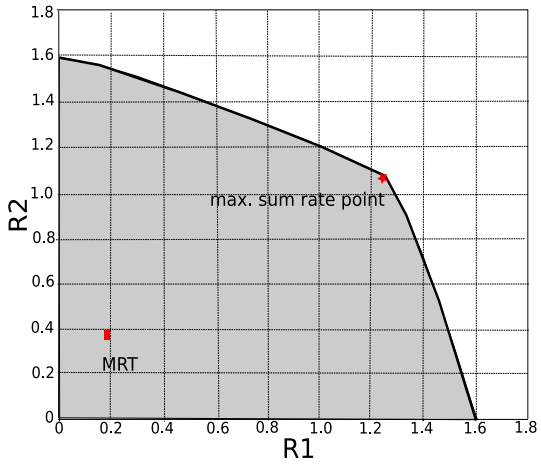

Figure 4.3: Achievable rate region of $\mathbf{R}^{dd}$: proposed parameterization achieves the Pareto Boundary at SNR 0dB.

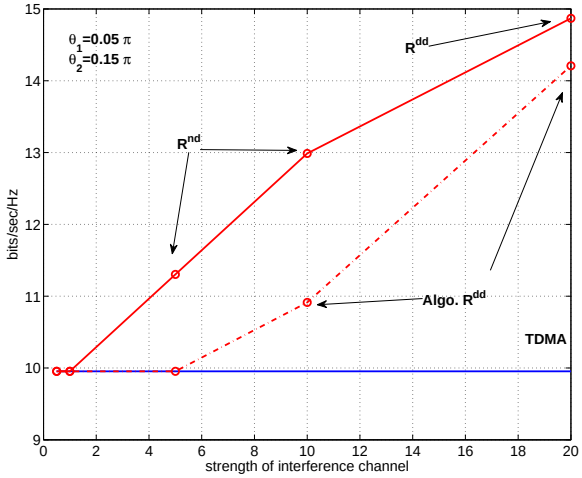

Figure 4.4: Sum rate optimal decoding structures when the strength of interference channel increases.

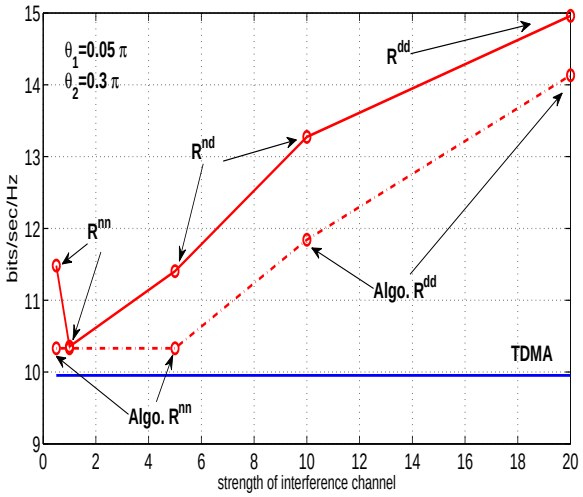

Figure 4.5: Sum rate optimal decoding structures when the strength of interference channel increases.

5 Fundamental Limits for Code, Signal, and Receiver Processing Design

5.1 Introduction

5.1.1 Wireless Network Coding with Hierarchical Decode and Forward Strategy

Background And Related Work

Multi-node and multi-source wireless communication scenarios are currently under intensive investigation in the research community. Generally, these can be seen as similar to the Network Coding (NC) paradigm [93]. NC operates with a discrete (typical binary) alphabet over loss-less discrete channels. It is in fact an operation on data rather than on the channel codewords. NC has great potential in substantially increasing the throughput of complicated communication networks. An extension of these principles into the wireless (signal space) domain is however non-trivial. Some attempts have been carried out using a simple concatenation of NC and a single-link physical layer modulation and coding technique. This has number of drawbacks and only limited optimality. An optimal solution is a direct signal space domain code synthesis.

Limited code design and capacity region results are available for the simplest possible scenario of the 2-Way Relay Channel (2-WRC). Authors of [94], [95], [96], [97] concentrate on the distance optimization of the relay hierarchical mapping regions as a function of the channel parametrization. A specific approach using a lattice code construction is taken by [98] and [99]. The authors of [98] and [99] provide lattice based code construction using principles of [100] but do not investigate the impact of the channel parametrization. The results of this section are also based on our earlier work [101], [102], [103].

Concept of Sharing PHY Layer in Multi-Source and Multi-Node Networks

The research target is a general *multi-source* and *multi-node* wireless communication network where all network nodes (relays) contribute to providing data flows *without* an explicit routing. It can be described as a flood of the information having different "colors" (from individual sources) at the inputs. The network processes

the "rainbow" mixture-color not distinguishing individual sources. The destinations pick a particular "color" from the received flood with the help of various forms of the side-information on other data streams available at the destination. Since the mixture-data flow represents jointly (but not necessarily individually distinguished) data stream, we call those data *hierarchical data* and corresponding relay processing a *hierarchical decode and forward* relay strategy.

This resembles the principles of Network Coding, but with important differences. (1) The information transfer is achieved through *signal-space wireless links* including all phenomena of *channel parametrization, fading and received signal superpositions*. (2) The distributed source coding joint with distributed channel coding can play an important role. The source-channel separation theorem does not hold generally for correlated sources. This problem arises mainly when we do not fully decode and re-code the hierarchical codewords at relays (e.g. due to the latency constraints). Then the resulting per-symbol relay processing must source-code the soft-symbol metric. These metrics are possibly correlated due to the codeword structure and due to the multi-path network flow topology.

The above stated concept relies on following tools.

- Network Coded Modulation is the network structure aware modulation and coding. Each node, either source or relay, transmits the signal that it can be processed in the remaining receiving nodes performing various joint relaying strategies.
- Relaying strategies should work on the hierarchical data using hierarchical decode and forward strategy, not on individual separated data streams.
- Combined distributed source and channel coding at various levels including full frame and also per-symbol soft-decoding metric for symbol-wise relay strategies can help improving the overall network efficiency.

The simplest particular network example capable of demonstrating some of the above stated concepts is the 2-Source Relay Network. (see also [SAPHYRE deliverable D3.2a] for details)

5.1.2 WNC and HDF in the context of SAPHYRE project

The WNC technique with HDF relaying strategy is a cooperative coding & relaying technique fulfilling the SAPHYRE project goals in the SAPHYRE TC (relaying) reference scenario (see SAPHYRE deliverable [D3.3a]). The ultimate target WNC/HDF based relaying scenario is shown on Fig. 5.1. Each system operation stage shares the wireless propagation medium at the same time and same frequency band. Each node uses Network Coded Modulation (NCM) which (1) has output codewords directly in the signal space (hence "modulation") and (2) fully respects the structure and connectivity of other nodes in the network including the comple-

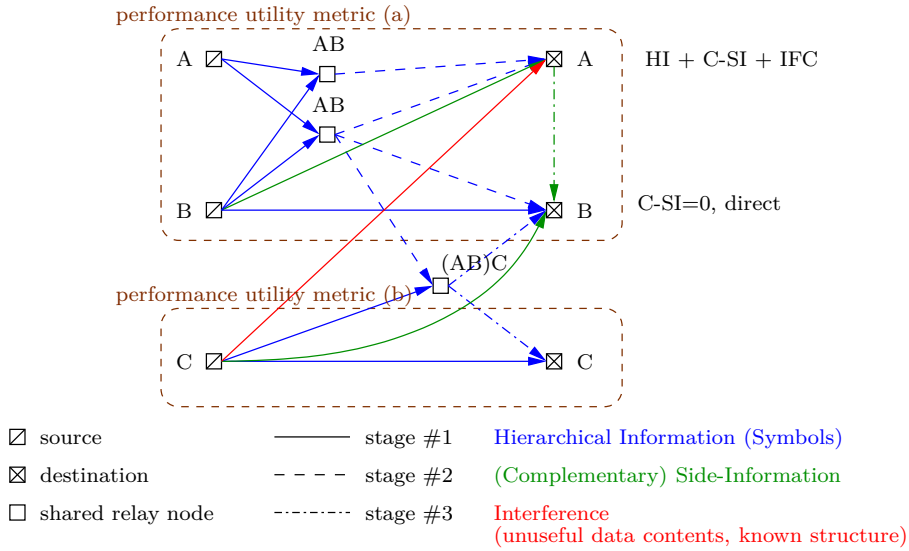

Figure 5.1: Ultimate sharing scenario with relaying using WNC and HDF relaying strategy.

mentary side-information available there (hence "network coded"). The information is thus propagated between the source and the destination by all available paths and with full respect of the amount of the information obtained by other paths (i.e. minimizing any redundancy). This approach is much more effective in comparison with multi-slot traditional packet network forwarding technique. In fact, the WNC/HDF overcomes to some extend any need of the network layer. All the information is "flooded" through all "pipes" purely by means of PHY layer technique. Additional details on WNC/HDF and NCM are provided in SAPHYRE [D3.2a] deliverable.

5.2 System model

5.2.1 2-Source Relay Network with Partial C-SI

A 2-Source Relay Network (2-SRN) consists of two independent data sources SA and SB which want to deliver their data to two destinations DA and DB through shared relay R. During the first (MAC) stage sources A and B transmit to the relay and also destination B collects complementary side information (C-SI) on the data A and destination A C-SI on the data B. The relay operates with HDF strategy. In the second (BC) stage, R produces on its output hierarchical symbols (details will be given later) carrying both data A and B only through the Hierarchical eXclusive Code (HXC). Both destination receive this common signal and combine that with the C-SI received in the MAC stage to decode the data. See Fig. 5.2. The figure also shows individual Signal-to-Noise Ratios (SNRs) of the individual links.

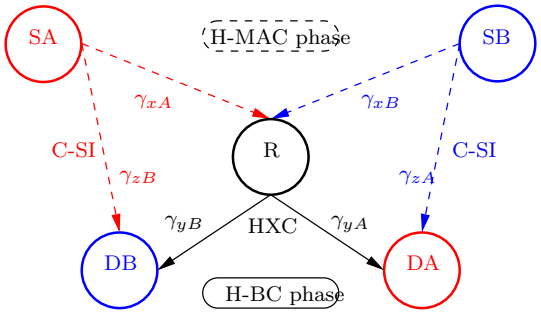

Figure 5.2: 2-Source Relay Network with Partial C-SI.

The system is symmetric in its structure (SA $\rightarrow$ R $\rightarrow$ DA, and SB $\rightarrow$ R $\rightarrow$ DB), which allows us to investigate it from the *perspective* of the *data flow A* with data B being only a nuisance parameter. All conclusions drawn for A should then be equally applicable to B.

Next sections define formal details. Subscripts A and B denotes variable associated with node A and B respectively. For notational simplicity, we omit the sequence number indices of individual symbols. We use also a slightly relaxed notation for the symbol and the codebook sets and the corresponding mapping and encoding operations. The notation uses the same letter symbol in two different contexts. This simplifies the reader's appreciation of the relatively large number of codebooks/alphabets involved. As an example, the codebook (the set of all codewords) is denoted by $\mathcal{C}$ and it is optionally supplemented by a subscript corresponding to the particular codeword. The notation $\mathcal{C}(\mathbf{d})$ denotes a codeword corresponding to the data input $\mathbf{d}$. A similar notation holds for symbol alphabets, denoted by $\mathcal{A}$, and corresponding mapping operations $\mathcal{A}(\centerdot)$. All continuous-valued time-domain signals are represented through their signal space (with an *orthonormal* basis) representations.

5.2.2 Exclusive Law and Hierarchical Exclusive Code/Alphabet

The *exclusive law* [95] is defined as a property of the joint representation of two data symbols through the function $\mathcal{X}_d(\mathbf{d}_A, \mathbf{d}_B)$. It must hold that

$$\mathcal{X}_d(\mathbf{d}_A, \mathbf{d}_B) \neq \mathcal{X}_d(\mathbf{d}'_A, \mathbf{d}_B), \quad \forall \mathbf{d}_A \neq \mathbf{d}'_A, \tag{5.1}$$

$$\mathcal{X}_d(\mathbf{d}_A, \mathbf{d}_B) \neq \mathcal{X}_d(\mathbf{d}_A, \mathbf{d}'_B), \quad \forall \mathbf{d}_B \neq \mathbf{d}'_B. \tag{5.2}$$

The functions fulfilling exclusive law will called exclusive mapping and denoted by the operator $\mathcal{X}_d(\centerdot, \centerdot)$ specifying also the corresponding symbol (in this case d) for which it applies. Simply speaking, the exclusive mapping allows an inverting the mapping function provided we have a side-information on one of the data symbols. Assuming that the destination node B has perfect Side Information (SI) on the

node's own data $\mathbf{d}_B$ it can then decode the message $\mathbf{d}_A$ (and similarly for node A). Data $\mathbf{d}_B$ will be called called *complementary* data from the perspective of the data $\mathbf{d}_A$ operations. The SI on the complementary data will be denoted as Complementary SI (C-SI).

The exclusive mapping can be applied at various levels — complete or partial codewords/messages or individual symbols. We define Hierarchical eXclusive Code (HXC) as a two-source codebook fulfilling the exclusive law. Similarly we define Hierarchical eXclusive Alphabet (HXA) when it is applied symbol-wise.

Assume a HXC codebook $\mathcal{C}_{AB}$ with mapping $\mathcal{X} : (\mathcal{C}_A, \mathcal{C}_B) \mapsto \mathcal{C}_{AB}$. In order for the exclusive law to hold, the relay hierarchical codebook cardinality must satisfy $|\mathcal{C}_{AB}| \geq \max(|\mathcal{C}_A|, |\mathcal{C}_B|)$. On the other hand, the cardinality is upper-bounded by all possible $\mathbf{d}_A$ and $\mathbf{d}_B$ message combinations $|\mathcal{C}_{AB}| \leq |\mathcal{C}_A||\mathcal{C}_B|$. The lower bound case requires perfect C-SI on the complementary data at the destination. The upper bound is in fact a classical MAC channel with joint and separate decoding of both data messages at the relay and requires *no* C-SI. Any situation in between those two extreme cases requires partial C-SI at the destination.

The HXC having the minimal cardinality $|\mathcal{C}_{AB}| = \max(|\mathcal{C}_A|, |\mathcal{C}_B|)$ will be called Minimal-HXC (M-HXC). This case puts minimum *throughput* requirements on the BC channel at the price of requiring perfect C-SI at the destination. All codebooks with a higher cardinality will be called Extended-HXC (E-HXC).

5.2.3 H-MAC Phase

Source data messages are $\mathbf{d}_A$, $\mathbf{d}_B$ and they are composed of data symbols $d_A, d_B \in \mathcal{A}_d = \{0, 1, \ldots, M_d - 1\}$, with alphabet cardinality $|\mathcal{A}_d| = M_d$. Source node codewords are $\mathbf{c}_A, \mathbf{c}_B$ with code symbols $c_A, c_B \in \mathcal{A}_c$, $|\mathcal{A}_c| = M_c$. The encoding operation is performed by the encoders $\mathcal{C}_A, \mathcal{C}_B$ with codebooks $\mathbf{c}_A \in \mathcal{C}_A$ and $\mathbf{c}_B \in \mathcal{C}_B$. Transmitted channel symbols are $s_A = s(c_A)$, $s_B = s(c_B)$, $s_A, s_B \in \mathcal{A}_s \subset \mathbb{C}^N$. We assume a common channel symbol mapper $\mathcal{A}_s(\centerdot)$. A signal space representation of the overall coded frame is $\mathbf{s}_A(\mathbf{c}_A)$ and $\mathbf{s}_B(\mathbf{c}_B)$.

The received signal at the relay in a parameterized flat fading (constant over the frame) channel is

$$u = s_A + h s_B. \tag{5.3}$$

The relative equivalent parameterization by $h \in \mathbb{C}$ represents the parametric channel with both parametric links $u' = h_A s_A + h_B s_B$ by a proper rescaling by $1/h_A$ and denoting $h = h_B/h_A$, $h_A, h_B \in \mathbb{C}^1$. The received signal at the relay is

$$x = u + w \tag{5.4}$$

where the circularly symmetric complex Gaussian noise w has the variance σ_w^2 per complex dimension. See Fig. 5.3.

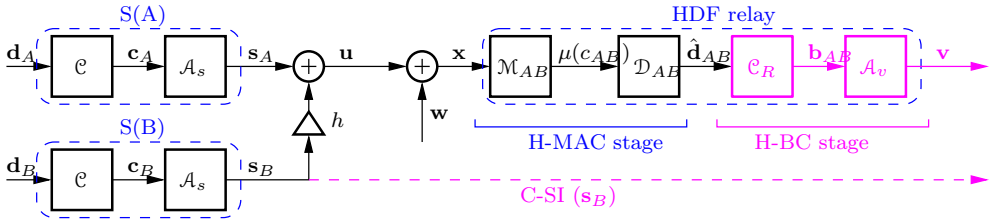

Figure 5.3: The system model for H-MAC phase with layered HXC design.

The SNR is defined as the ratio of the real base-band symbol energy of one source (e.g. A, to have a fair comparison for reference cases) to the noise power spectrum density ratio $\gamma_{xA} = (\mathcal{E}_{s_A}/2)/N_0$. Assuming orthonormal basis signal space complex envelope representation of the AWGN, we have $\sigma_w^2 = 2N_0$ and thus $\gamma_{xA} = \mathrm{E}\left[\|s_A\|^2\right]/\sigma_w^2$.

5.2.4 H-BC Phase

The HDF front-end (H-MAC phase) processing at the relay produces the hierarchical symbols $\mathbf{d}_{AB} = \mathcal{X}_d(\mathbf{d}_A, \mathbf{d}_B)$ which are the *minimal* HXC. The data $\mathbf{d}_{AB}$ are encoded at the back-end (H-BC phase) of the relay to produce codewords $\mathbf{b}_{AB} = \mathcal{C}_R(\mathbf{d}_{AB})$. The discrete code symbols are mapped in symbol-by-symbol manner on the signal space symbols $v = v(b_{AB}) \in \mathcal{A}_v$ and and broadcast to destinations DA and DB. At the destination for data A, the received signal space symbols are

$$y_A = v(b_{AB}) + w_A \tag{5.5}$$

where the complex circularly symmetric AWGN w_A has variance σ_A^2 per complex dimension. We denote the signal space symbols at node A (a destination for data B) similarly $y_B = v + w_B$. We define the SNR on the R to DA link as $\gamma_{yA} = \mathrm{E}\left[\|v\|^2\right]/\sigma_{w_A}^2$.

The C-SI on the data from the source SB are received at the destination DA during the first H-MAC phase and they are stored for the later processing at the second H-BC phase. The transmitted signal is identical to the one transmitted at H-MAC. The received signal is

$$z_A = s(c_B) + \xi_A \tag{5.6}$$

where the complex circularly symmetric AWGN ξ_A has variance $\sigma_{\xi_A}^2$ per complex dimension. The SNR of the C-SI link is $\gamma_{zA} = \mathrm{E}\left[\|s_A\|^2\right]/\sigma_{\xi_A}^2$. Fig. 5.4.

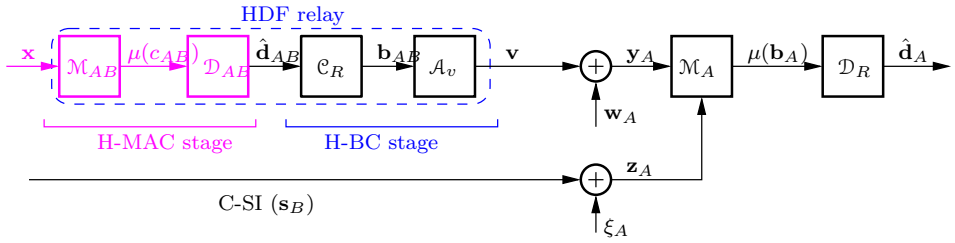

Figure 5.4: The system model for H-BC phase with layered HXC design.

5.3 Capacity/Throughput Regions of HDF strategy with Minimal mapping

5.3.1 Hierarchical MAC Rate Region

Hierarchical Mutual Information

It follows from the Layered HXC Design theorem that the throughput rate region is rectangular and given by the hierarchical mutual information $I(c_{AB}; x)$. It is evaluated for given chosen symbol alphabets $\mathcal{A}_s$ with given channel parameterization

$$x = u\left(s(c_A) + hs(c_B)\right) + w. \tag{5.7}$$

The hierarchical code symbols are mapped on the useful signal by $u(c_A, c_B) = \mathcal{A}_u(c_{AB})$. The transmitted signals, the useful H-MAC signal and the received signal are signal space representations $s(c_A), s(c_B), u, x \in \mathbb{C}^N$. The mutual information evaluation must respect the fact that the $\mathcal{A}_u(c_{AB})$ is generally a set (class) of multiple possible symbols for each particular c_{AB}.

The hierarchical mutual information (uniform-input capacity) is

$$C_{AB} = I(c_{AB}; x) = \mathcal{H}[x] - \mathcal{H}[x|c_{AB}] \tag{5.8}$$

$$= \mathcal{H}[x] - \mathcal{H}[x|\mathcal{A}_u(c_{AB})]\,. \tag{5.9}$$

The channel parameterization h and symbol space alphabets $s(\centerdot)$ are *implicitly* hidden in the hierarchical class $\mathcal{A}_u(c_{AB})$ definition and we do not use an explicit notation for that.

Received Signal Entropy

From the entropy definition, we get (all integrals are over $\mathbb{C}^N$ support)

$$\mathcal{H}[x] = -\int p(x) \lg p(x)\ \mathrm{d}\, x \tag{5.10}$$

where the PDF is

$$p(x) = \frac{1}{M_c^2} \sum_{c_A, c_B} p_w(x - u(c_A, c_B)) \tag{5.11}$$

and $p_w(w)$ is the PDF of complex signal space AWGN representation

$$p_w(w) = \frac{1}{(\pi \sigma_W^2)^N} \exp\left(-\frac{\|w\|^2}{\sigma_w^2} \right). \tag{5.12}$$

We assumed uniformly distributed code symbols $c_{A,}c_B$.

Conditional Entropy

An evaluation of the conditional entropy $\mathcal{H}[x|c_{AB}] = \mathcal{H}[x|\mathcal{A}_u(c_{AB})]$ is slightly more complicated compared to the classical point-to-point single user channel. Generally, it is *not* the entropy of the AWGN $\mathcal{H}[x|c_{AB}] \neq \mathcal{H}[w]$ as it would have been in the single user channel. This is because, given c_{AB}, the actual useful signal is a multi-symbol class $\mathcal{A}_u(c_{AB})$.

From the definition, we get

$$\mathcal{H}[x|c_{AB}] = -\sum_{c_{AB}} \Pr\{c_{AB}\} \int p(x|c_{AB}) \lg p(x|c_{AB}) \, \mathrm{d}\, x. \tag{5.13}$$

Then we apply the results of the $p(x|c_{AB})$ evaluation (see also [SAPHYRE deliverable D3.2a] for details). In a *special case* of a *minimal* exclusive code (M-HXC) and uniformly distributed c_A, c_B, the hierarchical symbols have $\Pr\{c_{AB}\} = 1/\sum_{c_A, c_B} \mathcal{I}_c(c_A, c_B, c_{AB}) = 1/M_c$ and the conditional PDF is simply

$$p(x|c_{AB}) = \frac{1}{M_c} \sum_{c_A, c_B : \mathcal{X}_c(c_A, c_B) = c_{AB}} p_w\left(x - u(c_A, c_B)\right). \tag{5.14}$$

Classical MAC and Cut-Set Bound Reference

As a reference case, we consider the classical MAC rate region first and second order limits

$$I(c_A; x|c_B), \;\; I(c_A, c_B; x). \tag{5.15}$$

Notice that the first order rate limit $I(c_A; x|c_B)$ is in fact a cut-set bound [104] with finite alphabet limitation. The second order limit $I(c_A, c_B; x)$ corresponds to the joint decode and forward strategy where individual data streams from A and B are separately decoded at the relay.

For comparison, we evaluate $I(c_A; x|c_B)$ as a limiting performance criterion. The value R_0 is in fact the mutual information of the single user A channel as if there is

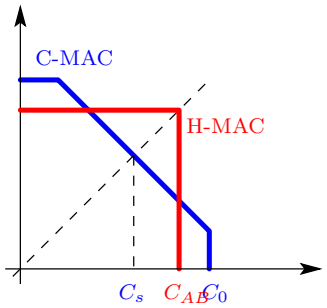

Figure 5.5: Capacity regions for H-MAC.

no user B at all. Notice that this can be quite easily modeled by setting the channel B transfer $h = 0$. The uniform-input alphabet constrained capacity is found as

$$C_0 = I(c_A; x|c_B) = \mathcal{H}[x|c_B] - \mathcal{H}[x|c_A, c_B] \tag{5.16}$$

where the second term is simply the entropy of AWGN

$$\mathcal{H}[x|c_A, c_B] = \mathcal{H}[w] = N \lg\left(\pi e \sigma_w^2\right). \tag{5.17}$$

The second order cut-set bound limit is in fact a sum-rate. We evaluate the sum-rate rescaled to one user (assuming symmetric rates from nodes A and B)

$$C_s = \frac{1}{2} I(c_A, c_B; x). \tag{5.18}$$

All capacities and regions are depicted in Fig. 5.5.

Unconstrained Capacity

We also include the true alphabet unconstrained cut-set bound capacity for given input variance which is

$$C_u = \lg\left(1 + \frac{\mathrm{E}\left[\|\mathbf{s}_A\|^2\right]}{\sigma_w^2}\right). \tag{5.19}$$

Numerical Results and Discussion

The hierarchical rate and single-user (alphabet limited cut-set bounds) rates were evaluated for a number of signal alphabets $\mathcal{A}_s$ and channel parameterizations. The alphabet $\mathcal{A}_s$ is indexed by symbols $c_A, c_B \in \{0, \ldots, M_c - 1\}$. We used a natural constellation index mapping for BPSK, QPSK and 8PSK constellations $\{\exp(\mathrm{j}\, i 2\pi/M_c\}_{i=0}^{M_c-1}$. The constellation denoted by QPSK-cross has indexing defined by $\{1, -1, \mathrm{j}, -\mathrm{j}\}$. 16QAM constellation uses a natural row-wise index mapping

starting from the south-west corner. The exclusive *minimal* hierarchical mapping is $c_{AB} = c_A \oplus c_B$. The amplitude of $h = |h| \exp(\mathrm{j}\,\psi)$ is kept constant ($|h| = 1$) in our setup to respect the symmetry of the rates from A and B.

Figs. 5.7, 5.8, 5.9, 5.10, 5.11 show comparisons of the hierarchical symmetric capacity with various channel parameterizations with the alphabet constrained cut-set bound (both first and second order bound) and the unconstrained AWGN cut-set bound capacity. There are two main observations. First, we see that HXA outperforms the classical C-MAC capacity second order cut-set bound (sum-rate per user) and closely approaches the first order cut-set bound for medium to high signal to noise ratios. This means that the 2-WRC behaves at the MAC stage as if there was just one user alone. In the region of very low signal to noise ratio, the C-MAC is marginally better. However this is strongly affected by the choice of constellations, which is ad-hoc and not optimized. An optimization of the component constellation could improve this. The second observation shows a relatively small dispersion of the capacity over all possible channel relative phase parameterizations for some component symbol constellations. This is strongly dependent on the constellation. For example, the QPSK-cross constellation is particularly vulnerable to this phenomenon. Again, proper selection and optional optimization of the alphabet components is an important aspect.

Encouraged by the previous observation, we also plot a relative H-MAC capacity degradation due to the phase channel relative rotation ψ (Figs. 5.12, 5.13, 5.14). Various channel phases cause a capacity degradation due to the movement of the composite hierarchical points u. Their mutual position influences the metric, the decision regions, and thus also the capacity. However we can observe two types of behavior. In the first case, the capacity is just a little lowered when the points occupy less favorable mutual positions. But for some constellations and a given indexing catastrophic failure of the exclusivity law may occur, where several points belonging to different hierarchical indices c_{AB} reach same position. Fortunately these phases are relatively isolated. This observation encourages an evaluation of the mean capacities, which indicates that they have only a limited impact on the mean capacity over all phase rotations. The mean capacity is quite close to the maximum and, most importantly, it also exceeds the C-MAC capacity.

The results on the mean value over all channel phases have a direct practical implication. They also suggest the use of *phase scrambling* schemes. The phase scrambling pattern would be known to the relay, which could easily unscramble it. This operation would effectively erase the influence of the particular critical phase channel rotation at the price of slightly lower throughput. Particular implementation details of this phase scrambling technique are not discussed here.

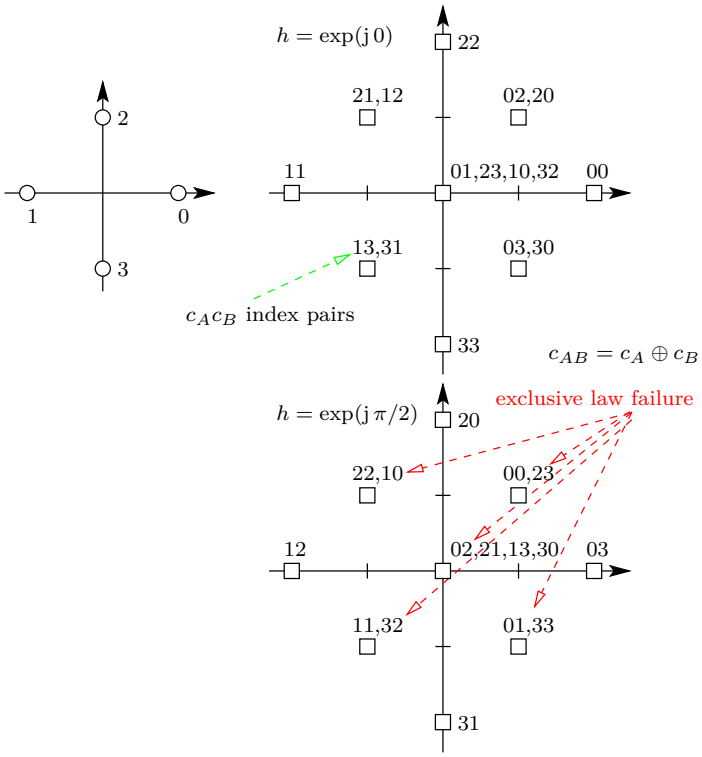

Figure 5.6: An example of the catastrophic exclusive law failure for QPSK-cross (cross indexing) and specific phase rotation.

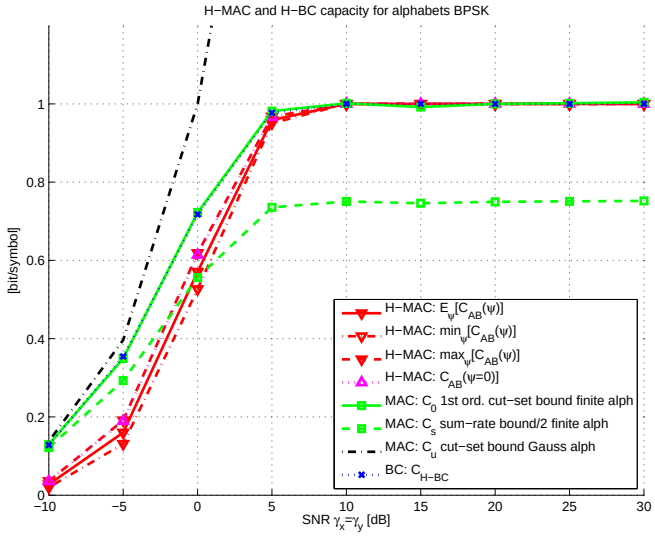

Figure 5.7: A comparison of capacities $C_{AB}, C_0, C_s, C_{\text{HBC}}$ for BPSK alphabet and various channel phase parameterizations.

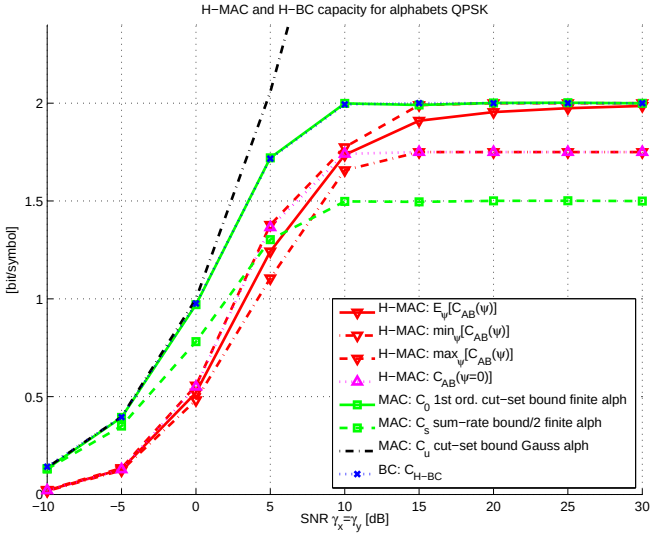

Figure 5.8: A comparison of capacities $C_{AB}, C_0, C_s, C_{\mathrm{HBC}}$ for QPSK alphabet and various channel phase parameterizations.

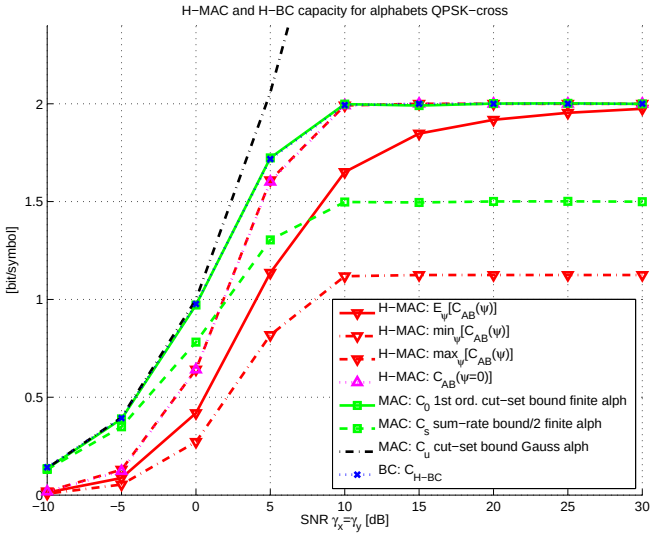

Figure 5.9: A comparison of capacities $C_{AB}, C_0, C_s, C_{\mathrm{HBC}}$ for QPSK-cross alphabet and various channel phase parameterizations.

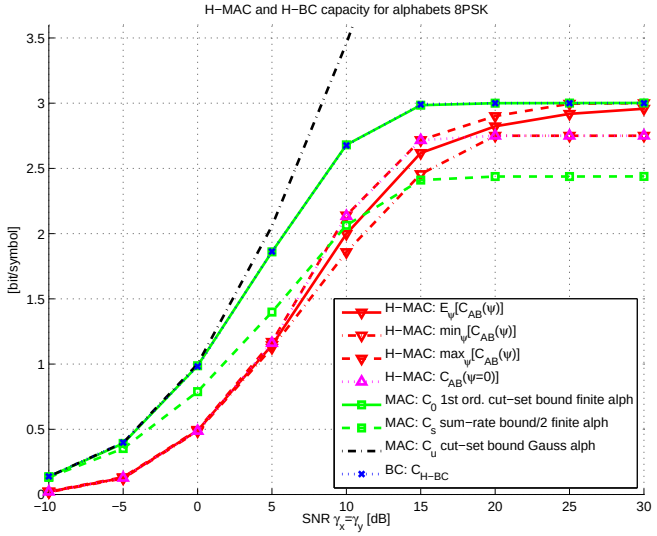

Figure 5.10: A comparison of capacities $C_{AB}, C_0, C_s, C_{\text{HBC}}$ for 8PSK alphabet and various channel phase parameterizations.

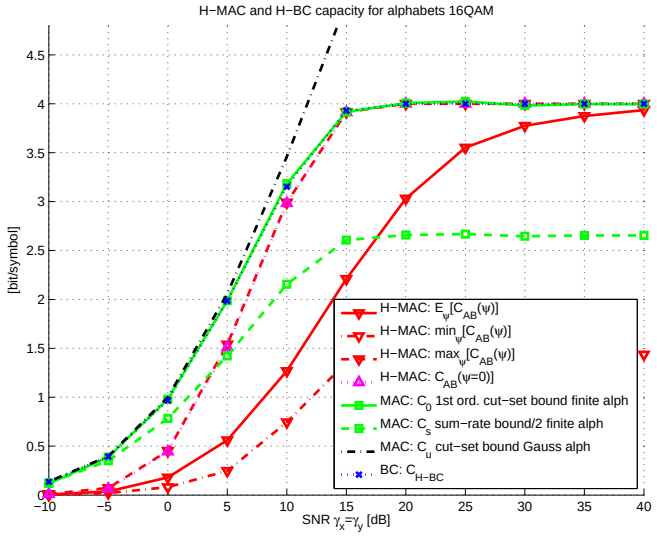

Figure 5.11: A comparison of capacities $C_{AB}, C_0, C_s, C_{\text{HBC}}$ for 16QAM alphabet and various channel phase parameterizations.

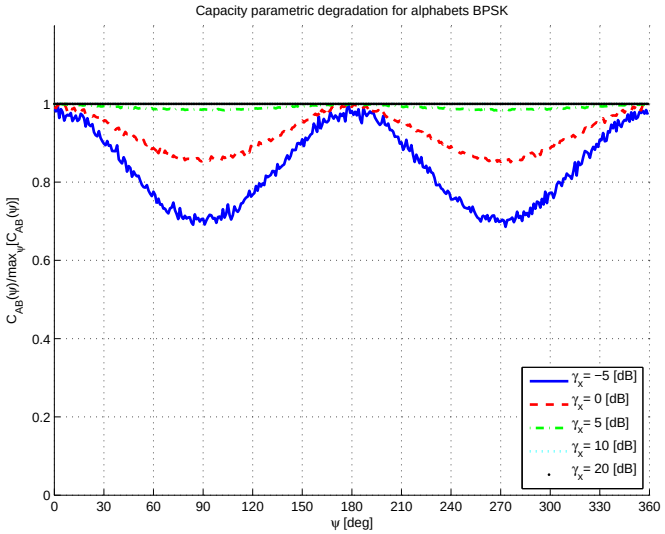

Figure 5.12: A degradation of the capacity $C_{AB}(\psi)/\max_{\psi'}[C_{AB}(\psi')]$ as a function or channel relative phase rotation for BPSK alphabet.

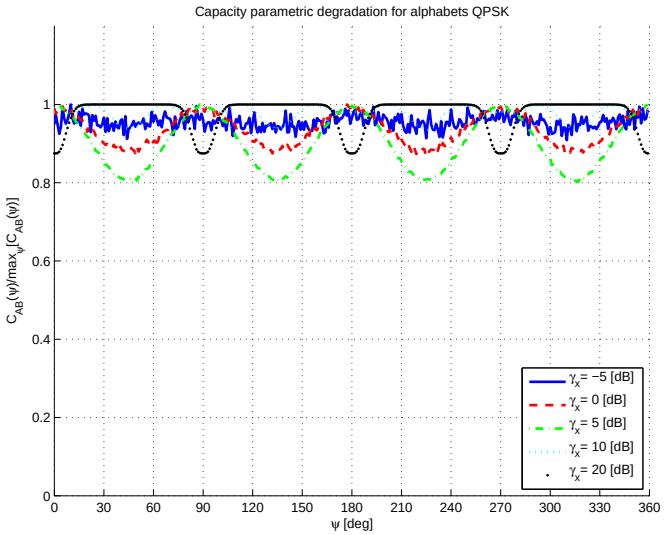

Figure 5.13: A degradation of the capacity $C_{AB}(\psi)/\max_{\psi'}[C_{AB}(\psi')]$ as a function or channel relative phase rotation for QPSK alphabet.

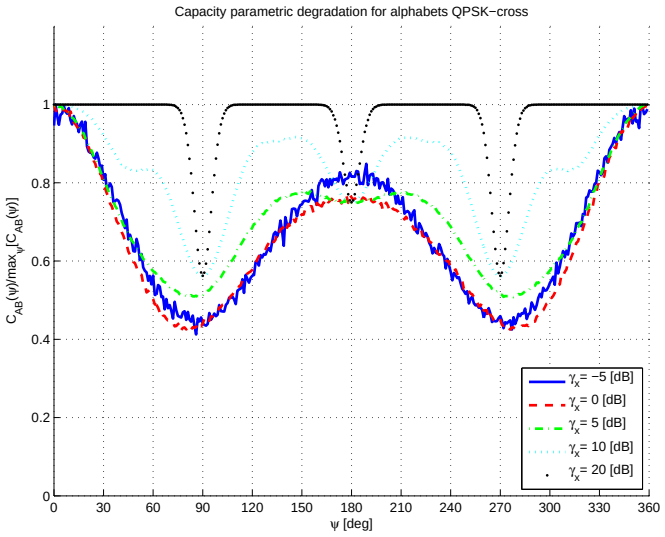

Figure 5.14: A degradation of the capacity $C_{AB}(\psi)/\max_{\psi'}[C_{AB}(\psi')]$ as a function or channel relative phase rotation for QPSK-cross alphabet.

Monte-Carlo Evaluation of the Integrals

All integrals involved in the entropy evaluations are complicated multi-fold integrals over the N-dimensional complex plane. Their direct evaluation by traditional numerical integration procedures is known to be complex and very slowly converging. Better computational efficiency is achieved by Monte-Carlo numerical evaluation of the integrals. This is not to be confused with Monte-Carlo simulation. We use it for the numerical evaluation of the integrals, not for running the system with some particular coding and signal processing algorithms. The method is usable for evaluation of any summation or integration of the form

$$I = \int f(x)g(x)\ \mathrm{d}\,x. \tag{5.20}$$

We consider $f(x)$ as a PDF, and hence the integral can be evaluated as

$$I = \mathrm{E}_{f(x)}[g(x)]. \tag{5.21}$$

Providing that we are able to generate random values with the distribution $f(x)$: $x \sim f(x)$ then the integral is approximated by evaluating the empirical mean $\hat{\mathrm{E}}[\centerdot]$ of $g(x)$. Generation of the random variable with given a density is a relatively easy task particularly for linear Gaussian mixture densities. We can also always resort to building a full system model producing the desired random variable and feeding that system with its all random excitations — typically data and noise sources.

A numerical evaluation of $\mathcal{H}[x]$ gives

$$\mathcal{H}[x] \approx -\hat{\mathrm{E}}_{x\sim p(x)}\left[\lg\left(\frac{1}{M_c^2}\sum_{c_A,c_B} p_w(x-u(c_A,c_B))\right)\right] \tag{5.22}$$

where x is generated with the distribution (5.11). The conditional entropy approximation is obtained as

$$\mathcal{H}[x|c_{AB}] = -\hat{\mathrm{E}}_{x,c_{AB}\sim p(x,c_{AB})}\left[\lg p(x|c_{AB})\right]. \tag{5.23}$$

5.3.2 Alphabet constrained Hierarchical BC with Partial Side Information

Destination decoding metric with partial complementary side-information

Invertibility of Minimal Exclusive Mapping

Lemma 1 (Reciprocal minimal exclusive mapping). Assume a *minimal* exclusive mapping $a_{AB} = \mathcal{X}(a_A, a_B)$ for finite alphabet symbols a_A, a_B, a_{AB} with the cardinality M. Then we can always construct some other *minimal* exclusive mapping $\mathcal{X}'$ such that $a_A = \mathcal{X}'(a_{AB}, a_B)$.

Proof. For a finite alphabet, we can always index the symbols by integers $i_A, i_B, i_{AB} \in \{0,\ldots,M-1\}$. The minimal exclusive mapping for the index alphabets can be implement by mod$M$ operations $i_{AB} = i_A \oplus i_B$. But it directly implies that $i_A = i_{AB} \ominus i_B$ which also forms a minimal exclusive mapping. □

This property simply means that given the knowledge of arbitrary 2 symbols out of a_A, a_B, a_{AB}, we can uniquely obtain the remaining one provided that the mapping is the minimal one.

Symbol-wise Destination Decoding Metric Assume a layered HXC with *common* H-MAC and H-BC relay code $\mathcal{C}_R = \mathcal{C}$ and transmitting the symbols at relay

$$v = v(b_{AB}),\ \ \mathbf{b}_{AB} = \mathcal{C}(\mathbf{d}_{AB}) \tag{5.24}$$

where symbol-wise mappings $d_{AB} = \mathcal{X}_d(d_A, d_B)$ and $b_{AB} = \mathcal{X}_b(b_A, b_B)$ are *minimal* exclusive mappings. The destination received signal symbols are $y_A = y_A(b_{AB})$. The function $y_A(b_{AB})$ represents a *general* input-output description of the H-BC observation at the destination including full channel model. An example is a special case of AWGN R to DA channel $y_A = y_A(b_{AB}) = v(b_{AB}) + w_A$.

Assume a C-SI transmitted signal *sharing* the same codebook as the H-MAC phase $s_B = s(c_B)$, $\mathbf{c}_B = \mathcal{C}(\mathbf{d}_B)$. The C-SI is in fact the same signal as it is transmitted

from the source at the H-MAC phase. The destination received signal symbols are $z_A = z_A(c_B)$ which is conditionally independent with observation y_A: $z_A \perp y_A|b_{AB}, c_B$. A general input-output description of the C-SI link is represented by $z_A(c_B)$.

From lemma 1, it must hold $d_A = \mathcal{X}'_d(d_{AB}, d_B)$. The symbols b and c are coded by the same codebook, thus they must share the same alphabet. Again, from the lemma 1, it holds $b_A \equiv c_A = \mathcal{X}'_c(b_{AB}, c_B)$ and also $b_B \equiv c_B$. The symbol equivalence comes from the common isomorphic indexing. The distributive law of the coding over the minimal per-symbol mapping (see [101] or [102]) gives

$$\mathcal{X}'_c(b_{AB}, c_B) = \mathcal{C}\left(\mathcal{X}'_d(d_{AB}, d_B)\right). \tag{5.25}$$

Therefore, d_A must be decodable from the observations $y_A = y_A(b_{AB})$ and $z_A = z_A(c_B)$.

The symbol-wise decoding metric $\mu(b_A) = p(y_A, z_A|b_A)$ is

$$\begin{aligned} p(y_A, z_A|b_A) &= \sum_{c_B} p(y_A, z_A|b_A, c_B)p(c_B) \\ &= \sum_{c_B} p(y_A|b_A, c_B)p(z_A|b_A, c_B)p(c_B) \\ &= \sum_{c_B} p(y_A|\mathcal{X}_c(b_A, c_B))p(z_A|c_B)p(c_B). \end{aligned} \tag{5.26}$$

This metric is used by the destination decoder $\mathcal{D}$ corresponding to the coded $\mathcal{C}$.

Equivalent H-BC Channel The destination B has two channel observations y_A and C-SI link z_A. The equivalent channel for the capacity evaluation has multi-output form

$$[y_A, z_B] = [y_A(b_{AB}), z_A(c_B)]. \tag{5.27}$$

H-BC Symmetric Capacity with Partial C-SI

The H-BC phase transmits a common HXC signal to both destinations. The H-BC capacity region is thus *rectangular* with maximum rates given by $I(b_A; y_A, z_A)$ and similarly for destination B.

The symmetric alphabet constrained H-BC capacity corresponds to the mutual information evaluated for the uniform code symbols distribution

$$C_{\text{HBC}} = I(b_A; y_A, z_A) = \mathcal{H}[y_A, z_A] - \mathcal{H}[y_A, z_A|b_A]. \tag{5.28}$$

Both entropies are relatively easy to evaluate

$$\mathcal{H}[y_A, z_A] = -\,\mathrm{E}_{y_A,z_A}\left[\lg p(y_A, z_A)\right], \tag{5.29}$$

$$\mathcal{H}[y_A, z_A|b_A] = -\,\mathrm{E}_{y_A,z_A,b_A}\left[\lg p(y_A, z_A|b_A)\right]. \tag{5.30}$$

For the Gaussian channels, it is

$$\begin{aligned} &p(y_A, z_A|b_A) = \\ &= \sum_{c_B} p_{w_A}\left(y_A - v\left(\mathcal{X}_c(b_A, c_B)\right)\right) p_{\xi_A}\left(z_A - s(c_B)\right) p(c_B) \end{aligned} \tag{5.31}$$

and

$$p(y_A, z_A) = \sum_{b_A} p(y_A, z_A|b_A) p(b_A) \tag{5.32}$$

where $p_{w_A}(\centerdot)$ is the PDF of the R to DA link additive noise and $p_{\xi_A}(\centerdot)$ is the PDF of the SB to DA side-information link additive noise (see Fig. 5.4).

For a comparison purposes, we also evaluate pure C-SI link capacity, as if there was no other signal at all. The capacity $C_{\mathrm{CSI}} = I(c_B; z_A)$ is a simple capacity of the Gaussian alphabet constrained channel.

Numerical Results

All symmetric alphabet constrained capacities were evaluated numerically by the Monte-Carlo integral evaluation. The detailed procedure follows similar principles as explained in [101] and [102]. We assumed identical alphabets $\mathcal{A}_s = \mathcal{A}_v$. The H-BC capacity as a function of the γ_z SNR for various alphabets and relay-to-destination SNR γ_x are on Figs. 5.15, 5.16, 5.17, 5.18. We also show a pure "stand-alone" capacity of the C-SI link for a comparison.

A slightly different perspective on the the same results is shown on Figs. 5.19, 5.20, 5.21, 5.22. We plotted the H-BC capacity as function of the stand-alone C-SI link capacity *implicitly* parameterized by all γ_Z. The curves are plotted for various alphabets and relay-to-destination link SNR.

Upper Bound & Product Capacity Law

The numerical results show some qualitative phenomena.

1. The H-BC capacity is upper bounded by the C-SI link capacity (Figs. 5.15, 5.16, 5.17, 5.18)

   $$C_{\mathrm{HBC}}(\gamma_y, \gamma_z) \leq C_{\mathrm{CSI}}(\gamma_z), \;\; \forall \gamma_y, \gamma_z. \tag{5.33}$$

   This is not surprising, and in fact, it directly follows from the assumption of the *minimal* HXC used. Unless the C-SI link is capable providing reliable

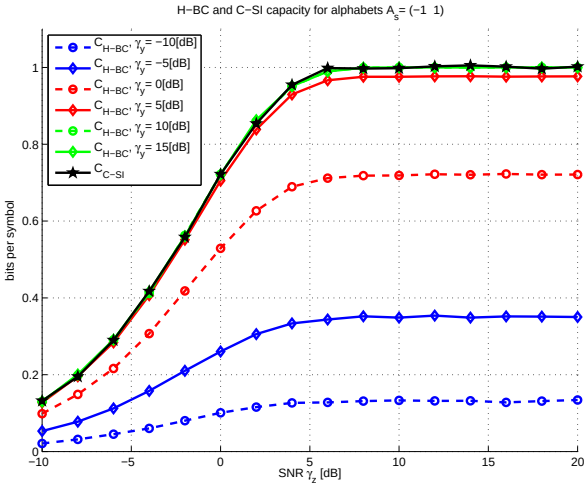

Figure 5.15: BPSK alphabet constrained capacity of H-BC stage and capacity of the complementary SI link.

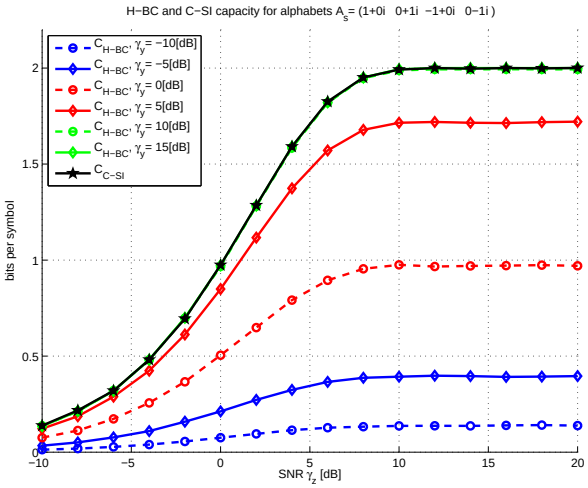

Figure 5.16: QPSK alphabet constrained capacity of H-BC stage and capacity of the complementary SI link.

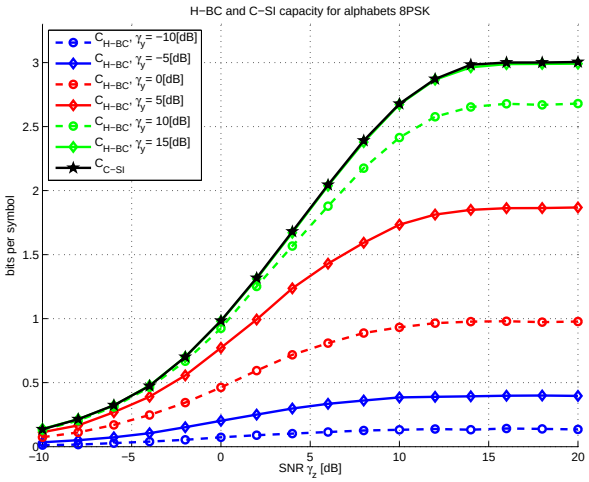

Figure 5.17: 8PSK alphabet constrained capacity of H-BC stage and capacity of the complementary SI link.

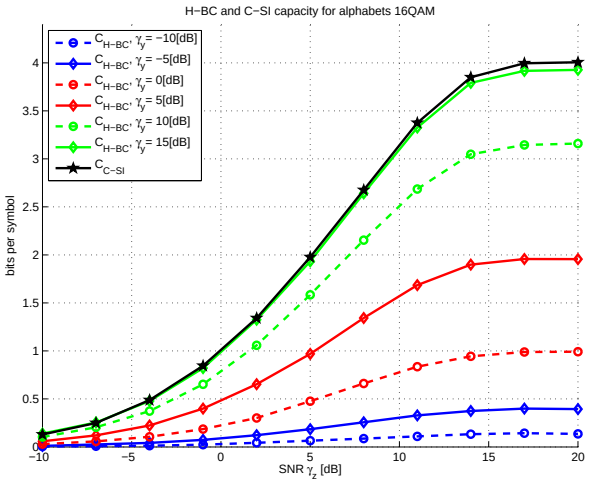

Figure 5.18: 16QAM alphabet constrained capacity of H-BC stage and capacity of the complementary SI link.

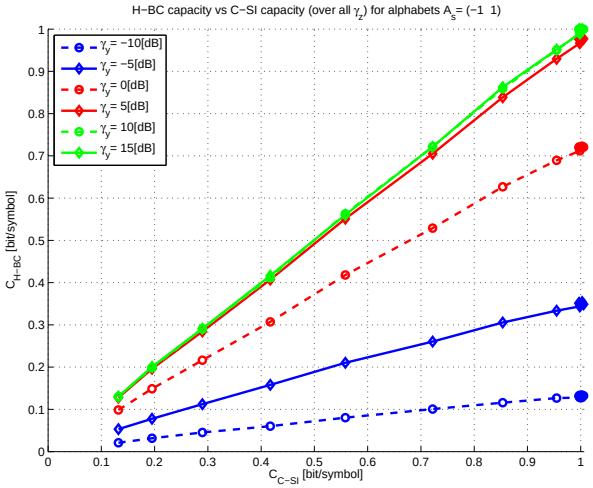

Figure 5.19: BPSK alphabet constrained capacity of H-BC versus capacity of C-SI link as a parametric plot over all γ_z.

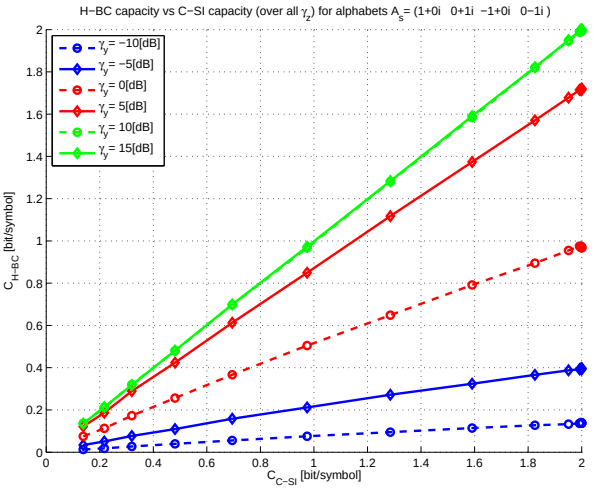

Figure 5.20: QPSK alphabet constrained capacity of H-BC versus capacity of C-SI link as a parametric plot over all γ_z.

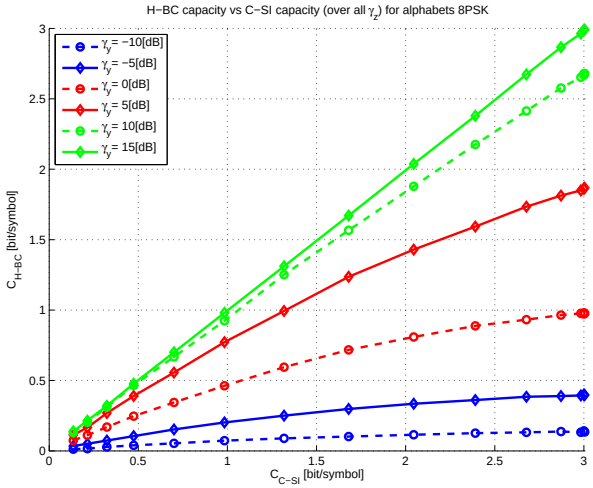

Figure 5.21: 8PSK alphabet constrained capacity of H-BC versus capacity of C-SI link as a parametric plot over all γ_z.

C-SI, we cannot decode the main data from the source A.

2. This cannot be exceeded even for the perfect relay-to-destination link $\gamma_y \to \infty$. Then the capacity is purely given by the C-SI capacity

$$C_{\mathrm{HBC}}(\gamma_y \to \infty, \gamma_z) = C_{\mathrm{CSI}}(\gamma_z). \tag{5.34}$$

This corresponds to the linear identity function in Figs. 5.19, 5.20, 5.21, 5.22.

3. However a rather surprising fact is that this linear law also holds for finite values of γ_y (see Figs. 5.19, 5.20, 5.21, 5.22)

$$C_{\mathrm{HBC}}(\gamma_y, \gamma_z) = \alpha C_{\mathrm{CSI}}(\gamma_z) \tag{5.35}$$

where

$$\alpha = \frac{C_{\mathrm{HBC}}(\gamma_y, \gamma_z \to \infty)}{C_{\mathrm{HBC}}(\gamma_y \to \infty, \gamma_z \to \infty)}. \tag{5.36}$$

We used the fact that the *perfect* C-SI case corresponds to $\gamma_z \to \infty$, with $C_{\mathrm{perfCSI}} = \lg |\mathcal{A}_S|$ and $C_{\mathrm{HBC}}^{\mathrm{perfCSI}}(\gamma_y) = C_{\mathrm{HBC}}(\gamma_y, \gamma_z \to \infty)$. The capacity $C_{\mathrm{HBC}}^{\mathrm{perfCSI}}$ is however given as a simple finite alphabet Gaussian link. The capacity

$$C_{\mathrm{HBC}}(\gamma_y \to \infty, \gamma_z \to \infty) = \lg |\mathcal{A}_v| = \lg |\mathcal{A}_s| \tag{5.37}$$

corresponds to both perfect (error-less) relay-to-destination and C-SI links.

The above stated facts leads to the following conjecture.

Conjecture 5.1 (Product capacity law of the H-BC)**.** *The H-BC finite alphabet constrained capacity with minimal HXC and common source and relay alphabet* $\mathcal{A}$

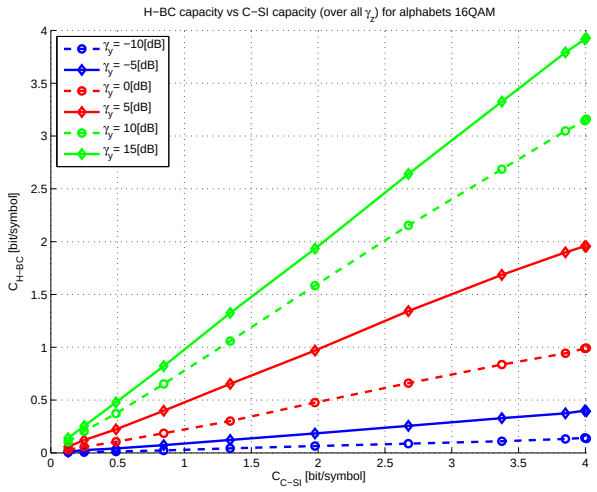

Figure 5.22: 16QAM alphabet constrained capacity of H-BC versus capacity of C-SI link as a parametric plot over all γ_z.

is given by

$$C_{\mathrm{HBC}}(\gamma_y, \gamma_z) = \frac{C_{\mathrm{HBC}}^{\mathrm{perfCSI}}(\gamma_y) C_{\mathrm{CSI}}(\gamma_z)}{\lg |\mathcal{A}|}. \tag{5.38}$$

Note The case of 8PSK exhibits very slight depart (a positive margin) from this law (see Fig. 5.21). An explanation of this phenomena is yet to be investigated.

5.4 Capacity/Throughput Regions of HDF strategy with Extended mapping

The extended mapping case is the case where the relay performs a decoding of the original sources data function, called Hierarchical Network Code map (HNC map), having the output cardinality $|\mathcal{C}_R|$ such that $\max(|\mathcal{C}_A|, |\mathcal{C}_B|) < |\mathcal{C}_R| < |\mathcal{C}_A||\mathcal{C}_B|$ where $|\mathcal{C}_A|, |\mathcal{C}_B|$ are the cardinalities of the source nodes A and B codebooks. In such a case, the destination complementary side-information does *not* need to the perfect one. The cardinality extension can be done at various levels, either on codeword symbol level on one side on the complete codebook size. A very natural system scenario which nicely demonstrates the potentials of extended HNC map and impacts of imperfect (partial) C-SI is the "butterfly" network (2-SRN) in Fig. 5.2.

Although an extension of the WNC principles from the 2-WRC system into a slightly advanced network structures like the *butterfly network* [105] could seem relatively straightforward, several new unconventional features of the WNC arise. First of all, the unreliable transmission of the C-SI can be overcome by an increased cardinality of the relay output (extended cardinality relaying [106, 107]) — the phenomenon

which does not have its counterpart in the traditional (binary) NC systems. The legacy of the NC approach is hence broken here, rising a huge number of new (and challenging) research problems.

It has been shown in [107] that the *extended cardinality* relaying/relay output mapping could (under specific channel conditions) outperform the minimal one (see e.g. [101]). This was demonstrated on an example of the butterfly network with 4-ary source and 8-ary relay constellation alphabets, using the Hierarchical Decode & Forward (HDF) strategy [101]. Moreover, as also proved in [107], the HDF strategy with a layered hierarchical coding approach (see e.g. [101]) and linear mapping can achieve the end-to-end capacity upper bound in the butterfly network.

One of the crucial steps in the HDF system design is the choice of a suitable Hierarchical Network Code (HNC) mapper at the relay. Simply speaking, this mapper defines how the separate data streams (from individual users) are mapped to the *hierarchical* (network-coded) data [101] stream at the relay node.

Design of the HNC mapper is quite simple in the case of the *minimal mapping* (see e.g. [101]) where it is usually given by a simple bit-wise xor operation. However, in case of the *extended mapping* the suitable HNC mapper should respect also the amount of destinations' C-SI (i.e. a quality of the C-SI links) to maximize the potential throughput of the system.

In this section we focus on this problem. We introduce a systematic approach to the design of a *set of HNC mappers* for relay output mapping in the Broadcast (BC) phase of communication in the butterfly network. Consequently, we focus mainly on a relay processing and the subsequent BC phase of communication. The parametric Multiple-Access (MAC) phase (essentially identical to that in the 2-WRC) is analyzed e.g. in [101, 108, 109].

In a numerical evaluation of the alphabet-constrained capacity (mutual information) we show how the performance of the butterfly network can be controlled by a suitable choice of the HNC mapper (from the pre-designed set) at the relay. These results pave the way for an idea of adaptive butterfly network, where the performance can be adapted to the actual channel conditions (and thus the quality of C-SI).

The topology of the butterfly network can be justified also from the point of view of the SAPHYRE project. Sources S_A, S_B correspond to the base stations of two different mobile operators. Since both mobile nodes (destinations D_A, D_B) are out of their respective operator's coverage area, the communication is not possible. However, if the operators implement the SAPHYRE approach, which in this case means that they will share their time-frequency slots (sharing resources) and deploy a common relay R (sharing infrastructure), they will both benefit from the situation, since a communication to both mobile nodes will be made possible (using the HDF strategy).

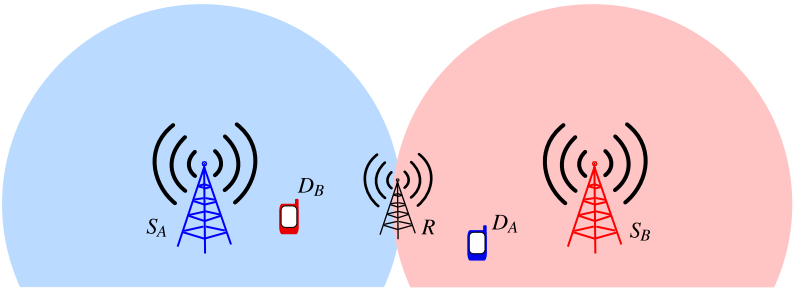

Figure 5.23: Butterfly network with HDF strategy – SAPHYRE project point of view.

5.4.1 Relay processing with Extended HNC mapping

After receiving x, the relay performs an eXclusive mapping operation (see [101] for details) to map the received signal to the relay output symbol $s_R\left(c_{AB}\right)$, where $c_{AB} = \mathcal{X}\left(c_A^i, c_B^j\right)$. This hierarchical symbol mapping is referred to as the *Hierarchical Network Code* (HNC map) in [110]. In principle, the hierarchical (network-coded) output signal from the relay must jointly represent the data from both sources (S_A, S_B), while a knowledge of respective C-SI at the destination is necessary for a successful decoding of the desired (separate) data stream [101].

For the purpose of this work we will assume that the HNC mapping operation can be described directly on the signal-space symbol level $s_R^{k_{ij}} = \mathcal{X}_s\left(s_A^i, s_B^j\right)$. In this case it is suitable to describe the specific HNC mapping by the HNC matrix

$$X_{\mathrm{HNC}} = \begin{bmatrix} k_{11} & \cdots & k_{1M} \\ \vdots & \ddots & \vdots \\ k_{M1} & \cdots & k_{MM} \end{bmatrix}, \tag{5.39}$$

where $k_{ij} = X_{\mathrm{HNC}}\left(i,j\right), i,j \in \{1,2,\ldots M\}$ is an index of the relay output (signal space) channel symbol $s_R^{k_{ij}} \in \mathcal{A}_s^R$. Note that for the cardinality of the relay output alphabet holds (see e.g. [101])

$$|\mathcal{A}_s| = M \leq \left|\mathcal{A}_s^R\right| \leq M^2 = |\mathcal{A}_s|^2 . \tag{5.40}$$

The equalities in (5.40) correspond to the minimal ($\left|\mathcal{A}_s^R\right| = |\mathcal{A}_s|$) and full ($\left|\mathcal{A}_s^R\right| = |\mathcal{A}_s|^2$) mapping (see e.g. [101, 106]). More details about the relay output alphabet cardinality and corresponding required amount of the C-SI will be provided later.

In the BC phase the relay transmits the signal to both destinations. The constellation space signals received at D_A, D_B are

$$y_A = s_R + w_A, \tag{5.41}$$
$$y_B = s_R + w_B. \tag{5.42}$$

Assuming that a suitable HNC mapper has been used at the relay, destinations are able to decode the desired data from the relay signal and C-SI.

5.4.2 The Role of Complementary Side Information

The amount of information on the complementary data stream (C-SI) which is available at D_i (after the MAC phase) is given by a number of reliably received bits c^i_{CSI}, $i \in \{A, B\}$. This corresponds to a level of granularity at which the destination can distinguish particular symbols received on the C-SI link, and consequently also to the partitioning of the HNC map (HNC matrix X_{HNC}). For the unambiguous decoding each destination needs to identify only the relay symbol inside the resulting subset of the HNC map (submatrix of X_{HNC}). This is obvious from the example system with $|\mathcal{A}_s| = 4$ in Figs. 5.24, 5.25, 5.26 for perfect, zero and partial C-SI (respectively).

As proved e.g. in [107], for unambiguous decoding in the presence of perfect C-SI at each destination each particular relay output symbol can appear at most once on each row and in each column of the HNC map (see Fig. 5.24). This corresponds to the *minimal cardinality* relay output mapping ($\left|\mathcal{A}^R_s\right| = M$). Similarly (as also noted in [107]), for the case of partial/imperfect C-SI each particular relay output symbol can appear at most once within a group of rows/columns (given by the HNC map partitioning – see Fig. 5.26). This corresponds to the *extended cardinality* relay output mapping. In the last case, i.e. in the butterfly network where the C-SI links are fully unreliable (Fig. 5.25), the relay needs to deliver data to both sources without assistance of the C-SI and hence a *full cardinality* relay output mapping ($\left|\mathcal{A}^R_s\right| = M^2$) is required.

As it is obvious from the discussion above, the C-SI (overheard by destinations in the MAC phase) has a crucial impact on the overall system performance, since it determines a required minimal cardinality of the relay output alphabet $\left|\mathcal{A}^R_s\right|$ (as proved e.g. in [107]). This is obviously a direct consequence of the eXclusive law (see e.g. [101]). Accordingly, the C-SI introduces some preconditions on a suitable HNC matrix design. In the following section we introduce an algorithm for the design of a set of HNC matrices for arbitrary source alphabet cardinality M (and the corresponding range of permissible values of c^A_{CSI}, c^B_{CSI}).

5.4.3 HNC Mapper Design

As noted in the previous section, the quality of the C-SI links defines the partitioning of the HNC matrix X_{HNC} (see examples in Figs. 5.24, 5.25, 5.26), where unique relay output symbols are required in all the resulting submatrices (for a given c^A_{CSI}, c^B_{CSI}). In this way the X_{HNC} can be partitioned into a set of (generally rectangular) blocks B_l (see examples in Fig. 5.27).

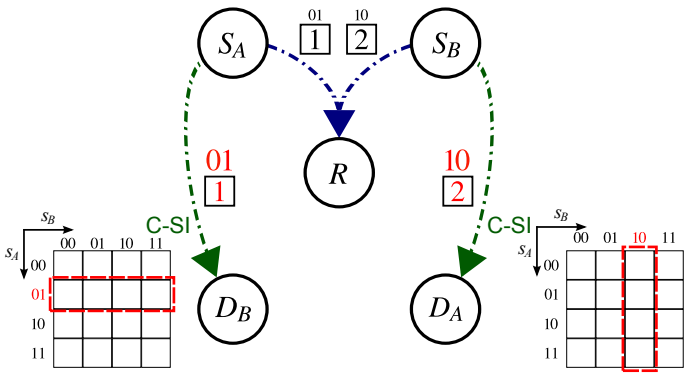

Figure 5.24: Butterfly network with perfect C-SI links ($c^A_{\text{CSI}} = c^B_{\text{CSI}} = 2$).

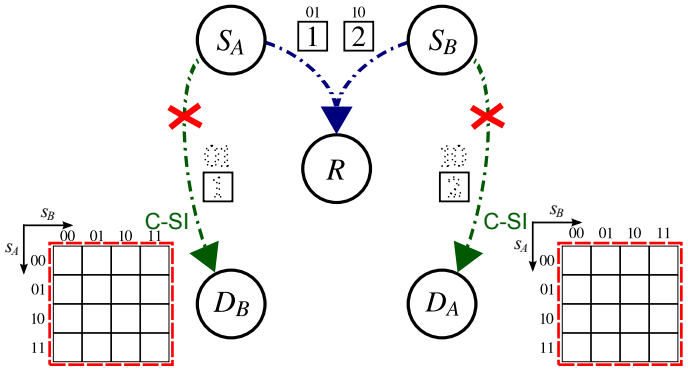

Figure 5.25: Butterfly network with unreliable/missing C-SI links ($c^A_{\text{CSI}} = c^B_{\text{CSI}} = 0$).

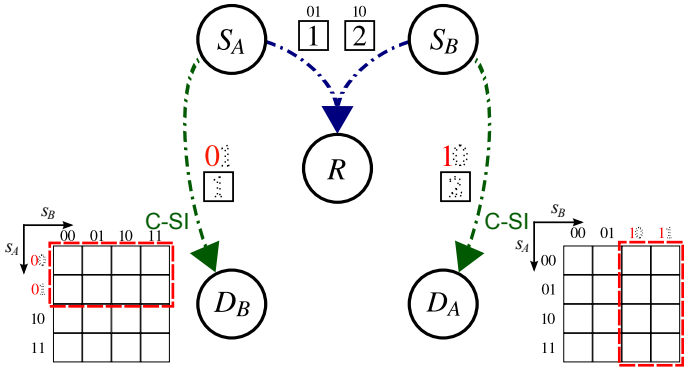

Figure 5.26: Butterfly network with imperfect C-SI links ($c^A_{\text{CSI}} = c^b_{\text{CSI}} = 1$). Imperfection of the C-SI links can be visualized as a loss of (several) least significant bits (only the last bit is lost in this example).

Algorithm 1 HNC matrix $X_M^{(m)}$ design ($M = |\mathcal{A}_s|$, $m = c_{\text{CSI}}$).

1. Assumptions:
   a) Block dimensionality: $\mathcal{B} = \frac{M}{2^m}$
   b) Number of unique blocks: $L = 2^m$
   c) Input elements: $k \in \mathcal{K} = \left\{0, 1, 2, \ldots \left(\frac{M^2}{L}\right) - 1\right\}$
2. Design the set of blocks $\{B_l\}_{l=0}^{L-1}$:
   a) Partition the set $\mathcal{K}$ into L non-overlapping subsets $\mathcal{K}_l$, where $|\mathcal{K}_l| = \mathcal{B}^2$, $\forall l \in \{0, \ldots L-1\}$
   b) Fill in successively (e.g. columnwise) the block B_l with unique elements from $\mathcal{K}_l$
3. Set up (block-by-block) the HNC matrix $X_M^{(m)}$:
   a) $A_{i,j} = B_{i \oplus j}$, where $i, j \in \{0, 1, \ldots L-1\}$ and $\oplus$ is a bit-wise XOR
   b) $X_M^{(m)} = \begin{bmatrix} A_{0,0} & \cdots & A_{0,L-1} \\ \vdots & \ddots & \vdots \\ A_{L-1,0} & \cdots & A_{L-1,L-1} \end{bmatrix}$

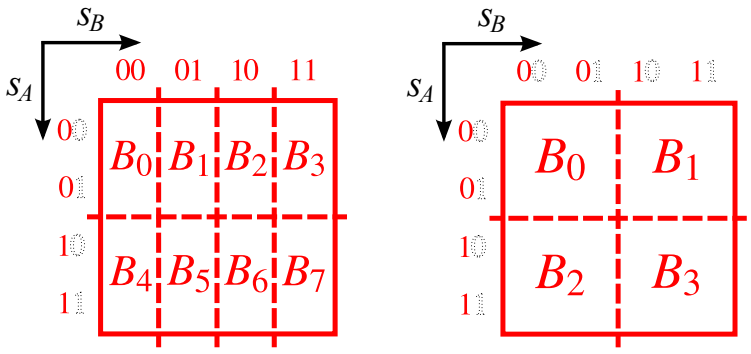

Figure 5.27: Examples of HNC matrix partitioning for $c^A_{\text{CSI}} = 2$, $c^B_{\text{CSI}} = 1$ and $c^A_{\text{CSI}} = c^B_{\text{CSI}} = 1$.

c_{CSI} = 1

$X_4^{(c_{\text{CSI}})}$

$$\left[\begin{array}{cc|cc} 0 & 2 & 4 & 6 \\ 1 & 3 & 5 & 7 \\ \hline 4 & 6 & 0 & 2 \\ 5 & 7 & 1 & 3 \end{array}\right]$$

c_{CSI} = 2

$$\left[\begin{array}{c|c|c|c} 0 & 1 & 2 & 3 \\ \hline 1 & 0 & 3 & 2 \\ \hline 2 & 3 & 0 & 1 \\ \hline 3 & 2 & 1 & 0 \end{array}\right]$$

Table 5.1: Example HNC matrices $X_4^{(1)}$ and $X_4^{(2)}$.

This observation leads to an idea of a systematic, block-based design of the HNC matrix. A suitable X_{HNC} must have unique symbols in each individual block B_l and also in all the respective subsets of blocks corresponding to the given partitioning (e.g. $\{B_0, B_1, B_2, B_3\}$, $\{B_4, B_5, B_6, B_7\}$ and $\{B_0, B_4\}$, $\{B_1, B_5\}$, $\{B_2, B_6\}$, $\{B_3, B_7\}$ in Fig. 5.27).

It is interesting to note that square building blocks B_l can be assumed without loss of generality (for arbitrary c^A_{CSI}, c^B_{CSI})[1]. Each individual block is hence a $\mathcal{B} \times \mathcal{B}$ submatrix of X_{HNC}. The block dimensionality is given by $\mathcal{B} = \frac{M}{2^{c_{\text{CSI}}}}$, where $c_{\text{CSI}} = \min\left\{c^A_{\text{CSI}}, c^B_{\text{CSI}}\right\}$. The HNC matrix designed for the source alphabet with cardinality M and CSI-links quality c_{CSI} will be denoted as $X_M^{(c_{\text{CSI}})}$. The design algorithm for the HNC matrix $X_M^{(c_{\text{CSI}})}$ is summarized in Algorithm 1.

The complete set of HNC matrices $X_M^{(c_{\text{CSI}})}$ for given M and all permissible values of

[1]The minimal required relay alphabet cardinality $\left|\mathcal{A}_s^R\right|$ is given by the weaker C-SI link. To clarify this statement we can consider an example where one C-SI link is fully unreliable (e.g. $c^A_{\text{CSI}} = 0$). In this case the relay must use full cardinality relaying in order to guarantee successful decoding at D_A (even if D_B has a perfect C-SI available). Hence for the purpose of the HNC mapper design we can assume the same level of partitioning given by $c_{\text{CSI}} = \min\left\{c^A_{\text{CSI}}, c^B_{\text{CSI}}\right\}$, resulting in the square blocks B_l.

c_{CSI} = 1

$X_8^{(c_{\mathrm{CSI}})}$

0	4	8	12	16	20	24	28
1	5	9	13	17	21	25	29
2	6	10	14	18	22	26	30
3	7	11	15	19	23	27	31
16	20	24	28	0	4	8	12
17	21	25	29	1	5	9	13
18	22	26	30	2	6	10	14
19	23	27	31	3	7	11	15

c_{CSI} = 2

0	2	4	6	8	10	12	14
1	3	5	7	9	11	13	15
4	6	0	2	12	14	8	10
5	7	1	3	13	15	9	11
8	10	12	14	0	2	4	6
9	11	13	15	1	3	5	7
12	14	8	10	4	6	0	2
13	15	9	11	5	7	1	3

Table 5.2: Example HNC matrices $X_8^{(1)}$ and $X_8^{(2)}$.

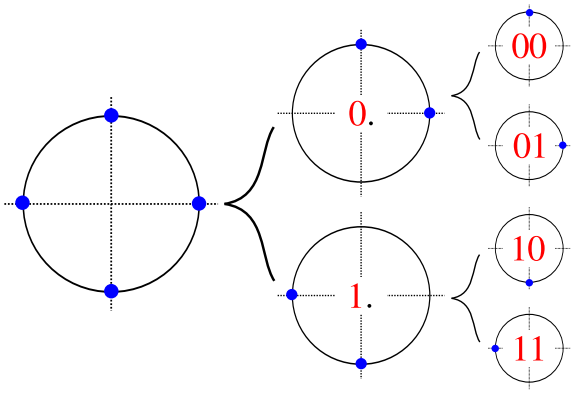

Figure 5.28: Partitioning of the QPSK source constellation alphabet.

c_{CSI} ($0 \leq c_{\mathrm{CSI}} \leq \log_2 M$) can be designed with Algorithm 1. This design algorithm is suitable even for the design of HNC mappers for minimal ($\mathcal{B} = 1$, $L = M$) and full cardinality ($\mathcal{B} = M$, $L = 1$) relaying. Some examples of the proposed HNC matrices are given in Tables 5.1, 5.2 for $M = 4$ and $M = 8$ (respectively). As it is also obvious from these tables, the cardinality of the relay output alphabet is given by

$$\left|\mathcal{A}_s^R\right| = |\mathcal{K}| = \frac{M^2}{L}. \tag{5.43}$$

Source Alphabet Partitioning

The HNC mapper design in Algorithm 1 is based on the assumption that each destination can identify (at least) first c_{CSI} bits from the constellation symbol received on the C-SI link (except for the full cardinality case) – see examples in Figs. 5.24, 5.26. Obviously, it is possible to increase the reliability of this (partial) C-SI by a suitable partitioning (and corresponding constellation indexing) of both source

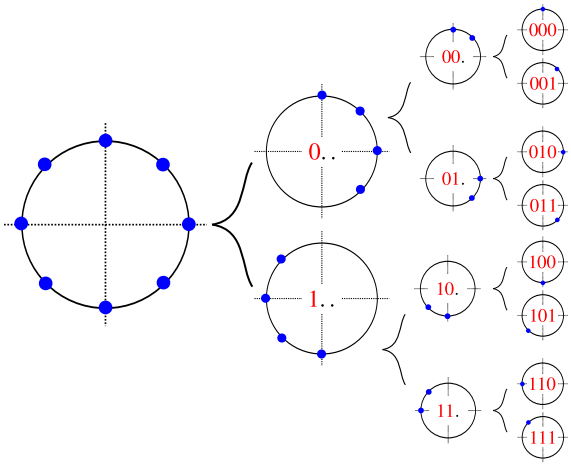

Figure 5.29: Partitioning of the 8PSK source constellation alphabet.

alphabets $\mathcal{A}_s$.

The idea is to partition the source constellation alphabet into smaller subsets (according to the principles similar to Ungerboeck mapping rules [111]) to increase the probability of successful (partial) C-SI retrieval at the destination. Hence the intention is to maximize the distance between the particular subsets (not the particular symbols)[2]. The principle of the proposed source constellation alphabet partitioning is visualized in Figs. 5.28, 5.29 for QPSK and 8PSK (respectively).

5.4.4 Numerical Evaluations

In this section we finally demonstrate a feasibility of the proposed HNC mapper design (Algorithm 1) for the butterfly network. Without loss of generality, we focus on the D_B processing. Destination D_B has two channel observations – the relay (network-coded) signal $y_B\,(c_{AB})$ and C-SI link $z_B\,(c_A)$.

Since the relay transmits a common signal to both destinations, the broadcast phase capacity region is *rectangular* [106] with maximum rate given by $I(c_B; y_B, z_B)$ (and similarly for D_A). The broadcast phase alphabet-constrained capacity [106] (mutual information) is given by

$$C_{\text{HBC}} = I(c_B; y_B, z_B) = \mathcal{H}[y_B, z_B] - \mathcal{H}[y_B, z_B|c_B]. \tag{5.44}$$

The pure C-SI link capacity $C_{\text{CSI}} = I(c_A; z_B)$ will be also evaluated (for a compar-

[2]This should be clear e.g. from Fig. 5.26, where symbols 00 and 01 define the same subset of the HNC map and consequently the successful decoding would be possible even if the destination is unable to distinguish between these two symbols on the C-SI link. Hence, these symbols should be grouped into one subset $\{00, 01\}$ (and similarly for the other symbols).

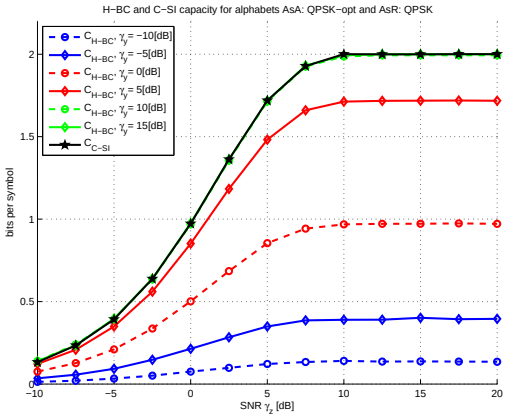

Figure 5.30: BC phase alphabet constrained capacity and capacity of the complementary SI link (minimal mapping, $\mathcal{A}_s$ = QPSK, $\mathcal{A}_s^R$ = QPSK).

ison)[3]. This capacity is simply a capacity of the Gaussian (alphabet constrained) channel [106].

The alphabet constrained capacities were evaluated numerically by the Monte-Carlo integral evaluation (for details see [106] and references therein). The broadcast phase capacity was evaluated as a function of the C-SI link SNR (γ_{z_B}) for various relay-to-destination SNR (γ_{y_B}). The results are on Figs. 5.30, 5.31, 5.32 (QPSK source alphabet) and on Figs. 5.34, 5.35, 5.36, 5.38 (8PSK source alphabet). For all these results the source alphabets were partitioned according to the Figs. 5.28, 5.29 and the HNC mappers (matrices $X_M^{(c_{\mathrm{CSI}})}$) were designed using the Algorithm 1.

For the extended relaying scenarios we have evaluated also the capacities for source alphabets with Ungerboeck [111] mapping (see Figs. 5.33, 5.37, 5.39). Here a significant degradation of the broadcast phase capacity can be observed (see Figs. 5.32 and 5.33; Figs. 5.36 and 5.37; Figs. 5.38 and 5.39), although the C-SI link capacity is identical for both compared source alphabet partitioning. Hence it is obvious that Ungerboeck source alphabet partitioning is not appropriate for the proposed HNC mappers.

Adaptive Butterfly Network Performance

As it is clear from the presented numerical results, the achievable broadcast phase capacity depends strongly on the employed HNC mapper. Obviously, by a suitable choice of the HNC mapper (according to the actual channel conditions) it would be possible to maximize the throughput of the system. Provided that the observed

[3]It is important to note that some caution is necessary when interpreting the numerically evaluated C-SI link capacity and the C-SI link "quality indicator" c_{CSI} used in this work. Obviously, the particular value of c_{CSI} does not directly correspond to the C-SI link capacity and the proper relation between these quantities needs further investigation.

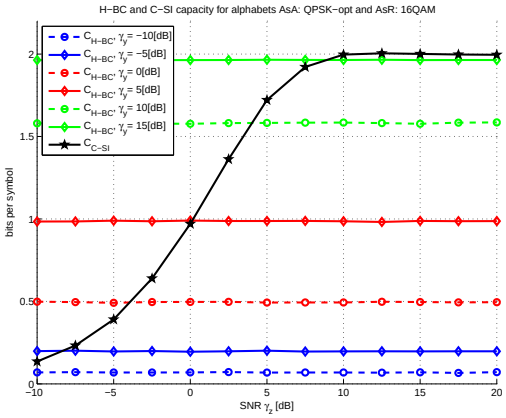

Figure 5.31: BC phase alphabet constrained capacity and capacity of the complementary SI link (full mapping, $\mathcal{A}_s = \text{QPSK}$, $\mathcal{A}_s^R = 16\text{QAM}$).

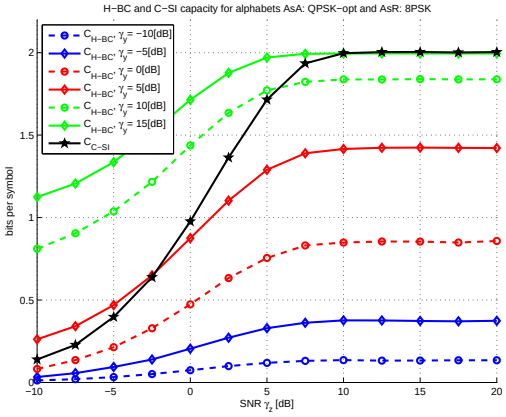

Figure 5.32: BC phase alphabet constrained capacity and capacity of the complementary SI link (extended mapping, $\mathcal{A}_s = \text{QPSK}$, $\mathcal{A}_s^R = 8\text{PSK}$).

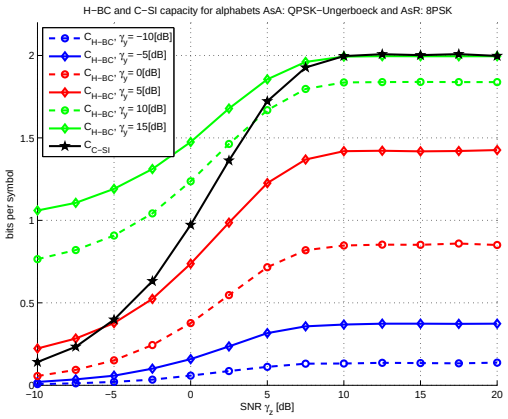

Figure 5.33: BC phase alphabet constrained capacity and capacity of the complementary SI link (extended mapping, $\mathcal{A}_s$ = QPSK with Ungerboeck mapping, $\mathcal{A}_s^R$ = 8PSK). Compare with Fig. 5.32.

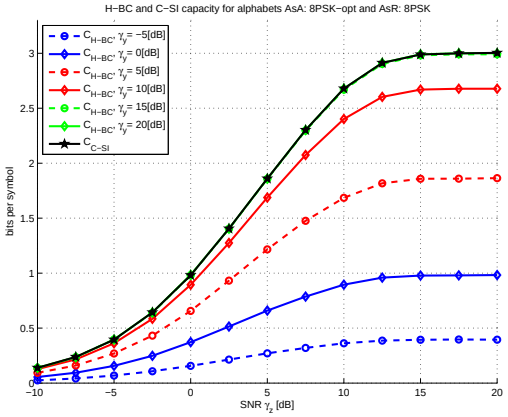

Figure 5.34: BC phase alphabet constrained capacity and capacity of the complementary SI link (minimal mapping, $\mathcal{A}_s$ = 8PSK, $\mathcal{A}_s^R$ = 8PSK).

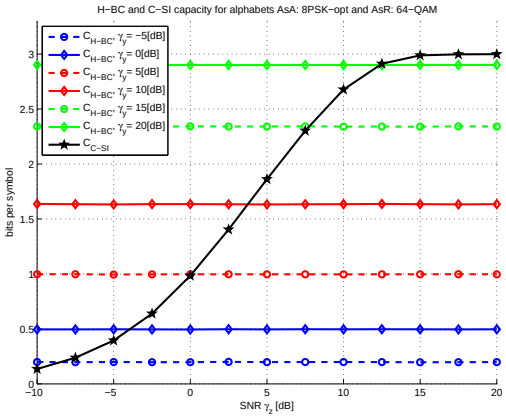

Figure 5.35: BC phase alphabet constrained capacity and capacity of the complementary SI link (full mapping, $\mathcal{A}_s = 8\text{PSK}$, $\mathcal{A}_s^R = 64\text{QAM}$).

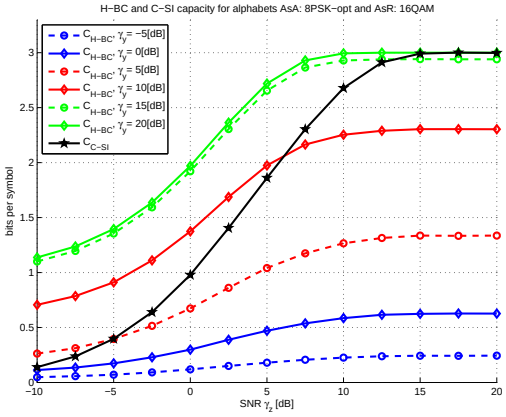

Figure 5.36: BC phase alphabet constrained capacity and capacity of the complementary SI link (extended mapping, $\mathcal{A}_s = 8\text{PSK}$, $\mathcal{A}_s^R = 16\text{QAM}$).

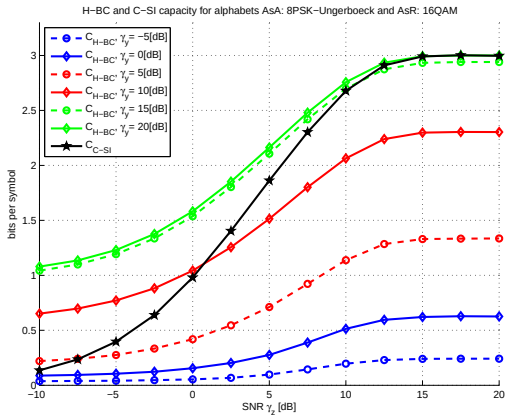

Figure 5.37: BC phase alphabet constrained capacity and capacity of the complementary SI link (extended mapping, $\mathcal{A}_s$ = 8PSK with Ungerboeck mapping, $\mathcal{A}_s^R$ = 16QAM). Compare with Fig. 5.36.

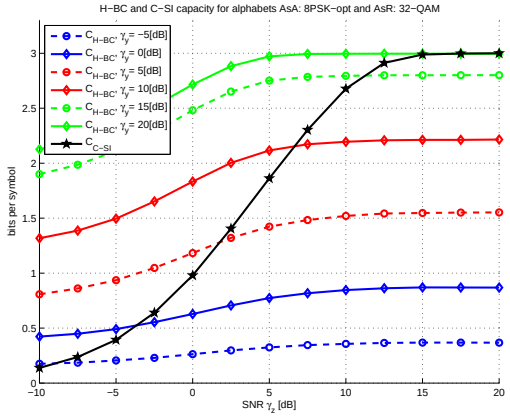

Figure 5.38: BC phase alphabet constrained capacity and capacity of the complementary SI link (extended mapping, $\mathcal{A}_s$ = 8PSK, $\mathcal{A}_s^R$ = 32QAM).

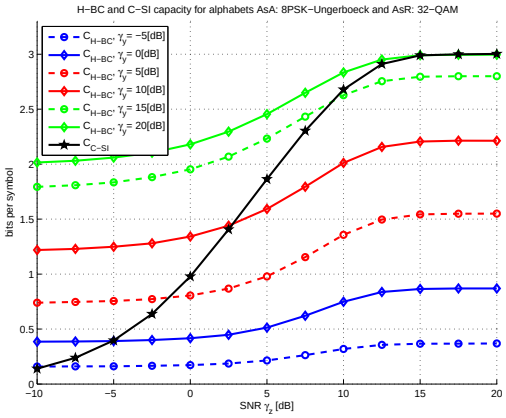

Figure 5.39: BC phase alphabet constrained capacity and capacity of the complementary SI link (extended mapping, $\mathcal{A}_s$ = 8PSK with Ungerboeck mapping, $\mathcal{A}_s^R$ = 32QAM). Compare with Fig. 5.38.

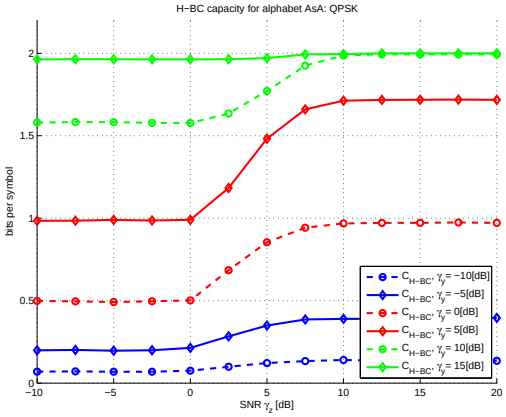

Figure 5.40: Maximum achievable BC phase (alphabet constrained) capacity for the adaptive butterfly network ($\mathcal{A}_s$ = QPSK).

quality of the C-SI link is delivered to the relay by both destinations D_A, D_B, a suitable HNC mapper can be chosen (from the predesigned set) to maximize the achievable capacity of the network.

To demonstrate a potential performance of such a system, we will assume a genie-aided relay which possess a perfect knowledge about the actual quality of the C-SI links quality (γ_{z_A}, γ_{z_B}) and the respective relay to destination links (γ_{y_A}, γ_{y_B}). The achievable broadcast phase capacity of this (genie-aided) system is evaluated in Figs. 5.40, 5.41 for QPSK and 8PSK (respectively) source alphabets.

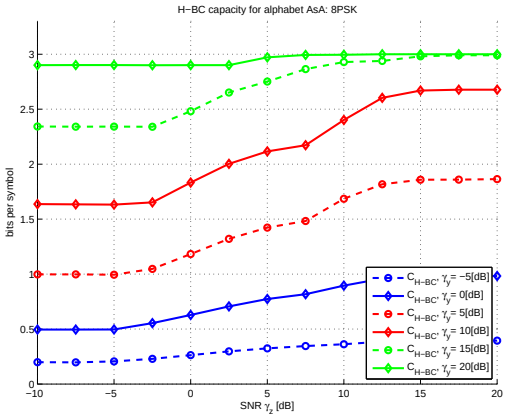

Figure 5.41: Maximum achievable BC phase (alphabet constrained) capacity for the adaptive butterfly network ($\mathcal{A}_s = 8\text{PSK}$).

5.4.5 Conclusion

In this work we have proposed a systematic algorithm for the HNC mapper design (see Algorithm 1) for relaying in the butterfly network with HDF strategy. The feasibility of the proposed HNC mappers was demonstrated by evaluation of the broadcast phase capacity. We have shown that suitable source alphabet partitioning should be performed by the sources to increase the probability of successful (partial) C-SI retrieval at destinations (to maximize the achievable capacity of the system). The observed behavior of the broadcast phase capacities gives rise to the idea of adaptive butterfly network, where the performance of the system can be adapted to the actual quality of the C-SI and relay to destination links.

6 Conclusions

The first part of the deliverable provides achievable rate regions for the downlink of the spectrum sharing scenario where the multi-antenna base stations of different operators transmit over the same channel, each to its own single-antenna mobile station. This scenario is modeled by the multiple-input single-output interference channel. Thereby, the base stations are assumed to have perfect channel state information. The two distinct cases of systems with single-user decoding or multi-user decoding capabilities are considered. With single-user decoding, we further investigate the scenario where the channel state information at the base station is not perfect. The second part of the deliverable studies a physical layer resource sharing technique, which is based on a hierarchical decode and forward strategy. It is a network aware modulation and coding for multi-terminal and multi-relay communications. The results of the deliverable are organized in the following structure.

In Chapter 2 achievable rate regions of the MISO IC have been studied under the assumption that all receivers treat the interference as additive Gaussian noise. The main results are:

- In Section 2.2 an explicit parametrization of the Pareto boundary is given for an arbitrary number of users and antennas. The parametrization describes the boundary in terms of a low-dimensional manifold.
- In Section 2.3 the maximum sum-rate operating point, the proportional-fair operating point and the max-min rate point have shown to be non-convex optimization problems. A corresponding non-convex optimization framework which takes as much as possible of the problem structure into account has been developed.
- In Section 2.4 a computationally-efficient method is proposed for computing the Pareto boundary of the MISO IC achievable rate region. It is shown that the problem of finding an arbitrary Pareto-optimal rate pair, along with its enabling beamforming vector pair, is quasi-convex and hence, it can solved very efficiently using interior-point algorithms.
- In Section 2.5, the condition in which spectrum sharing (as in MISO IC) provides benefits over non-sharing scenario (as in MISO BC) is investigated. A new fast algorithm is proposed for finding a lower bound on the sum-rate of the BC using linear beamforming. The bounds are used to numerically evaluate the potential gain of non-orthogonal spectrum sharing.

Chapter 3 studies the achievable rate region of MISO IC in the scenario of imperfect CSI. The main results are:

- In Section 3.1, the robust achievable rate region of MISO is investigated. Considering the worst case achievable rate of the links, we characterize the beamforming vectors that achieve points on the Pareto boundary of the robust rate region. The spectral efficiency gain with spectrum sharing over baseline TDMA (non-sharing) is larger in the mid SNR regime.
- Section 3.2 studies the outage rate region for MISO IC. The definitions, which differ on whether the rates are declared in outage jointly or individually and whether there is instantaneous or statistical channel state information (CSI) at the transmitters, are given. Outage probabilities are given in closed form for the statistical CSI scenario.

Chapter 4 considers the case where the receivers have interference decoding capability such that the interference, when strong enough, can be decoded and subtracted from the received signal. The main results are:

- The achievable rate regions are explored and the improvement compared with the single-user detection is shown.
- The achievable rate region for the cases with two users is formulated and it is shown that the Pareto-optimal transmit covariance matrices are rank one, i.e. beamforming attains the Pareto boundary.
- The Pareto boundary is characterized, in terms of both power allocation and transmit beamforming vectors.

In Chapter 5, a general multi-source and multi-destination wireless communication network where all network nodes (relays) contribute to providing data flows without explicit routing has been investigated. The main results are:

- In Section 5.1.1, a bare-bone scenario has been identified, capturing all fundamental elements and still being simple enough to allow theoretical analysis.
- The capacity regions of the hierarchical multiple-access channel and hierarchical broadcast channel stage have been analyzed under various direct component and complementary side-information quality.
- Results on achievable rate regions for two new scenarios have been carried out. The first relaxes the minimum cardinality requirement of the exclusive code used in HDF strategy at the relay. The second is focused on minimal hierarchical distance conditions in parametric channel under various symbol alphabet size and dimensionality.
- A general technique for input-output description of the wireless network coding with arbitrary network topology and HDF strategy has been developed and achievable rate regions for finite alphabet extended HXC codes were evaluated.
- Section 5.4 deals with the fundamental limits of HDF strategy with *extended* cardinality mapping and the closely related impact of *imperfect* complemen-

tary side-information.

- The relay HDF extended cardinality map allows a trade-off between side information quality and the required throughput over the relay. Such situation captures more realistic scenarios where sources and destinations are not collocated. We evaluate quantitatively the limits and the relation between complementary side-information and the relay throughput and we also design a proper extended mapper.

Bibliography

[1] Y.-F. Liu, Y.-H. Dai, and Z.-Q. Luo, "On the complexity of optimal coordinated downlink beamforming," in *Proc. of IEEE International Conference on Acoustics Speech and Signal Processing (ICASSP)*, 2010.

[2] E. A. Jorswieck and E. G. Larsson, "The MISO interference channel from a game-theoretic perspective: A combination of selfishness and altruism achieves pareto optimality," in *Proc. of IEEE International Conference on Acoustics Speech and Signal Processing (ICASSP)*, 2008, pp. 5364–5367.

[3] ——, "Monotonic optimization framework for the two-user MISO interference channel," *IEEE Transactions on Communications*, vol. 58, no. 7, pp. 2159–2168, 2010.

[4] R. Zakhour and D. Gesbert, "Coordination on the MISO interference channel using the virtual SINR framework," in *Proc. of ITG International Workshop on Smart Antennas (WSA)*, 2009.

[5] R. Zakhour, K. M. Z. Ho, and D. Gesbert, "Distributed beamforming coordination in multicell MIMO channels," in *Proc. of IEEE Vehicular Technology Conference (VTC)*, 2009.

[6] Z. K. M. Ho and D. Gesbert, "Spectrum sharing in multiple-antenna channels: A distributed cooperative game theoretic approach," in *Proc. PIMRC*, Sept. 2008, pp. 1–5.

[7] J. Lindblom and E. Karipidis, "Cooperative beamforming for the MISO interference channel," in *Proc. of 16th European Wireless Conference (EW'10)*, 2010.

[8] Z. K. M. Ho and D. Gesbert, "Balancing egoism and altruism on the interference channel: The MIMO case," in *Proc. of IEEE International Conference on In Communications (ICC)*, 2010, pp. 1–5.

[9] R. Mochaourab, E. A. Jorswieck, Z. K.-M. Ho, and D. Gesbert, "Bargaining and beamforming in interference channels," in *Proc. of IEEE Asilomar Conference on Signals, Systems, and Computers (ACSSC)*, 2010, to be published.

[10] Y. Lebrun, J. Nsenga, V. Ramon, A. Bourdoux, F. Horlin, and R. Lauwereins, "Maximum SINR-based beamforming for the MISO interference channel," in *Proc. of European Signal Processing Conference (EUSIPCO)*, 2009.

[11] E. A. Jorswieck, E. G. Larsson, and D. Danev, "Complete characterization of the pareto boundary for the MISO interference channel," *IEEE Transactions*

on Signal Processing, vol. 56, no. 10, pp. 5292–5296, 2008.

[12] X. Shang, B. Chen, G. Kramer, and H. V. Poor, "Capacity regions and sum-rate capacities of vector Gaussian interference channels," *IEEE Transactions on Information Theory*, vol. 56, no. 10, pp. 5030–5044, 2010.

[13] R. Zhang and S. Cui, "Cooperative interference management with MISO beamforming," *IEEE Transactions on Signal Processing*, vol. 58, no. 10, pp. 5450–5458, 2010.

[14] A. Goldsmith, S. A. Jafar, I. Maric, and S. Srinivasa, "Breaking spectrum gridlock with cognitive radios: An information theoretic perspective," *Proceedings of the IEEE*, vol. 97, no. 5, pp. 894–914, 2009.

[15] E. Bjornson, R. Zakhour, D. Gesbert, and B. Ottersten, "Cooperative multicell precoding: Rate region characterization and distributed strategies with instantaneous and statistical CSI," *IEEE Transactions on Signal Processing*, vol. 58, no. 8, pp. 4298–4310, 2010.

[16] E. Bjornson, M. Bengtsson, and B. Ottersten, "Pareto characterization of the multicell MIMO performance region with simple receivers," in *Proc. of IEEE International Conference on In Communications (ICC)*, 2011, submitted.

[17] C.-B. Chae, I. Hwang, J. Robert W. Heath, and V. Tarokh, "Interference aware-coordinated beamform system in a two-cell environment," *IEEE Journal on Selected Areas in Communications*, 2010, to be published.

[18] X. Shang, B. Chen, and H. V. Poor, "Multi-user MISO interference channels with single-user detection: Optimality of beamforming and the achievable rate region," *IEEE Transactions on Information Theory*, 2009, submitted.

[19] A. B. Gershman, N. D. Sidiropoulos, S. Shahbazpanahi, M. Bengtsson, and B. Ottersten, "Convex optimization-based beamforming," *IEEE Signal Processing Magazine*, vol. 27, no. 3, pp. 62–75, 2010.

[20] N. D. Sidiropoulos, T. N. Davidson, and Z.-Q. Luo, "Transmit beamforming for physical-layer multicasting," *IEEE Transactions on Signal Processing*, vol. 54, no. 6, pp. 2239–2251, 2006.

[21] D. Tomecki and S. Stanczak, "On feasible SNR region for multicast downlink channel: Two user case," in *Proc. of IEEE International Conference on Acoustics Speech and Signal Processing (ICASSP)*, 2010, pp. 3474–3477.

[22] H. Tuy, "Monotonic optimization: Problems and solution approaches," *SIAM Journal on Optimization*, vol. 11, no. 2, pp. 464–494, 2000.

[23] E. A. Jorswieck, "Optimal beamforming in interference networks," *IEEE Transactions on Signal Processing*, 2010, in preparation.

[24] S. Katz, A. Tal, and R. Basri, "Direct visibility of point sets," *ACM Transactions on Graphics*, vol. 26, no. 3, pp. 24/1–24/11, 2007.

[25] E. G. Larsson and E. A. Jorswieck, "Competition versus cooperation on the MISO interference channel," *IEEE Journal on Selected Areas in Communications*, vol. 26, no. 7, pp. 1059–1069, 2008.

[26] ——, "Competition and collaboration on the MISO interference channel," in *Proc. of Allerton Conference on Communications, Control and Computing*, 2007, invited.

[27] J. Lindblom, E. Karipidis, and E. G. Larsson, "Selfishness and altruism on the MISO interference channel: The case of partial transmitter CSI," *IEEE Commun. Lett.*, vol. 13, no. 9, pp. 667–669, 2009.

[28] E. Karipidis, A. Gründinger, J. Lindblom, and E. G. Larsson, "Pareto-optimal beamforming for the MISO interference channel with partial CSI," in *Proc. of IEEE International Workshop on Computational Advances in Multi-Sensor Adaptive Processing (CAMSAP)*, 2009, pp. 13–16.

[29] M. Bengtsson and B. Ottersten, "Optimal and suboptimal transmit beamforming," in *Handbook of Antennas in Wireless Communications*, L. C. Godara, Ed. CRC, 2001, ch. 18.

[30] S. Boyd and L. Vandenberghe, *Convex Optimization*. Cambridge University Press, 2004.

[31] Y. Ye, *Interior Point Algorithms: Theory and Analysis*. John Wiley & Sons, 1997.

[32] D. Tse and P. Viswanath, *Fundamentals of Wireless Communications*. Cambridge University Press, 2005.

[33] M. Grant and S. Boyd, "CVX: Matlab software for disciplined convec programming, version 1.21," http://cvxr.com/cvx, 2010.

[34] SAPHYRE, "Sharing physical resources," http://www.saphyre.eu.

[35] E. A. Jorswieck, L. Badia, T. Fahldieck, M. Haardt, E. Karipidis, J. Luo, and R. Pisz, "Spectrum sharing improves the network efficiency for wireless operators," *IEEE Commun. Mag.*, 2012, submitted.

[36] A. Carleial, "Interference channels," *IEEE Trans. Inf. Theory*, vol. 24, pp. 60–70, Jan. 1978.

[37] E. G. Larsson and E. A. Jorswieck, "Competition versus cooperation on the MISO interference channel," *IEEE J. Sel. Areas Commun.*, vol. 26, pp. 1059–1069, Sep. 2008.

[38] E. A. Jorswieck, E. G. Larsson, and D. Danev, "Complete characterization of the Pareto boundary for the MISO interference channel," *IEEE Trans. Signal Process.*, vol. 56, pp. 5292–5296, Oct. 2008.

[39] J. Lindblom, E. Karipidis, and E. G. Larsson, "Closed-form parameterization of the Pareto boundary for the two-user MISO interference channel," in *Proc.*

IEEE Int. Conf. on Acoustics, Speech, and Signal Process. (ICASSP), Prague, Czech Republic, May 2011, pp. 3372–3375.

[40] R. Mochaourab and E. Jorswieck, "Exchange economy in two-user multiple-input single-output interference channels," *IEEE J. Sel. Topics Signal Process.*, vol. 6, no. 2, pp. 151–164, Apr. 2012.

[41] R. Zakhour, Z. K. M. Ho, and D. Gesbert, "Distributed beamforming coordination in multicell mimo channels," in *Proc. IEEE Veh. Tech. Conf. (VTC)*, Barcelona, Spain, Apr. 2009.

[42] A. Leshem and E. Zehavi, "Game theory and the frequency selective interference channel," *IEEE Signal Process. Mag.*, vol. 26, no. 5, pp. 28–40, Sep. 2009.

[43] E. A. Jorswieck and E. G. Larsson, "Linear precoding in multiple antenna broadcast channels: Efficient computation of the achievable rate region," in *Proc. ITG Workshop on Smart Antennas (WSA)*, Vienna, Austria, Feb. 2008, pp. 21–28.

[44] S. Karmakar and M. K. Varanasi, "Capacity of the MIMO interference channel to within a constant gap," in *Proc. IEEE Int. Symp. on Inf. Theory (ISIT)*, Aug. 2011, pp. 2193–2197.

[45] G. Caire and S. Shamai, "On the achievable throughput in the multiple antenna Gaussian broadcast channel," *IEEE Trans. Inf. Theory*, vol. 49, no. 7, pp. 1691–1706, Jul. 2003.

[46] H. Weingarten, Y. Steinberg, , and S. Shamai, "The capacity region of the Gaussian multiple-input multiple-output broadcast channel," *IEEE Trans. Inf. Theory*, vol. 52, no. 9, pp. 3936–3964, Sep. 2006.

[47] T. Han and K. Kobayashi, "A new achievable rate region for the interference channel," *IEEE Trans. Inf. Theory*, vol. 27, no. 1, pp. 49–60, Jan. 1981.

[48] G. Kramer, "Outer bounds on the capacity of Gaussian interference channels," *IEEE Trans. Inf. Theory*, vol. 50, no. 3, pp. 581–586, Mar. 2004.

[49] S. Vishwanath and S. A. Jafar, "On the capacity of the vector Gaussian interference channel," in *Proc. IEEE Inf. Theory Workshop (ITW)*, San Antonio, TX, Oct. 2004, pp. 365–369.

[50] X. Shang, B. Chen, G. Kramer, and H. V. Poor, "Capacity region and sum-rate capacities of vector Gaussian interference channels," *IEEE Trans. Inf. Theory*, vol. 56, no. 10, pp. 5030–5044, Oct. 2010.

[51] S. Vishwanath, N. Jindal, and A. Goldsmith, "Duality, achievable rates, and sum-rate capacity of Gaussian MIMO broadcast channels," *IEEE Trans. Inf. Theory*, vol. 49, no. 10, pp. 2658–2668, Oct. 2003.

[52] S. Vishwanath and S. A. Jafar, "On the capacity of vector Gaussian interfer-

ence channels," in *Proc. of Information Theory Workshop (ITW)*, 2004, pp. 365–369.

[53] R. Zhang and S. Cui, "Cooperative interference management with MISO beamforming," *IEEE Trans. Signal Process.*, vol. 58, no. 10, pp. 5454–5462, Oct. 2010.

[54] R. Mochaourab and E. A. Jorswieck, "Optimal beamforming in interference networks with perfect local channel information," *IEEE Trans. Signal Process.*, vol. 59, no. 3, pp. 1128–1141, Mar. 2011.

[55] J. Lindblom, E. G. Larsson, and E. A. Jorswieck, "Parameterization of the MISO IFC rate region: the case of partial channel state information," *IEEE Trans. Commun.*, vol. 9, no. 2, pp. 500–504, Feb. 2010.

[56] S. Vorobyov, A. Gershman, and Z.-Q. Luo, "Robust adaptive beamforming using worst-case performance optimization: a solution to the signal mismatch problem," *IEEE Trans. Signal Process.*, vol. 51, no. 2, pp. 313–324, Feb. 2003.

[57] R. Lorenz and S. Boyd, "Robust minimum variance beamforming," *IEEE Trans. Signal Process.*, vol. 53, no. 5, pp. 1684–1696, May 2005.

[58] J. Li and P. Stoica, Eds., *Robust Adaptive Beamforming*. Hoboken, NJ: Wiley, 2006.

[59] A. Tajer, N. Prasad, and X. Wang, "Robust linear precoder design for multi-cell downlink transmission," *IEEE Trans. Signal Process.*, vol. 59, no. 1, pp. 235–251, Jan. 2011.

[60] R. Mochaourab and E. Jorswieck, "Robust pareto optimal beamforming in two-user multiple-input single-output interference channel, invited," in *Proc. EUSIPCO*, Aug. 2011.

[61] A. Lozano, A. Tulino, and S. Verdu, "High-SNR power offset in multiantenna communication," *IEEE Trans. Inf. Theory*, vol. 51, no. 12, pp. 4134–4151, Dec. 2005.

[62] S. Verdu, "Spectral efficiency in the wideband regime," *IEEE Trans. Inf. Theory*, vol. 48, no. 6, pp. 1319 –1343, Jun. 2002.

[63] J. Lindblom, E. G. Larsson, and E. A. Jorswieck, "Parametrization of the MISO IFC rate region: The case of partial channel state information," *IEEE Trans. Wireless Commun.*, vol. 9, pp. 500–504, Feb. 2010.

[64] E. A. Jorswieck and H. Boche, "Outage probability in multiple antenna systems," *European Trans. on Telecommun.*, vol. 18, pp. 217–233, Apr. 2007.

[65] L. Li, N. Jindal, and A. J. Goldsmith, "Outage capacities and optimal power allocation for fading multiple-access channels," *IEEE Trans. Inf. Theory*, vol. 51, pp. 1326–1347, Apr. 2005.

[66] L. Li and A. J. Goldsmith, "Capacity and optimal resource allocation for fad-

ing broadcast channels–Part II: Outage capacity," *IEEE Trans. Inf. Theory*, vol. 47, pp. 1103–1127, Mar. 2001.

[67] V. Ntranos, N. D. Sidiropoulos, and L. Tassiulas, "On multicast beamforming for minimum outage," *IEEE Trans. Wireless Commun.*, vol. 8, no. 6, pp. 3172–3181, Jun. 2009.

[68] R. Narasimhan, "Individual outage rate regions for fading multiple access channels," in *Proc. IEEE Int. Symp. on Inf. Theory (ISIT)*, Nice, France, Jun. 2007, pp. 1571–1575.

[69] X. Kang, Y.-C. Liang, and H. K. Garg, "Fading cognitive multiple access channels: Outage capacity regions and optimal power allocation," *IEEE Trans. Wireless Commun.*, vol. 9, pp. 2382–2391, Jul. 2010.

[70] S. Kandukuri and S. Boyd, "Optimal power control in interference-limited fading wireless channels with outage-probability specifications," *IEEE Trans. Wireless Commun.*, vol. 1, pp. 46–55, Jan. 2002.

[71] X. Lei, L. Cottatellucci, and K. Avrachenkov, "Equilibriums in slow fading interfering channels with partial knowledge of the channels," in *Proc. IEEE INFOCOM*, Shanghai, China, Apr. 2011, pp. 481–485.

[72] Y. Weng and D. Tuninetti, "Outage analysis of block-fading gaussian interference channels: General case," in *Proc. IEEE Int. Conf. on Commun. (ICC)*, Cape Town, South Africa, May 2010, pp. 1–5.

[73] W.-C. Li, T.-H. Chang, and C.-Y. Chi, "A convex approximation approach to weighted sum rate maximization of multiuser MISO interference channel under outage constraints," in *Proc. IEEE Int. Conf. on Acoustics, Speech, and Signal Process. (ICASSP)*, Prague, Czech Republic, May 2011, pp. 3368–3371.

[74] J. Lindblom, E. Karipidis, and E. G. Larsson, "Outage rate regions for the MISO IFC," in *Proc. IEEE Asilomar Conf. Signals, Systems, and Computers*, Pacific Grove, CA, Nov. 2009, pp. 1120–1124.

[75] X. Shang, B. Chen, and H. V. Poor, "On the optimality of beamforming for multi-user MISO interference channels with single-user detection," in *Proc. IEEE Global Telecommun. Conf. (GLOBECOM)*, Honolulu, HI, USA, Nov. 2009, pp. 1–5.

[76] A. Goldsmith, S. A. Jafar, N. Jindal, and S. Vishwanath, "Capacity limits of MIMO channels," *IEEE J. Sel. Areas Commun.*, vol. 21, no. 5, pp. 684–702, 2003.

[77] S. M. Ross, *Introduction to Probability Models*. Academic Press, 2003.

[78] A. Bletsas, H. Shin, and M. Z. Win, "Cooperative communications with outage-optimal opportunistic relaying," *IEEE Trans. Wireless Commun.*, vol. 6, pp. 3450–3460, Sep. 2007.

[79] H. Shin and M. Z. Win, "MIMO diversity in the presence of double scattering," *IEEE Trans. Inf. Theory*, vol. 54, pp. 2976–2996, Jul. 2008.

[80] A. B. Carleial, "Interference channels," *IEEE Transactions on Information Theory*, vol. 24, no. 1, pp. 60–70, 1978.

[81] M. H. M. Costa, "On the gaussian interference channel," *IEEE Transactions on Information Theory*, vol. 31, no. 5, pp. 607–615, 1985.

[82] X. Shang, G. Kramer, and B. Chen, "A new outer bound and the noisy-interference sum-rate capacity for Gaussian interference channels," *IEEE Transactions on Information Theory*, vol. 55, no. 2, pp. 689–699, 2009.

[83] S. A. Motahari and A. K. Khandani, "Capacity bounds for the Gaussian interference channel," *IEEE Transactions on Information Theory*, vol. 55, no. 2, pp. 620–643, 2009.

[84] I. Sason, "On achievable rate regions for the gaussian interference channel," *IEEE Transactions on Information Theory*, vol. 50, no. 6, pp. 1345–1356, 2004.

[85] R. H. Etkin, D. N. C. Tse, and H. Wang, "Gaussian interference channel capacity to within one bit," *IEEE Transactions on Information Theory*, vol. 54, no. 12, pp. 5534–5562, 2008.

[86] Y. Weng and D. Tuninetti, "On gaussian interference channels with mixed interference," in *Proceedings of International Symposium of Information Theory*, 2008.

[87] B. Bandemer, A. Sezgin, and A. Paulraj, "On the noisy interference regime of the MISO Gaussian interference channel," in *Proc. of IEEE Asilomar Conference on Signals, Systems, and Computers (ACSSC)*, 2008, pp. 1098–1102.

[88] M. Charafeddine, A. Sezgin, and A. Paulraj, "Rate region frontiers for n-user interference channel with interference as noise," in *Proc. of Allerton Conference on Communications, Control and Computing*, 2007.

[89] T. S. Han and K. Kobayashi, "A new achievable rate region for the interference channel," *IEEE Transactions on Information Theory*, vol. 27, no. 1, pp. 49–60, 1981.

[90] Z. K.-M. Ho, D. Gesbert, E. Jorswieck, and R. Mochaourab, "Beamforming on the MISO interference channel with interference decoding capability," *in preparation*, 2010.

[91] Y.-F. Liu, Y.-H. Dai, and Z.-Q. Luo, "Coordinated beamforming for miso interference channel: Complexity analysis and efficient algorithms," *IEEE Transactions on Signal Processing*, 2010, submitted.

[92] V. S. Annapureddy and V. V. Veeravalli, "Sum capacity of MIMO interference channels in the low interference regime," *IEEE Transactions on Information*

Theory, Sep. 2009, submitted.

[93] R. W. Yeung, S.-Y. R. Li, N. Cai, and Z. Zhang, *Network Coding Theory*. now Publishers, 2006.

[94] P. Popovski and T. Koike-Akino, "Coded bidirectional relaying in wireless networks," in *Advances in Wireless Communications*, V. Tarokh, Ed. Springer, 2009.

[95] T. Koike-Akino, P. Popovski, and V. Tarokh, "Denoising maps and constellations for wireless network coding in two-way relaying systems," in *Proc. of IEEE Global Telecommunications Conference (GlobeCom)*, 2008.

[96] ——, "Denoising strategy for convolutionally-coded bidirectional relaying," in *Proc. of IEEE International Conference on In Communications (ICC)*, 2009.

[97] ——, "Optimized constellations for two-way wireless relaying with physical network coding," *IEEE Journal on Selected Areas in Communications*, vol. 27, no. 5, pp. 773–787, 2009.

[98] W. Nam, S.-Y. Chung, and Y. H. Lee, "Capacity bounds for two-way relay channels," in *Proc. Int. Zurich Seminar on Communications*, 2008.

[99] I.-J. Baik and S.-Y. Chung, "Network coding for two-way relay channels using lattices," in *Proc. of IEEE International Conference on In Communications (ICC)*, 2008, pp. 3898–3902.

[100] U. Erez and R. Zamir, "Achieving $1/2 \log(1 + \mathrm{SNR})$ on the AWGN channel with lattice encoding and decoding," *IEEE Transactions on Information Theory*, vol. 50, no. 10, pp. 2293–2314, 2004.

[101] J. Sykora and A. Burr, "Layered design of hierarchical exclusive codebook and its capacity regions for HDF strategy in parametric wireless 2-WRC," *IEEE Trans. Veh. Technol.*, vol. 60, no. 7, pp. 3241–3252, Sep. 2011.

[102] ——, "Hierarchical exclusive codebook design using exclusive alphabet and its capacity regions for HDF strategy in parametric wireless 2-WRC," in *Proc. of COST Management Committee Meeting*, 2009, pp. 1–9.

[103] ——, "Hierarchical alphabet and parametric channel constrained capacity regions for HDF strategy in parametric wireless 2-WRC," in *Proc. of IEEE Wireless Communications and Networking Conference (WCNC)*, 2010, pp. 1–6.

[104] T. M. Cover and J. A. Thomas, *Elements of Information Theory*. John Wiley & Sons, 1991.

[105] R. Ahlswede, N. Cai, S.-Y. R. Li, and R. W. Yeung, "Network information flow," *IEEE Trans. Inf. Theory*, vol. 46, no. 4, pp. 1204–1216, Jul. 2000.

[106] J. Sykora and A. Burr, "Network coded modulation with partial side-information and hierarchical decode and forward relay sharing in multi-source

wireless network," in *Proc. European Wireless Conf. (EW)*, Lucca, Italy, Apr. 2010, pp. 1–7.

[107] A. Burr and J. Sykora, "Extended mappings for wireless network coded butterfly network," in *Proc. European Wireless Conf. (EW)*, Vienna, Austria, Apr. 2011, pp. 1–7.

[108] T. Uricar and J. Sykora, "Non-uniform 2-slot constellations for bidirectional relaying in fading channels," *IEEE Commun. Lett.*, vol. 15, no. 8, pp. 795–797, Aug. 2011.

[109] ——, "Design criteria for hierarchical exclusive code with parameter-invariant decision regions for wireless 2-way relay channel," *EURASIP J. on Wireless Comm. and Netw.*, vol. 2010, no. Article ID 921427, pp. 1–14, Jul. 2010.

[110] J. Sykora and E. A. Jorswieck, "Network coded modulation with HDF strategy and optimized beam-forming in 2-source 2-relay network," in *Proc. IEEE Vehicular Technology Conf. (VTC)*, San Francisco, USA, Sep. 2011, pp. 1–6.

[111] G. Ungerboeck, "Channel coding with multilevel/phase signals," *IEEE Trans. Inf. Theory*, vol. 28, no. 1, pp. 55–67, Jan. 1982.